CHARACTERISTICS OF ALTERNATIVE FUELS AND ALTERNATIVE COOLING OF THERMAL POWER PLANTS

By

Christopher David Bolin

A DISSERTATION

Submitted to
Michigan State University
in partial fulfillment of the requirements
for the degree of

Mechanical Engineering - Doctor of Philosophy

2014

ABSTRACT

CHARACTERISTICS OF ALTERNATIVE FUELS AND ALTERNATIVE COOLING OF THERMAL POWER PLANTS

By

Christopher David Bolin

In regions of the world where the infrastructure for electrical power generation and distribution is unreliable or outdated moving to a distributed power generation is a viable strategy for the future. Gas turbine engines at all scales can be used to meet local power demands efficiently. Remote sites will require small engines relying on a variety of fuel sources including alternative fuels (i.e., fuels derived from non-fossil sources) as well as cleaner, from an emissions standpoint, methods of using fossil sources. Near larger industrial and domestic loads larger co-generation plants will be necessary. These co-generation plants will require cooling for a steam condenser to maximize the efficiency of the vapor cycle. In arid locations surface and sub-surface water sources may be insufficient to meet cooling demands for both environmental and regulatory reasons. At such locations an alternative cooling strategy will be required. This work is divided into two parts that investigate fundamental questions regarding alternative fuel issues for small scale gas turbine engines and cooling issues for larger co-generation plants.

In the first part of this work the application of biogas to small scale generation systems is explored. Biogas is a term used for the collection of gases produced by the anaerobic digestion of organic waste materials such as garbage and animal manure. The resulting gas consists of CH_4 diluted with varying amounts of CO_2, H_2O, N_2, and other trace species. The content of biogas is feedstock dependent and thus variable. This poses a challenge to combustor designers. Many modern gas turbine combustors use a fuel-lean, premixed strategy to meet

strict emissions standards. Operating under such conditions, often near the lean-extinction limit, can be difficult with fuel variability. Empirical relations, determined with simplified experimental devices, can be used by the designer to provide a first-order approximation of the operating envelope of a new system. Such relations are available for a range of traditional fuels but are lacking for newer alternative fuels. Stability limits for a range of biogas fuel contents are investigated here using stirred-reactor theory. Correlations to predict lean-extinction limits based on content are developed. Finally, a facility for expanding this research with a laboratory well-stirred reactor (WSR) for the investigation of biogas extinction limits and combustion emissions will be described.

The second part of this work explores the use of vapor-compression refrigeration systems for steam condenser cooling. Larger loads invite the use of combined cycle power systems. These systems use large industrial or aero-derivative gas turbine topping cycles with conventional steam power bottoming cycles to increase fuel efficiency. An alternative cooling system using vapor compression refrigeration is an alternative method of cooling that can reduce or eliminate the need for cooling water. A novel facility for small scale experiments to explore the operating envelope of the proposed system is described here. The results of preliminary investigations into the use of R-410a as a steam condenser coolant are also presented.

To my mother Carole and father Steven for the patience and encouragement

ACKNOWLEDGMENTS

In the completion of this work I have been assisted, supported and encouraged by many individuals. I would like to thank Dr. Wei Liao, Dr. Norbert Mueller, Dr. Tonghun Lee and Dr. Patrick Kwon for their guidance and support as committee members. All of the small details involved with conducting research work as well as classwork would not have been possible without the assistance of Aida Montalvo, Mary Pease, Lindsey Niesen and Suzanne Kroll of the Department of Mechanical Engineering office. Many ideas on the design, construction and maintenance of various lab equipment were greatly assisted by Roy Bailiff of the department machine shop.

I would also like to thank those of my colleagues who acted as both collaborators and distractions. In the early portion of this work I collaborated with Dr. Joseph Zelina of the Air Force Research Laboratory, Dr. Scott Stouffer of the University of Dayton, Dr. Samuel Manzello of the National Institute of Standards and Technology and Dr. Saeed Jahangirian and Mr. Daejung Kim of MSU, their assistance in getting my feet under me is greatly appreciated. A special thanks to Dr. Marco Vagani who acted as a research collaborator and a helpful distraction as appropriate. Thank you to Ryan, Amol, Venkat and Avinash for being willing to play some golf or generally get out of the building whenever it was necessary and several times when it wasn't.

My family played a large roll in maintaining my balance during this work. Thank you for your patience, encouragement and understanding throughout this extended process. Mom, whenever I needed a break you were always there with a lovingly prepared meal and someone to talk to. Dad, if I needed to do something to take my mind of research, you could always find some task, usually involving physical labor, to keep me busy. Matt, Sarah and Kelsey,

you were always there to talk to about anything other than research or do anything other than work. For these little distractions, I am extremely grateful.

Finally, I wish to acknowledge and thank my advisor Dr. Abraham Engeda. A quick hallway meeting in the fall of 2008 started this endeavor. Along the way, you have provided copious amounts guidance, support, advice, encouragement and patience. I sincerely thank you for all that you have done for me to reach this point.

TABLE OF CONTENTS

LIST OF TABLES

LIST OF FIGURES

KEY TO SYMBOLS AND ABBREVIATIONS

$\bar{\mathrm{Nu}}$	Average Nusselt Number
c_{P}	Isobaric Specific Heat Capacity
$\dot{m}$	Mass Flow Rate
T	Period of Oscillation
$\mathrm{S_L}$	Laminar Flame Speed
$\tilde{\mathrm{Re}}$	Two-phase Reynolds number
A	Arrhenius Coefficient
D	Diameter
Da	Damköhler Number
E	Activation Energy
h	Specific Enthalpy
k	Reaction Constant of Proportionality
L	Length
MW	Molecular Weight
P	Pressure
Q	Heat Release
q_c	Specific Heat of Reaction
R_{u}	Universal Gas Constant
s	Specific Entropy
$S.G.$	Specific Gravity
T	Temperature
t	Time
u	Velocity
U_{o}	Overall Heat Transfer Coefficient
V	Volume

W	Work
x_f	CH_4 Mole Fraction of Biogas
Y	Species Mass Fraction
α	Third Body Efficiency
β	Fraction of Fuel Consumed
χ	Mole Fraction
δ	Flame Thickness
γ	Ratio of Specific Heats
ν	Stoichiometric Coefficient
ω	Rate of Change in Concentration
ϕ	Equivalency Ratio
ϕ_{LE}	Equivalence ratio at fuel-lean extinction
ρ	Mass Density
τ	Residence Time
τ_{ig}	Autoignition time
η	Efficiency
F/A	Fuel-to-Air Ratio
LHV	Lower Heating Value
$\mathrm{NO_x}$	Total oxides of nitrogen $\mathrm{NO} + \mathrm{NO_2}$
CHP	Combined Heat and Power
COP	Coefficient of Performance
EGR	Exhaust Gas Recirculation
GRI	Gas Research Institute
GT	Gas Turbine
HRSG	Heat Recovery Steam Generator
IHX	Intermediate Heat Exchanger
LMTD	Log-Mean Temperature Difference

LP Chemical Loading Parameter

LP Fuel-Lean, Premixed

LPP Fuel-Lean Premixed, Prevaporized

MN Methane Number

MON Motor Octane Number

PaSR Partially-Stirred Reactor

PFR Plug Flow Reactor

PSR Perfectly-Stirred Reactor

RCL Rich-Catalytic-Lean

RQL Rich-Quench-Lean

SCR Selective Catalytic Reduction

SNCR Selective Non-Catalytic Reduction

UHC Unburned Hydrocarbons

VCRS Vapor Compression Refrigeration System

WI Wobbe Index

WSR Well-Stirred Reactor

Chapter 1

Introduction and Objectives

1.1 Introduction

The related national goals of energy independence, reducing the emission of various pollutant species and updating the electrical grid present an intriguing set of engineering challenges. As methods to achieve the first two of these goals, the development of alternative fuels (*i.e.*, fuels derived from non-fossil sources) as well as cleaner, from an emissions standpoint, methods of using domestic fossil sources have generated great interest. Some of these alternative fuels can be produced at a useful scale near their point of use. A more distributed power generation system would be well suited to utilize such local local sources and is also a strategy to achieve the third goal of updating the electrical infrastructure. Such a system would require a large number power generating facilities of different sizes based on the available local fuel source. Alternative fuel sites traditionally support small generators ($\leq$ 10 MW_e) driven by clean, fuel-flexible heat-engines. Natural gas production sites may support generating systems up to hundreds of MW_e. These conventionally fired power generation facilities would be used in conjunction with other alternative energy sources (*e.g.*, solar, wind and tidal) to produce electricity for local use. By generating electrical power near its use point, the losses inherent in long distance transmission of both fuel and electricity can be reduced or eliminated. Combining distributed generation and alternative fuels presents path towards a more efficient, cleaner system of power generation.

Two alternative fuels in particular are promising candidates for adoption: biogas and syngas. These fuels are both gaseous at standard atmospheric conditions, which eliminates the parasitic loss required to vaporize the fuel before combustion, and can be produced from feedstock readily available in the U.S. Generally, syngas refers to H_2 and CO based fuels. One of the more abundant sources for syngas in the U.S. is coal, though it can also be produced from biomass and natural gas. Biogas is a term used for the collection of gases produced by the anaerobic digestion of organic waste materials. This is a process which takes place naturally in sanitary landfills, manure storage and other sealed organic waste containers. The result is a mixture of primarily CH_4 and CO_2. In the case of large landfills, the biogas can be pumped from the subsurface in a similar manner to natural gas. Biogas derived from animal waste or human sewage requires collection of the waste and is normally produced in specialized digesters located near the collection point.

Both of the primary products of the anaerobic digestion of organic waste, CO_2 and CH_4, are known greenhouse gases. In terms of warming, CH_4 is a 21 times more effective greenhouse gas than CO_2 [5]. To prevent buildup of CH_4 and ecological damage, gas must removed in locations like sanitary landfills where it may naturally collect. This effluent may be required by law to undergo treatment to reduce its impact on the local environment. One method of treating biogas is to burn it using flares. The combustion of the CH_4 in biogas, which ideally results only in the emission of CO_2 and H_2O, acts as a net reduction in CO_2 equivalent greenhouse gas emissions and eliminates a potential fire hazard. There are, however, no other benefits from the flaring. Using the biogas to generate electricity or hot water takes the greenhouse gas reduction of flaring and adds useful by-product.

One of the more efficient options for driving electrical generators is the gas-turbine (GT) engine [6]. GT engines may be roughly subdivided into two groups: micro-turbines and

industrial turbines. Micro-turbines produce less than 500 kWe and were developed over the last 25 years from turbocharger technology or scaling of industrial turbine designs [7]. The small scale of the GTs often used in alternative fuels applications makes achieving high a thermal efficiency, a general attribute of GTs, a challenge. As a result, many micro-turbines run a recuperated cycle. Industrial turbines may be further subdivided into two categories: pure industrial and aero-derivative. Pure industrial models were purpose designed from the outset as ground based power generators. Aero-derivative, as the name implies, are based on engines intended to power aircraft. Modifications are often made to aero-derivative engines to reduce cost and make them better suited to ground based power production.

The two scales of turbines rely on similar basic architecture to produce power. A common arrangement is that of a compressor driven by a turbine on a single shaft. In the case of a micro-turbine, these are typically a single-stage centrifugal compressor and a single stage radial turbine. This grouping of radial flow turbomachinery may be used through the smaller scales of industrial turbines (ca. 2MW). Larger industrial and aero-derivative engines rely primarily on multi-stage axial compressors and turbines. Aero-derivatives also maintain their multi-spool arrangements for driving different stages of compression at different speeds. In the flow path between the rotating devices sits the combustor. It takes the compressor discharge, adds fuel, and reacts the mixture to generate high temperature gas. A portion of the energy in the gas extracted by the turbine is used to drive the compressor. Any energy in excess of that required to drive the compressor can be used to drive an electrical generator, drive other rotating machinery, or produce thrust. Of these components only the combustor is particularly affected by the additional challenges posed by alternative fuels and fuel flexibility.

Regardless of scale, fuel efficiency can be improved by using the remaining energy in the

turbine exhaust for heating a second fluid yielding a combined heat and power (CHP) system or a co-generation plant. The small scale and recuperated cycle of micro-turbines generally limits them to the production of hot water. The water may be used for a variety of purposes including domestic hot water, energy for absorption chillers, building or process heating, and boiler feed water pre-heating. Industrial turbines, due to the high mass flow rates and lack of recuperation, can co-generate high quality steam. This steam is then often used in a secondary Rankine cycle loop to generate additional electrical power thereby increasing the fuel efficiency of the system. To maximize the efficiency of the secondary Rankine cycle, a steam condenser is typically employed to reduce the minimum cycle temperature. As they do in more typical Rankine cycle systems, these condensers use or consume large quantities of water. If these larger industrial turbines are to be used in a more distributed fashion, alternative cooling methods for the steam condensers are required for regions where the water supply is limited and ambient conditions make evaporative cooling unappealing.

1.1.1 Gas Turbine Combustors

In both aircraft and ground-based GT engines the purpose of the combustor is to convert the chemical energy, stored in the fuel and air, into high-quality thermal energy. The combustor's two main components are the casing and the liner, see Figure 1.1. The casing provides pressure containment for the system, and the liner is designed to hold the hot combustion gasses. Fresh air flows into the casing and takes one of three paths into the liner. The first path, labeled primary air in Figure 1.1, carries the air into a mixing zone where fuel is added. This mixture then flows into the high temperature region where it acts as the primary combustion charge. A second path provides cooling air to the liner to prevent mechanical failure due to excessive temperatures. The final path dumps any remaining air into the liner

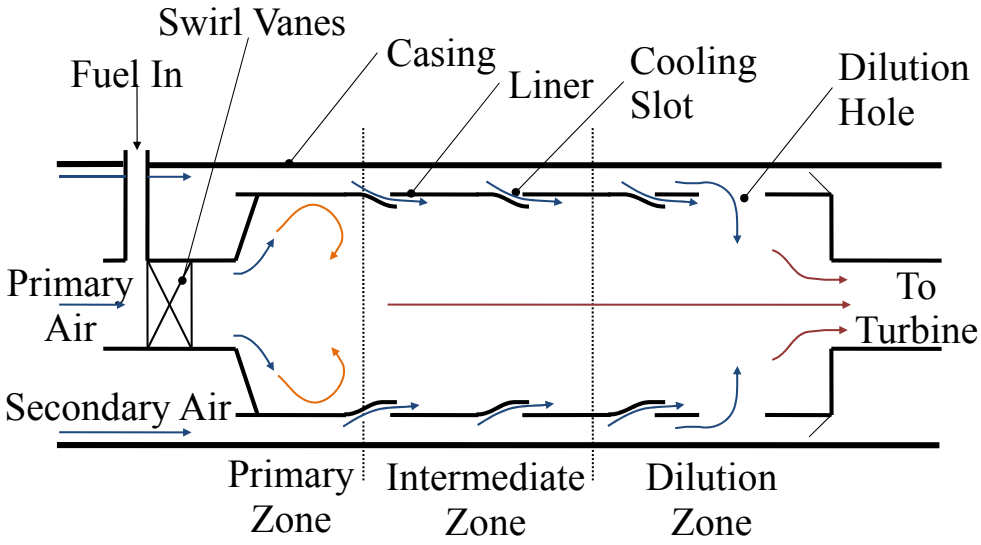

Figure 1.1: Sketch of a gas turbine combustor, blue lines indicate cool air, orange lines indicate recirculation/flame stabalization zones and red lines indicate product gases. For interpretation of the references to color in this and all other figures, the reader is referred to the electronic version of this dissertation.

near the exit through the dilution holes to achieve the desired temperature profile. It follows that the high temperature region within the liner is commonly divided into three zones: the primary zone, intermediate zone and dilution zone. Each have different functions and present their own design challenges [8].

The primary zone is the portion of the combustor that provides space for ignition and completion of a majority of the combustion processes. It is important for the geometry of this region to generate sufficient turbulence for the mixing of the reactants, provide a location for anchoring the flame, and sufficient temperature for the combustion process to occur. In this zone there may be regions where temperatures are high enough to dissociate CO_2 into CO, which is both a fuel and a pollutant, and O_2. Alternatively, regions may exist where temperatures are low enough to retard the completion of the conversion of CO to CO_2. To

recoup the losses caused by dissociation or complete the burnout of CO an intermediate combustion zone is used.

The length of the intermediate zone is necessary to perform two tasks. First, in ground-based and aircraft GTs at low altitude it serves as a zone for the reduction of CO in the product gases from the primary zone. In the case of dissociation due to high temperatures in the primary zone, this is done by the addition of small amounts of air through the liner wall which drops the temperature of the mixture. The additional O_2 also helps to complete the combustion of any pockets of unburned fuel. The second role of the intermediate zone takes place at high altitudes or other operating conditions that slow the reactions in the primary zone. Here it provides additional space for the primary combustion process to occur. This compensates for the lower reaction rates at high altitude due to the lower concentration of O_2 or at lower altitudes due to low combustion temperatures. At the end of the intermediate zone temperatures are still to extreme for injection into the turbine.

In the dilution zone more cool air is added to the combustion products to reduce their temperature to one suitable for the turbine inlet. The cooling air is injected through the wall of the liner in such a way to generate the desired temperature profile. This increases the life of the turbine blades and sealing materials by reducing the temperature where the mechanical stresses are highest. Because the limiting factor on GT performance is normally the thermal capabilities of the turbine, a major effort is devoted to producing the desired temperature profile.

1.1.2 Challenges of Alternative Fuels

Alternative fuels require a combustor of special design. These fuels tend to be of lower calorific content relative to common fossil fuels like natural gas. Thus, a greater fuel flow is

required to attain the same heat release. To compensate, the fuel handling and combustion systems may need to be larger than systems intended for natural gas. The composition of many alternative fuels tends to be site specific and can vary from day-to-day or even hour-to-hour which requires a degree of fuel flexibility. To be able to respond to the changes in fuel, specialized control systems and, in some cases, variable geometry are necessary to adjust fuel flow to meet power demand. Finally, the ongoing desire to further reduce pollutant emissions, particularly oxides of nitrogen (NO_x) and unburned hydrocarbons, adds yet another layer of difficulty by requiring careful control of the combustion environment to avoid conditions where these species are produced.

There are a number of techniques for overcoming the challenges posed by alternative fuels. One method is 'upgrading' which is a process that increases the calorific content by removing diluent. For fuels whose primary combustible component is CH_4, upgrading essentially scrubs the alternative fuels into natural gas before it enters the combustor. Additional capital equipment in the form of filters, separators, and absorption columns are required to clean the gas. The energy required to run the upgrading equipment is a parasitic loss to any stand-alone system. Upgrading may alleviate two difficulties associated with alternative fuels, energy content and variability, but it does little to address pollutant emissions other than to reduce the H_2S content of the fuel.

The modern practice of fuel-lean premixed, prevaporized (LPP) combustion is a method for reducing NO_x emissions by decreasing combustion temperature. LPP has the added benefit of reducing fuel consumption which is the only method of reducing CO_2 emissions. Operating in the fuel-lean regime is not without complications which are discussed in Sections 2.2 and 2.3 some of which are exacerbated by the content variation of alternative fuels. Clearly, the most desirable solution would be a flexible combustor that operate at fuel-lean

conditions on relatively low heating value fuels.

To aid the design such a combustor, a systematic analysis of the combustion properties of alternative fuels of varying constituency is required. It is important to know how much, if any, processing of the raw alternative fuels beyond that required to remove matter hazardous to other elements of the GT is necessary for successful, stable combustor operation. Further, it is necessary to have a baseline understanding of the content and properties of the gas which will be fed into the turbine and eventually into the atmosphere as exhaust to design for modern and future emissions requirements. For these reasons, a laboratory model of a GT combustor in which combustion stability and emissions investigations can be carried out in a controlled manner is of great use [9]. From experiments performed using such a model the necessary background knowledge on the combustion characteristics of various grades of alternative fuels for the design of future combustors can be attained.

1.2 Laboratory Modeling of a GT Combustor

Many of the major steps of the combustion process in a GT take place in the primary zone of the combustor. Therefore, if an investigation into the use of alternative fuels in a GT is to be undertaken, an accurate model of this zone required. While it is possible to use the combustor out of a production GT, the flow patterns tend to be geometry specific. Thus, results may not be applicable to all systems. For this reason using a simplified model of the primary zone is a preferred way to investigate the combustion properties new fuels [9].

Two primary methods of modeling are available: numerical and physical experiments. Each has its benefits and drawbacks. Numerical experiments are convenient, from a safety standpoint, in that they do not require physical combustion to take place. They also allow

for very precise variation of the boundary conditions. However, without experiments to calibrate them, the model's predictions cannot be guaranteed to be valid. Experimental data, when gathered carefully, accurately characterizes what actually happens in a system, but practical considerations affect the resolution and precision of the information. Following either route requires a model whose complexity should be a compromise between its ease of application and accuracy of representation. To which extreme the model approaches is based on the nature of data desired.

One relatively simple model, useful in both numerical and physical experiments, of the primary zone of a GT combustor is the well-stirred reactor (WSR). The WSR is a laboratory version of the theoretical perfectly-stirred reactor (PSR). Like the primary zone, the combustion inside a WSR is characterized by intense turbulent mixing of burned and unburned gases. Additionally, operating conditions within the WSR can be controlled reasonably and safely in a laboratory setting allowing for the investigation of basic combustion science problems. Thus, the WSR provides a benchmark useful for combustor modeling and design [2, 8, 10].

1.3 Cooling of co-generation steam loops

Steam-cycle power generating facilities are the largest consumers of water in the United States [11, 12]. The primary consumer of water in the Rankine cycle is the steam condenser. Though they consume less water than traditionally fired Rankine cycles, combined-cycle GT applications may still require large quantities of water depending on condenser design. Three different condenser designs are commonly used. The once-through design relies on a continuous stream of water to cool the steam exiting the turbine. Condensers of this

type are large users of water but not large consumers. Due to the large quantity of water required, power plants using once-through condensers must be located near rivers, lakes or ocean coasts. If a large source of water is not available, closed-cycle condensers may be employed. Instead of using high flow rates like once-through designs, closed-cycle systems employ evaporative cooling. The primary coolant is recycled through the condenser in a closed loop. This reduces the usage of water, but greatly increases the consumption of water due to the evaporation of a portion of the cooling water. Finally, there is the dry cooling option which relies on air movement to condense the steam. No additional water is required, so plant location is less dependent on the availability of local water sources. However, minimum temperatures are dictated by the ambient wet bulb temperature leading to seasonal swings in plant efficiency.

The design of a condenser is limited by both the load of the cycle and statutory limits on thermal pollution. For once-through condensers the limit is the temperature rise of the cooling water supply. Limits may be placed on both the temperature rise and the maximum temperature of the body of water into which cooling water is discharged [13]. For closed-loop cooling systems the issues arise from the thermal plume of saturated air created by the cooling towers. The plumes, if located near roadways or airports, can cause visibility issues or lead to surface icing in sub-freezing atmospheric conditions. Both open and closed-loop cooling systems operate in a range of temperatures that promote the growth of the *legionella* bacteria which can be carried by plumes from cooling towers [12].

Combined-cycle plants generally consume less water that steam cycle plants. To further reduce usage most new combined-cycle power plants opt for a closed-loop cooling systems. Closed-loop systems offer better temperature stability that dry systems [14]. Water usage may be eliminated for the full range of steam power plant sizes is to use closed-loop refrig-

eration systems to remove heat in the condenser. In this case the condenser of the Rankine cycle acts as the evaporator in the refrigeration cycle.

The use of refrigerants offers three basic advantages over water. The most obvious is the elimination of water from the cooling circuit. Second, refrigerants have higher heat transfer rates than water or air increasing the efficiency of the condenser. Lastly, using a refrigerant cycle will stabilize the efficiency of the Rankine cycle by providing a nearly constant minimum cycle temperature regardless of season. The primary disadvantage of such a system is the parasitic load it imposes on the power cycle.

1.4 Research Objectives

The objectives of the present research are as follows:

- Study the effect of CO_2 dilution on laminar flame speeds of CH_4-air combustion in a WSR with detailed chemical kinetics
- Study the effect of CO_2 dilution on the fuel-lean extinction limits of CH_4-air combustion in a WSR with detailed chemical kinetics
- Design of a laboratory scale WSR for alternative fuels combustion research at MSU
- Investigate the cycle impact of refrigerant cooling on combined-cycle steam plants
- Design a laboratory scale model of a steam power plant condenser with refrigerant cooling for more detailed investigations

Chapter 2

Alternative Fuels in Gas Turbine Combustion

There are many aspects of combustion in stationary GTs that are challenging to the design engineer. These include, but are not limited to: fuel flexibility, combustion stability and emissions. In this chapter a review of the archival literature is presented to provide necessary background information on these issues. Some focus will be on the development and use of WSR models to study and combustion phenomena.

2.1 Emissions

Since the passage of the Clean Air Act in 1955 and its updates in 1963, 1970, 1977, and 1990, designers have been challenged to create ever cleaner combustion systems. Methods of controlling the emission of pollutant species like unburned hydrocarbons (UHC), CO, and NO_x are competitive. The conditions that lead to a reduction of UHC and CO cause the rate of NO_x production to increase and vice versa. This section will examine the processes that lead to the production of pollutant species as well as some modern methods that are used to reduce emissions of these controlled pollutants.

2.1.1 Oxides of Nitrogen

The pollutant species nitric oxide (NO) is a minor product formed primarily by the oxidation of nitrogen, present in either the oxidizer or fuel, in high temperature regions (above 1800K). It is a key component of photochemical smog and, when further oxidized to NO_2, acid rain. In the upper atmosphere NO is converted to NO_2 in reactions that consume ozone which can lead to increased ultraviolet radiation reaching Earth's surface. For these reasons, NO_x ($NO_x = NO + NO_2$) is one of the more tightly controlled pollutant species around the world [15]. In this section the three primary mechanisms for the production of NO_x in a GT engine are introduced.

The thermal, or Zeldovich, mechanism is the major source of NO in high temperature (> 1800 K) regions of the combustor. This is a mechanism for the oxidation of atmospheric N_2 in the following chain reactions [16]

$$O + N_2 \rightleftarrows NO + N \tag{2.1}$$

$$N + O_2 \rightleftarrows NO + O \tag{2.2}$$

$$N + OH \rightleftarrows NO + H \tag{2.3}$$

The mechanism is controlled by Eq. (2.1) which requires high temperatures to provide the energy necessary to split N_2. Generally the peak production of NO is found slightly fuel-lean of stoichiometric, see Section 2.2 for definitions. Under these conditions there are both an excess of oxygen and sufficiently high temperatures to drive the mechanism. Compared to fuel oxidation, NO formation is slow and generally occurs downstream of the flame [8].

Many techniques for reducing NO_x emissions, as will be discussed later, rely on keeping

temperatures low enough to reduce the effectiveness of the thermal pathway. In these situations other mechanisms become responsible of for NO production. The N_2O mechanism has been shown to be important in the production of NO, especially in fuel-lean conditions. This mechanism consists of three steps

$$O + N_2 + M \rightleftarrows N_2O + M \tag{2.4}$$

$$H + N_2O \rightleftarrows NO + NH \tag{2.5}$$

$$O + N_2O \rightleftarrows 2NO \tag{2.6}$$

The importance of this pathway increases with pressure in fuel-lean combustion and dominates in low emissions combustors [17, 18]

The third mechanism for forming NO_x acts in regions of a combustor where insufficient time has passed for the thermal pathway to have completed. NO_x generated in such regions is termed 'prompt'. In experiments, Fenimore [19] discovered that near the flame front, NO production is linked to the combustion chemistry of the hydrocarbon fuel. In these zones the hydrocarbon radicals attack the molecular nitrogen in the following series of rapid reactions

$$CH + N_2 \rightleftarrows HCN + N \tag{2.7}$$

$$CH_2 + N_2 \rightleftarrows HCN + NH \tag{2.8}$$

$$CH_2 + N_2 \rightleftarrows H_2CN + N \tag{2.9}$$

$$C + N_2 \rightleftarrows CN + N \tag{2.10}$$

From here the exact path to NO production varies depending on the fuel/air ratio [20]. Generally, the next step is the formation of amines and cyano compounds. These are then oxidized to produce NO. This process is coupled with the thermal mechanism and can become complex.

Nitric oxide emissions are closely tied to a few combustion parameters. Combustion temperature is considered to be the most important of these [21, 22, 23]. Temperatures most obvious impact is on production via the thermal pathway which, as discussed above, becomes important only at sufficiently high temperatures. A second parameter of some importance is residence time in the hot zone. The thermal mechanism is slow relative to other reactions. Thus, sufficient residence time at high temperatures are required for significant production. There is also a slight negative dependence on pressure [17, 22]. These factors primarily influence the production of NO_x through the thermal pathway. Most of the control strategies discussed in Section 2.1.3 are designed to avoid this pathway.

2.1.2 CO and UHC

The production of CO is closely related to the reactant mix as well as the temperature of the primary zone. A fuel-rich, see Section 2.2 for definition, primary zone will have CO as a major product species due to a lack of O_2 to complete the oxidation to CO_2. If the primary zones is designed to operate at stoichiometric or slightly fuel-lean, then the presence of CO in the product gases is due to dissociation of CO_2 at high temperature. Accordingly, the gradual addition of cooling air should, in principle, reduce CO emissions.

In contrast to predictions made with equilibrium theory, CO production is highest when combustion temperatures are low (< 1100K). This has three likely causes [8]:

- Residence time or fuel-to-air ratios too small to produce adequate burning rates.
- Poor mixing of fuel and air leading to locally rich zones as well as zones too fuel-lean to support combustion.
- Reaction quenching along cool liner walls.

Oxidation of CO is often the determining factor in the design of practical combustors with respect to average temperature and residence time [8]. Dry oxidation of the CO present after the primary zone is difficult to sustain due to the high activation energy of the reaction between CO and O_2. In practical systems where a certain amount of water from the combustion of a hydrocarbon fuel is present, oxidation takes place in one of two wet reactions dependent on temperature. At high temperatures the equilibrium reaction

$$CO + OH \rightleftarrows CO_2 + H \tag{2.11}$$

is the primary means of reducing CO. At lower temperatures the water-gas shift reaction

$$CO + H_2O \rightleftarrows CO_2 + H_2 \tag{2.12}$$

becomes the important reaction [24].

Unburned hydrocarbons, like CO, are the result of rich combustion and low temperatures. The majority of UHC emitted are the products of incomplete combustion and may take different forms. They may take the form of the fuel species or, if the fuel was a blend or consisted of higher hydrocarbons, they can be smaller hydrocarbon species that result from the break down of the original fuel. Liquid fuel droplets may also pass through the combustor when inadequately atomized [8]. In fuel-lean mixtures, UHC often occurs due to poor flame

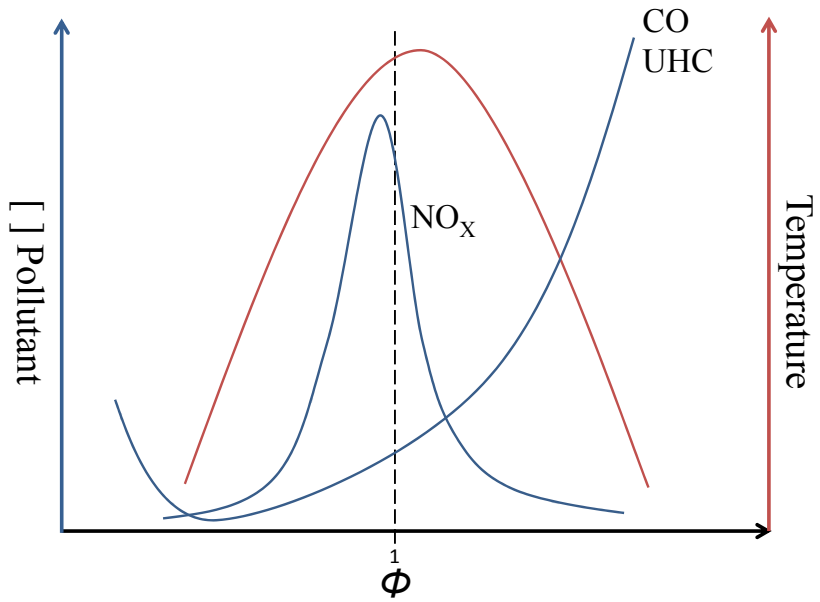

Figure 2.1: Sketch of the relation between fuel-air mixture, temperature (red line), and emissions of various pollutant species (blue lines).

propagation through the mixture [24].

2.1.3 Methods of Emissions Control

There is a narrow range of temperatures where UHC, CO, and NO_x can be reduced simultaneously, see Figure 2.1. Older combustion systems, sometimes called 'traditional', employed diffusion flames. In these combustors fuel and air are introduced into the primary zone where both reactant mixing and combustion take place. Thus, the combustion is diffusion controlled and tends to take place at near stoichiometric conditions ($\phi = 1$ in Figure 2.1) leading combustion temperatures that fall outside the ideal zone for pollutant emission reduction [25]. A number of methods have been developed over the last 40 years to either promote combustion in the ideal temperature range for pollutant emissions reduction or abate emissions from more traditional designs. Much of this effort has been focused on

limiting NO_x emissions. The reduction of CO and UHC is sometimes compromised by this technological focus [26].

The primary goal of combustor design strategies to reduce NO_x emissions to limit the rate of production from the thermal mechanism [8]. This is accomplished mainly by reducing maximum combustor temperatures. Reduction of average maximum temperature is not sufficient to meet NO_x emissions goals. As such, effective mixing is also required to attempt to eliminate local hot spots. Mixing in the flame front has been shown to increase NO_x emissions, so mixing must take place before combustion to create a homogeneous incoming charge [18]. Finally, residence time in the primary zone is minimized to further reduce the production of NO_x [17]. Several methods have been developed to accomplish these tasks with varying degrees of popularity.

2.1.3.1 Diluent Injection

Early methods of reducing NO_x production in the combustor included the injection of various diluents. The additional mass acts to reduce the combustion temperature, thereby avoiding the thermal mechanism, and increase power output at the same turbine inlet temperature by increasing mass flow through the turbine [27]. Using diluents also allows the combustor to operate near stoichiometric conditions for added stability.

One of the first diluents tested was H_2O. Liquid H_2O injection reduces combustor temperatures by using combustion energy for vaporization. If available, steam may also be injected to act as a thermal sink. Several methods of water/steam injection have been used [25, 27, 28]. Special nozzles that inject the fuel and either water or steam co-locally are commonly used. Liquid water may also be injected upstream of the combustor and allowed to vaporize in the air stream before fuel mixing. In terms of NO_x emissions reduction, liquid

water is more effective than steam [29, 30]. If either liquid water or steam are to be injected into the combustor, they must be of high purity to avoid fouling or damage to downstream components. Damage to these systems may lead to increased CO and UHC emissions.

Recirculating gas from the exhaust stream back into the combustor (EGR) as a diluent is another way reducing primary zone temperatures [31]. The exhaust gas has two effects. First, it reduces the concentration of O_2 in the reactants which slows the kinetics and reduces maximum flame temperatures. Second, the presence of CO_2 and water vapor in the exhaust increases the heat capacity of the reactants [24, 25]. The implementation of EGR may require the use of an intercooler to reduce the temperature of the exhaust before injection into the combustor [8, 32]. OxyFuel combustion, fuel and oxygen rather than air, combined with EGR also has potential as a CO_2 capture technique [32].

Diluent injection alone may not always be sufficient to achieve the levels of NO_x required by current and future standards [23]. This has led to the development of methods requiring more complex changes to combustor geometry or operation in different combustion regimes. These techniques have the advantage of not requiring additional plumbing to facilitate the injection of species other than fuel and oxidizer into the GT.

2.1.3.2 Catalytic Combustion

Enhancing combustion reactions using catalysts is another method of reducing NO_x. In systems employing catalytic combustion, fuel and air are premixed, below flammability limits, prior to entering the combustor. Within the combustor is a catalyst matrix carried by a support structure to initiate the combustion reaction. The limited energy content of the mixture prevents combustion temperatures from approaching those required for activation of the thermal NO_x pathway. Ideally, because the mixture is below the flammability limit,

flashback is not a possibility. However, autoignition in the mixing apparatus is possible near the fuel injectors where locally flammable mixtures may be present [26]. It is vitally important that the fuel and air be well mixed before reaching the catalyst as the efficiency of the reactions is dependent on stoichiometry. The reactions are also temperature dependent and, at part load, may require a pre-burner to reach the required temperature range. Temperatures that are too high lead to scintering of the catalyst and its support structure and vaporization of the catalyst. In large industrial GTs increasing combustor exit temperatures for greater thermal efficiency has led to the development of staged catalytic combustion. To avoid overheating the catalyst and its support structure, only a portion of the fuel is reacted. The rest is added downstream in a secondary burner which is stabilized by the hot gas from the catalytically supported section of the combustor [33, 34, 35].

2.1.3.3 Fuel-Air Mixture Adjustment

Adjusting the combustion mixture to be fuel-rich is another method of reducing combustion temperatures. Systems of this type also premix the fuel and air to ensure that the combustion takes place at the desired ratio. Unlike catalytic combustors, the fuel-rich primary zone is capable of maintaining a stable flame. The excess of fuel and dearth of O_2 in the primary zone reduces combustion temperatures but leads to excessive quantities of CO and UHC. Careful addition of air in the intermediate zone and dilution zone may be used to complete the combustion process [8]. Another technique to burn out the CO and UHC is the rich-quench-lean (RQL) combustor. Through the addition of air and the geometry of the liner, the reactions of the rich primary zone are quickly quenched to pass through the stoichiometric point as rapidly as possible. The now fuel-lean mixture maintains sufficient temperature to complete the burnout of CO and UHC in a second combustion zone [36, 37, 38]. RQL com-

bustors have been shown to be promising in instances where fuel bound N_2 is a concern [38]. Rich-catalytic-lean (RCL) combustors use a catalyst rather than just liner geometry flame stabilization in the fuel-lean zone. Using a fuel rich mixture allows a wider range of catalysts to be employed and helps catalyst life [39].

Fuel-lean premixed (LP) combustion follows an approach that is a middle ground between the catalytic and rich primary zone methods. Fuel is premixed with an excess of air, but the mixture is maintained above the lower flammability limit. The excess air acts as a diluent and reduces the combustion temperature to mitigate NO_x production from the thermal pathway. LP combustion is a popular method of reducing NO_x emissions in ground based GT engines [26]. The ideal scenario is to maintain combustion near the fuel-lean flammability limit throughout its range of operation. Practically, this is not possible without some form of fuel or air staging. Fuel staging is the easiest to implement. As load demand changes some of the fuel nozzles are alternately fed or cut-off from the fuel supply to maintain the desired combustor temperature and fuel-air mix. Staging is generally either radial or axial. In either method a pilot flame using a locally richer mixture may be used to stabilize the combustion [25]. Air staging is mechanically more complex as it requires the diversion of the high-temperature compressor discharge. When combined with fuel staging, air staging is preferable because it increases the operating range [40, 41]. Due to its popularity, Section 2.2 is dedicated to this fundamentals of this technique.

2.1.3.4 Post Combustion Treatment

Post combustion treatment options generally involve reduction of NO_x to N_2 and H_2O using injected chemicals and catalysts. In selective non-catalytic reduction (SNCR) nitrogen containing compounds (e.g., ammonia, urea, and cyanuric acid) are injected into the exhaust

stream. In a narrow temperature range (1200 - 1370 K) these chemicals reduce NO_x. Addition of these chemicals outside of this temperature range leads to either little or no decrease in NO_x (low temperatures) or increased levels of NO_x (high temperature) [42, 43]. The addition of catalysts to the process, now called selective catalytic reduction (SCR), allows for the reactions to take place at lower temperatures. The catalysts are commonly base metal oxides, precious metals in a ceramic matrix or zeolites. The reduction agent is injected into the effluent stream before the mixture passes across the catalytic bed. Catalysts reduce the necessary reaction temperatures to 400 - 700 K [43, 44]. In both SNCR and SCR the reductant must be added in the proper proportion and be well mixed in the flue gas to prevent ammonia, a controlled pollutant as well, from passing through the system [45]. A reduction of NO_x content of up to 95% is possible with these techniques. The added complexity of SCR and SNCR systems limits their practicality in some applications [46].

Other methods of NO_x abatement include: non-thermal plasma, absorption, electron beam flue gas treatment, and bioprocesses (e.g., using nitrogen fixing bacteria in compost or soil). These techniques are either still in the development phase or in limited implementation [44]. It is apparent that if a post combustion solution is to be implemented, additional capital equipment in the form of storage tanks, reductant injectors and control systems, and catalytic or growth beds are required.

2.1.3.5 CO and UHC

The rates of UHC and CO emissions are decreased by similar methods. The most effective solutions involve higher combustion temperatures and longer residence times at elevated temperature. This is contradictory to most methods used to reduce NO_x which rely on lowering combustion temperatures. Better mixing of reactants, also useful for reducing

NO_x, helps to avoid pockets with a local excess of fuel, in systems designed to operate with excess air, where UHC and CO can be produced. Fuel or air staging like that used in LP combustion can also be used to increase combustion efficiency and thereby reduce emissions of UHC and CO over an engines operating range. Finally, careful addition of cooling air avoids reaction quenching near the walls of the combustor [8, 24].

2.2 Lean Premixed Combustion

The increased interest in fuel-lean combustion systems in the stationary GT market has been driven by need for more fuel efficient, cleaner power generation. Volatility in the fuel market, both currently and projected in the future, is pushing consumers to demand increased fuel efficiency. Meanwhile, regulatory pressure to decrease emissions of pollutant species requires original equipment manufacturers to design cleaner systems. Some clean-up is possible with post combustion treatment systems (e.g., SCR as discussed earlier), but decreasing pollutant production is preferable based on capital and operational considerations [47]. Lean combustion is beneficial in that it produces lower combustion temperatures, reduced NO_x production, and fuel consumption rates. LP combustion has become one of the most popular methods of balancing pollutant emissions with efficiency.

Combustion can be categorized by its global chemistry as fuel-lean, stoichiometric or fuel-rich. The boundaries between zones are defined using the equivalency ratio, ϕ, which can be defined as

$$\phi = \frac{F/A}{(F/A)_s} \tag{2.13}$$

where F/A is the molar fuel to air ratio and the subscript s indicates stoichiometric conditions (i.e., only CO_2, H_2O, N_2 in the products). When ϕ is unity, the combustion is

stoichiometric. Fuel-lean combustion takes place at $\phi < 1$ and fuel-rich when $\phi > 1$. The excess of oxidizer or fuel in off-stoichiometric combustion cools the reaction and introduces additional major species into the product mix.

In general, fuel-lean combustion has multiple benefits. The lower combustion temperatures of fuel-lean mixtures inhibits the thermal NO_x pathway decreasing the emission of the controlled species. Decreased fuel consumption has obvious economic advantages. Lower carbon levels in the reactants means that possible emissions of CO_2 and CO are reduced. Lastly, the thermodynamic properties of the reactants in a fuel-lean system lead to increased thermal efficiency [48]. Lean combustion systems are more complex than traditional combustors, and their implementation introduces an interesting set of engineering challenges.

Inside a GT combustor, fuel-lean combustion refers specifically to a fuel-lean primary-zone. This often requires special geometry to ensure combustion occurs under the desired conditions. For cooling purposes, regardless of the primary-zone ϕ, the overall fuel-to-air ratio is always fuel-lean in a GT combustor. A larger percentage of the total air is required to flow through the primary zone in LP systems than in diffusion controlled combustors. This limits the available air for liner cooling and dilution which affect liner life and the temperature profile entering the turbine, respectively [47].

Combustion in the fuel-lean regime can be accomplished only through premixing of the fuel and oxidizer. If not premixed, the fuel and oxidizer will tend to combust under stoichiometric or near-stoichiometric conditions after diffusion mixing in the combustor. The degree of premixing is important to emissions. Incomplete mixing will lead to pockets of relatively rich mixtures. These pockets will yield hot spots which can increase NO_x emissions [49]. Conversely, relatively fuel-lean pockets can increase UHC emissions due to incomplete combustion.

In practice the mixing section of a LP combustor uses geometry to enhance mixing without greatly increasing residence time in the mixer. The addition of swirl inducing vanes and step geometry changes are common methods for increasing mixing rates. Rapid mixing ensures that ignition takes place in sections designed for high-temperatures and at the intended ϕ.

Of major importance to the design of the premixing section of LP systems is the autoignition process. In premixed systems the rate at which the combustion reactions take place is exponentially dependent on temperature. For autoignition this is captured in ignition delay time, τ_{ig}, which is a measure of the time required for combustion reactions to accelerate. When combined with the bulk through flow velocity, τ_{ig} can be used to size the premixer. Ignition delay may be calculated from a correlation taking the form [50]

$$\tau_{\mathrm{ig}} = A \exp\left(\frac{E}{R_{\mathrm{u}} T}\right) [\mathrm{O_2}]^a [f]^b \tag{2.14}$$

where A, a, and b are constants, E is the activation energy of the global reaction, R_{u} is the universal gas constant and $[\mathrm{O_2}]$ and $[f]$ are the molar concentrations of oxygen and fuel in the reactant mix, respectively. The constants of Eq. (2.14) are determined experimentally using a variety of methods, see [50].

Once lit, a combustor's continuously stable operation is critical to the function of a GT. Determining the static instability limit of a specific combustor or range of similar combustors is often the result of extensive testing [51]. In traditional combustors, blowout determined the turndown for the system. The limits are even more critical for the various dry low-$\mathrm{NO_x}$ approaches. To effectively reduce temperatures, LP combustors need operate near the fuel-lean extinction limit. The importance of stability issues in LP combustors combined with

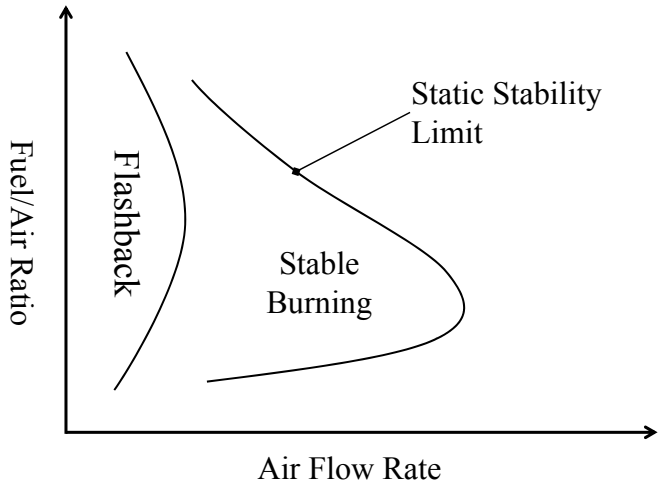

Figure 2.2: A general combustion stability loop, adapted from [1].

their popularity has led to an intense research focus

2.3 Stability

Under ideal circumstances the combustor would operate at a ϕ that generates the minimum combination of UHC, CO and NO_x. However, practical considerations may force ϕ to be richer or leaner than this ideal case. In either direction there are static stability limits. Even when operating between these limits there may be combinations of ϕ and air flow-rate where the acoustic and heat release characteristics of the combustor couple causing dynamic instabilities. Either avoidance or control of these instabilities is of great importance to the reliable operation of LP combustors.

The stability of a GT combustor depends on its operating condition as characterized by ϕ, $\dot{m}$ and fuel constituency. Within the primary-zone the flame anchors in areas where the local flame speed and matches the gas speed [52]. The effects of changing ϕ (flame speed) and air flow rate (gas speed) on the stability of a combustor are plotted against each other

in a stability loop. A general stability loop for a GT combustor, fuel type, and operating pressure, adapted from [1], is shown in Figure 2.2. The static stability limit, extinction or blowout, is divided into two parts about the maximum air flow rate which occurs at $\phi \approx 1$. Above this point the combustion is extinguished by an excess of fuel, rich-extinction, and below it by an excess of air, lean-extinction. At low air flow rates there is a risk of the flame propagating upstream (i.e., flame speed is greater than bulk flow speed) out of sections of the combustion system designed to withstand high temperatures, a condition known as flashback. Stable burning within the combustion chamber occurs when the conditions lie within the space bounded by the stability loop and the flashback limit.

The major drawback to LP combustion is its susceptibility to a variety of instabilities. Depending on the proximity of the fuel-lean extinction limit to the operating point of the combustor, slight variations in the fuel or air flow rates can lead to the flame being blown out of the combustor. Flashback may occur due to changes in fuel content that increase the flame speed. Temperatures in the mixing section must be carefully controlled to avoid autoignition in components not designed to survive combustion temperatures. Variations in fuel composition or air flow rate may cause the combustor to enter a dynamically unstable operation point. Due to the benefits of LP combustors, control and identification of phenomena that affect their stability has been an area of intense research.

2.3.1 Static Instability

Static instabilities are important to all GT combustion systems. They represent the hard operating bounds of the combustor. In traditional diffusion based systems, these bounds limited turndown which is of prime importance to both aircraft and ground application [8]. Static limits have an increased level of importance in LP combustors relative to traditional

systems. The weak extinction limit not only affects turndown but also limits the lowest possible NO_x emissions. Identifying and, if possible, extending the stability limits is an important part of the development of a combustor design.

Stability limits are governed by combustor geometry as well as combustion parameters. For a combustor under development, the static stability limits are identified experimentally. Stable combustion is established and fuel flow is decreased until the flame is blown-out of the combustor. This establishes the value of ϕ at fuel-lean extinction. Increasing fuel flow until blow out identifies ϕ at rich-extinction. The procedure is repeated for several air flow-rates. When plotted they establish the stability loop for the combustor. In aircraft applications stability loops are determined for a variety of pressures (real or simulated by water injection or nitrogen dilution [10]) to simulate altitude [8].

2.3.2 Dynamic Instability

When operating near the stability limits the combustor may exhibit dynamic instabilities which are a coupling of the acoustics of the combustor and variations in heat release from the combustion process [53]. Depending on their strength, dynamic instabilities may cause excess noise, prematurely extinguish combustion, or mechanical failure of the combustor. While static instabilities have been a concern since the advent of the GT [8], the issue of dynamic instabilities has become more prevalent as GT combustors have pushed LP technology.

The onset of such dynamic instabilities is governed by the modified Rayleigh criterion [54]

$$\int_V \int_0^{\mathsf{T}} P'(\mathbf{x},t)\, Q'(\mathbf{x},t)\, \mathrm{d}t\mathrm{d}V \geq \int_V \int_0^{\mathsf{T}} \sum L_i(\mathbf{x},t)\, \mathrm{d}t\mathrm{d}V \tag{2.15}$$

where P' is the combustor pressure oscillation, Q' is the oscillation in heat release, $\sum L_i$

represents the net acoustic losses in the combustor, $\mathbf{x}$ is the position vector within the combustor, t is time, and T is the period of oscillation. The left-hand-side of Eq. (2.15) represents the addition of acoustic energy to the system. The right-hand-side represents the removal of acoustic energy. When the combustor is unstable, the energy production outweighs the removal of energy.

Forcing a combustor into unstable operation may be accomplished by increasing the magnitude Q', decreasing the phase difference between P' and Q', or a combination of the two. Much of the instability is controlled by the geometry of the combustor, fuel and air injection strategies, and flame patterns [55]. Models have been developed to predict the conditions for a given combustor and fuel will lead to dynamic instabilities [53, 56, 57]. Dynamic instabilities are beyond the scope of this work and the interested reader is directed to Lieuwen's book on combustion instabilities [58].

When an LP combustor is exposed to a fuel supply whose content varies, its regions of stable operation shift with the changing fuel. The effect of various minor hydrocarbon species as well as diluents can be counterintuitive. In natural gas, changes in the C_2H_6 and C_3H_8 content affects the flamespeed and thereby the risk of flashback. In biogas CO_2 does not behave as an inert diluent and fluctuations in its mole fraction lead to a variety of stability issues. The desire for future GT systems to be as fuel-flexible as possible has led to interest in methods to expand the stability envelopes of LP combustors.

2.4 Fuel Flexibility & Alternative Fuels

Since the fuel crises of the latter part of the 1970's and early 1980's, it has been recognized that fuel sources of non-fossil origin would eventually be necessary to meet the world's energy

needs. Early work on the effect of alternative fuels and the merits of the fuel flexibility of GTs with traditional combustors took place at this time [59]. It was also in this time frame that the demand for tighter emissions controls led to the development of LP combustion systems. Subsequent drops in fossil fuel prices relative to income in the US limited alternative fuels to a niche market through the end of the century. Fluctuation in fossil fuel costs, geo-political instability in resource-rich regions, the desire to develop technology able to use otherwise flared gas and public concern over the climatological effects of greenhouse gas emissions during the first decade of the 21^{st} century have greatly increased interest in alternatives to traditional fuels.

Generally, individual LP combustors are designed to operate on a limited variety of fuels for stability and plumbing reasons. Beyond the intended range, changes must be made to the fuel handling and control systems and, possibly, to the combustor itself. This is a trade-off between fuel flexibility and emissions. In aviation, the quality standards of the various fuel types are tightly controlled for obvious safety reasons. However, the stationary GTs used to generate electrical power are forced to operate on fuels whose content is not as strictly controlled. Natural gas, a primary fuel source for many stationary GTs, is generally controlled to energy content, but it's constituents can vary widely depending on source [60]. Alternative fuels such as biogas and syngas have contents that vary based on the feedstock to their respective production processes [61, 62, 63, 64, 65]. Thus, there has been a focus on the effects of fuel variation on the operation of GT engines using LP combustion in power generation applications [26].

2.4.1 Fuel Conditioning

Due to corrosion and fouling issues that may arise, manufacturers often require that some minor species be removed before any gaseous fuel is used in their prime movers. Included in this group of species are those that form controlled pollutants when oxidized, those that can clog passages and species that may condense in the fuel system. This process is known as fuel conditioning. These fuel cleaning steps are required regardless of fuel source in order to meet emissions and operability constraints.

Oxidized sulfur compounds, SO_2 and SO_3 collectively known as SO_x, are controlled pollutants. In addition to being toxic, SO_3 reacts with H_2O to form H_2SO_4. If this occurs in the hot section of the GT, especially in the presence of alkali metals, corrosion becomes a serious issue [66]. Virtually all sulfur in the fuel is converted into SO_x in the combustion chamber; thus, the only available method of reducing SO_x production is to eliminate sulfur compounds in the fuel [8, 24].

If sufficiently high combustion temperatures are reached, siloxanes present in the fuel oxidize into SiO_2. In downstream components the SiO_2 collects as a powder on turbine blades and can fill the narrow passages in heat-exchangers and catalytic reducers [67]. Like H_2S and SO_x, the only method of reducing these effects is the removal of siloxanes from the fuel stream.

Liquids and gases that are near their dew point present a number of challenges. Fuel is typically passed through a liquid knock-out step to remove volatile organics and/or water. Aromatics and other higher hydrocarbons are precursors to soot and slow to react [68]. these volatile organics, if they pass through or are formed in the combustor, contribute to UHC emissions and are also found in photochemical smog [24]. They are removed to avoid this as

well as their condensation in the fuel handling system.

2.4.2 Fuel Characterization

As a first step to ensure that a change in fuel does not greatly alter the effectiveness of the combustion system, it must be able to deliver sufficient energy content to the system. To identify fuels which can deliver similar total heat release using fixed fuel system geometry and combustor pressure drop the Wobbe Index is often used

$$\mathrm{WI} = \frac{LHV}{(S.G.)^{0.5}} \tag{2.16}$$

where LHV is the fuel's lower heating value and $S.G.$ is the fuel's specific gravity relative to air at a standard condition (293K, 101.32kPa). Fuels with identical WI can be expected to generate the same heat output in a combustor using the same pressure drop and fuel control valve settings. Typically, a window of $\pm 5\%$ WI from design point is allowed in a GT without modification to the control system or combustor [59]. Outside this range control valves, fuel compressors, fuel nozzle pressure drops, and combustor liner modifications are necessary to meet the various performance and environmental restrictions placed on a unit [47]. A modified Wobbe index is also used

$$WI_T = \frac{LHV}{(S.G.)^{0.5}} \left(\frac{T_{\mathrm{std}}}{T} \right)^{0.5} \tag{2.17}$$

where T_{std} is a standard temperature (293K) and T is the fuel temperature in K, is often used to correct for the effect of variation in fuel temperature due to the fuel preparation or production processes.

Other methods of characterizing CH_4 based fuels exist. To characterize the knock resistance of fuels for use in piston engines, the motor octane number (MON) is often used

$$\text{MON} = -406.14 + 508.04\left(\frac{H}{C}\right) - 173.55\left(\frac{H}{C}\right)^2 + 20.17\left(\frac{H}{C}\right)^3 \tag{2.18}$$

where $\frac{\text{H}}{\text{C}}$ is the hydrogen to carbon ratio for the fuel, excluding the carbon in the diluents. An empirical relation has been developed to relate the MON of a gaseous fuel to that of CH_4. The so-called 'methane number' (MN) [69]

$$\text{MN} = 1.624\text{MON} - 119.1 \tag{2.19}$$

is an index that characterizes the effect of various minor hydrocarbon species found in natural gas on combustion phenomena related to knock (i.e., autoignition). This correlation is limited to fuels with $\text{H/C} \geq 2.5$ and diluent mole fractions less than 5%. Experiments using a commercial micro-GT and natural gas fuel with various diluents, both higher hydrocarbons and inerts, have shown relatively poor correlation between both the WI and MN and emissions when inert diluents are added [70].

As discussed in Section 2.3, LP combustion is susceptible to a variety of instabilities many of which are directly affected by fuel type. While useful, the WI and MN are not fully capable of characterizing the effect of fuel content change on the operation of a GT combustor. Fuels may have similar WI and yet have differing flame speeds, combustion chemistry, and flame temperatures. These properties directly affect the static and dynamic stability of the combustor as well as the emission of controlled pollutants [1, 60, 70].

2.4.3 Biogas

Using waste derived fuels to offset energy costs is not a new concept. Treatment plants for human sewage used CH_4 produced by anaerobic digestion to generate electrical and mechanical power for the plant in the middle part of the 20^{th} century [71]. This fell out of favor as electrical power from centralized generating stations became more affordable. In the late 1970's the concept of offsetting fossil fuel use through the production of fuels from solid wastes was once again considered. Much of this work focused on the direct combustion of municipal wastes in steam boilers, but it was recognized that the quantity of potential fuel available from human/animal sewage and sanitary land fills was promising [72].

2.4.3.1 Biogas Production

Biogas, depending on source, may have a range of constituents and is generally characterized as a low to medium-energy content fuel [59]. The feedstock is waste organic material from a number of sources. Biogas for industrial usage is collected from two general sources: sanitary landfills and animal/human sewage. In both cases, microbes break down the organic material in a chemically complex process to generate a combination of CH_4, CO_2, H_2, N_2, and H_2S. The anaerobic digestion process which results in biogas stores more of the chemical energy present in the organic waste in a useful form, CH_4, than aerobic processes which convert much of the energy to sludge [71]. The content of the product gas is tied to the organic feedstock and other process variables. The trace species in both digester and landfill gas vary but can include volatile organics, H_2S, siloxanes, and aromatics [61].

Digestion takes place in two steps. First, the large organic molecules are broken down by enzymes, the exact process is dependent on the organic molecule, producing smaller molecules that are useful for microorganisms. Anaerobic bacteria metabolize the smaller

molecules to low molecular weight acids. In the second step methanogenic bacteria degrade the acids into CH_4, CO_2, and H_2. Digestion can take place over a range of temperatures ($4 - 60°C$) if the temperature is held constant. Variations in temperature, however, can upset the process causing the content and quantity of gas to change or shutdown the process entirely. Other factors that influence gas production are pH and moisture content [71].

Landfill biogas contains CH_4, CO_2, N_2, and O_2 in varying amounts depending on garbage content and environment. The ratio of CH_4 to CO_2 typically ranges from 60%/35% to 35%/55% [73]. Because the gas is drawn from the landfill using a vacuum system and the landfill is not a fully sealed enclosure, atmospheric air may be drawn in to the landfill as the fuel demand changes. This has two effects. First, O_2 is introduced into the fuel stream. In most cases O_2 only appears in trace amounts and has little influence on combustion. The second effect is to change the chemistry of the digestion process by adding oxygen and promoting aerobic digestion which leads to higher CO_2 content gas [61]. Rain, or lack thereof, also affects the output of the landfill. Higher moisture contents promote gas production and increase the ratio of CH_4 to CO_2 [74].

Biogas from anaerobic digestion systems using either human or animal waste tends to be more consistent in content than gas from landfills. This is due to the more controlled nature of their operation relative to landfills [61]. Waste is collected by a sewage system and processed in specially constructed in digesters. Control systems are used to maintain digester temperature (typically $30 - 40°C$ known as the mesophilic range), moisture content, feed rate, and pH [71]. Like landfills, digesters are subject to process upset when the narrow range of conditions in which the bacteria thrive is violated. The ratio of CH_4 to CO_2 ranges from 75%/25% to 55%/45% [62, 73, 75].

2.4.3.2 Biogas Combustion

The diluents remaining in biogas after fuel conditioning, primarily CO_2, H_2O, and N_2, affect the combustion in a variety of ways. Fuel N_2 affects the adiabatic flame temperature and specific heat of the reactant mixture much as it does as a component of air [1, 76]. Though typically assumed to be chemically inert at the conditions in an LP combustion system, CO_2 and H_2O do affect other aspects of the combustion [77]. Both affect the specific heat and flame temperature in much the same way as N_2, but the effect is more pronounced. As discussed in Section 2.1.3, this is the reason EGR and water/steam injection are used to reduce NO_x. However, the presence of CO_2 and H_2O vapor in both the products and reactants also increases the radiative heat transfer and thereby the preheating the fuel. Preheating increases flame speed, the extent of the flammability limits, and the risk of flashback especially in fuel-lean mixtures [78]. Computational studies in a variety of systems have shown that, when radiation is ignored, dilution with CO_2 rather than N_2 slows flame speeds by retarding the kinetics [79].

A number of studies in laboratory combustors have been undertaken to explore the effect of dilution on flame stability. Experiments in a representative swirl-stabilized combustor demonstrated that flow effects (i.e., centrifugal stratification) may limit the effect of CO_2 dilution on blowout [76]. Experimental and numerical studies in a simplified LP combustor show that the effect of CO_2 dilution on flame stability and anchoring location is pronounced. For similar equivalency ratios, biogas (61% CH_4, 34% CO_2, 5% N_2) and methane flames have different anchoring patterns. Anchoring patterns, viewed via chemillumensence of CH, that were associated with instability, as measured by a dynamic pressure transducer, in pure methane flames were stable when the fuel was biogas [80].

Studies of emissions and static instabilities in biogas combustion have primarily been limited to application-specific experiments or simplified aerodynamic systems. Multiple workers have reported on the effect of running various sizes GT generator systems on a biogas from different sources on emissions and power output (e.g., [81, 82, 83, 84, 85]). Lafay et al. used a simplified GT configuration to investigate the stability of biogas flames and found that laminar flame speed best correlated with flame structure [80]. In a further simplification of the flow system, Qin et al. studied simulated landfill gas under fuel-lean conditions in a stagnation flow geometry both experimentally and numerically. They found that the presence of CO_2 in the fuel mixture effected the kinetics of the reaction through radiation and CH_2 reactions, that increased fuel CO_2 increases NO_x emissions by increasing fuel demand and prompt NO_x, and reduces the laminar flame speed [86]. Jahangirian et al. determined using counterflow diffusion flame experiments with simulated, diluted biogas that fuel CO_2 reduces the presence of soot precursors, NO_x, and greenhouse gases even when temperatures are similar to those of a pure CH_4 flame. Fackler et al. studied LP combustion of CH_4 flames diluted with CO_2 and N_2, to simulate landfill gas, in a jet-stirred reactor to determine the effect of diluents on NO_x production. They found that dilution with N_2 increases NO_x emissions compared to CO_2 dilution at similar temperatures and that NO_x emissions increase with dilution [87].

The effect of dilution of CH_4-air flames with CO_2, N_2, and H_2O has also studied in machines using EGR. Cold EGR in a perfectly premixed system is similar to raw biogas combustion. A concern in combustors with cold EGR is a reduction in the extent of the stability limits [88]. A limiting factor for combustor stability is considered to be an O_2 percentage of 16-18% in the reactant mix [89]. Røkke and Hustad tested the addition CO_2, N_2 and O_2, individually, to either the fuel or air inlet of a research combustor capable

of operating in premixed and diffusion modes. They determined that diluents, including O_2, increase the fuel-lean extinction limit in both premixed and diffusion flames [90]. This was confirmed by ElKady et al. in their study of EGR in a research combustor using a commercial GT fuel nozzle. They found that stability limits could be extended through the use of a diffusion pilot flame. With pilot flames the limit of EGR was identified as CO emissions levels [91]. Stability limits may also be extended through the addition of H_2 [92]. In their studies of methane-oxycombustion, a condition where the N_2 has been removed from the air and replaced by exhaust gas, Amato et al. showed that in CO_2 diluted CH_4/O_2 flames the extent of the extinction limits are contracted by the kinetic effect of CO_2. The effect may be predicted qualitatively by chemical time scaling near stoichiometric operation [77].

2.5 The Well-Stirred Reactor

It has long been recognized that laboratory models that simulate GT combustion processes are a preferred method for evaluating the effect of changes in fuel types [9]. Several different experimental apparati have been designed to approach WSR operation with varying degrees of success. Their results have proven useful in the development of modern computational codes and kinetics models [93]. This section introduces the governing theory behind WSR operation, the design of laboratory devices, and the use of WSR theory in numerical simulations of GT combustors.

2.5.1 WSR Theory

The theory governing the operation of the WSR is a combination of fluid mechanics, thermodynamics, heat transfer and chemical kinetics. Briefly, the WSR is a fixed volume with a

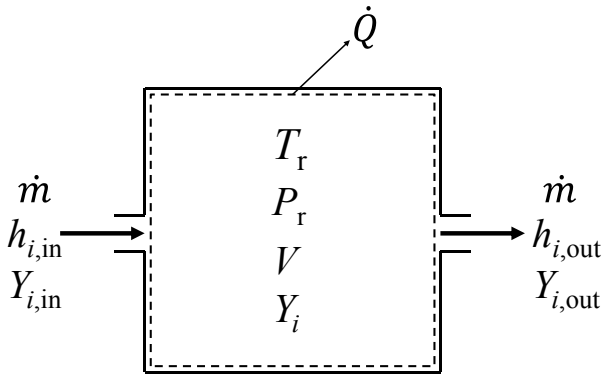

Figure 2.3: General WSR schematic with control volume.

constant influx of fuel and air at a constant temperature, see Figure 2.3. Near instantaneous mixing of the reactants and products is achieved through the careful design of the reactor. Inside the volume the mixture of gases is at a steady temperature and pressure. Due to the intense mixing, the gas mixture exiting is identical in composition to that within the volume. Finally, the reactor is essentially adiabatic.

A more detailed analysis begins with the conservation of species i for the control volume shown in Figure 2.3

$$\frac{\mathrm{d}m_{i,\mathrm{cv}}}{\mathrm{d}t} = \dot{m}_i''' V + \dot{m}_{i,\mathrm{in}} - \dot{m}_{i,\mathrm{out}} \tag{2.20}$$

where the left-hand-side represents the rate at which i accumulates within the control volume and the terms on the right-hand-side represent the rate-of-production within the volume, influx and out-flux of i, respectively. The production term is a consequence of the chemical reactions taking place within the WSR. It acts as a sink for reactant species and a source for product species.

From chemical kinetics the production of species i can be described in terms of reaction

rates. A chemical reaction involving N species can be written as

$$\sum_{i=1}^{N} \nu_i' X_i \leftrightarrows \sum \nu_i'' X_i \tag{2.21}$$

where ν_i is the stoichiometric coefficient of species X_i and the single and double primes indicate reactant and product side, respectively, for the forward reaction. Reactions rarely consist of a single-step, often referred to as 'global', rather several intermediate reactions occur involving multiple additional species. These multi-step reactions are called mechanisms. According to the law of mass action, the rate of change in concentration, ω, of species i in reaction j is proportional to the product of the concentrations of the reacting species, $[X_i]$ which has dimensions of moles per unit volume, raised to ν_i' [68]

$$\omega_j = \left(\nu_i'' - \nu_i'\right) \left(k_{\mathrm{f}j} \prod_{i=1}^{N} [X_i]^{\nu_i'} - k_{\mathrm{r}j} \prod_{i=1}^{N} [X_i]^{\nu_i''} \right) \tag{2.22}$$

where $k_{\mathrm{f}j}$ and $k_{\mathrm{r}j}$ are the reaction specific constants of proportionality for the forward and reverse reactions, respectively. For irreversible reactions k_{bj} is zero. The concentration exponents, stoichiomehtric coefficients ν_i' or ν_i'' in EQ. (2.22), can take a variety of values and do not have to be a whole number and may not even be indicative of the number of molecules participating in the reaction [20]. This is more common in global and quasi-global mechanisms. If a reaction requires a third body, Eq. (2.22) is modified by multiplying the right-hand-side by

$$\sum_{l}^{N} \alpha_{lj} \, [X_l] \tag{2.23}$$

where α_{lj} specify the increased efficiency of species l in reaction j. If a species is ineffective as a third body, the α_{lg} takes a value of zero [94].

Arrhenius' law is generally used to determine the value and temperature dependence of k_j using

$$k_j = A_j T^{c_j} \exp\left\{\frac{-E_{\mathrm{a}j}}{R_{\mathrm{u}} T}\right\} \tag{2.24}$$

where A_j is the Arrhenius factor which takes into account molecular collisions, T^{β_j} is a temperature correction and $E_{\mathrm{a}j}$ is the activation energy required to start the reaction. The pressure sensitivity of the reaction may be modeled in a variety of ways. Above or below certain pressure limits the reaction approach limiting reactions which may be modeled with Eq. (2.24). Between these limits the reaction behaves like a combination of the limiting reactions and its rate description is complex [94]. Different practical methods of dealing with pressure dependent reactions are described in Section 2.5.5. The production term of Eq. (2.20) can now be written as

$$\dot{m}_i''' = \sum_{j=1}^{M} \left(\nu_{ij}'' - \nu_{ij}'\right) \omega_j M W_i \tag{2.25}$$

where and MW_i is the molecular weight of species i.

A further set of simplifications can be made to Eq. (2.20) based on the operating state of the WSR. If the WSR is operated at steady-state, the left hand side is zero. Additionally, composition is the same in the outflow as it is with in the reactor. By substituting Eq. (2.25) and ignoring any diffusional transport, Eq. (2.20) can be rewritten for an M-step reaction mechanism as

$$\sum_{j=1}^{M} \left(\nu_{ij}'' - \nu_{ij}'\right) \omega_j M W_i V + \dot{m}\left(Y_{i,\mathrm{in}} - Y_{i,\mathrm{out}}\right) = 0 \tag{2.26}$$

where Y_i is the mass fraction of species i and is related to the molar concentration by

$$Y_i = \frac{[X_i]\, MW_i}{\sum_{j=1}^{N} [X_j]\, MW_j} \tag{2.27}$$

For a system of N reacting species Eq. (2.26) yields N equations with $N+1$ unknowns.

The conservation of energy is used to close the system resulting from Eq. (2.26). In a control volume under steady-state conditions with steady inflow and outflow and negligible changes in kinetic and potential energies, the conservation of energy is

$$\dot{Q} = \dot{m}\,(h_{\text{in}} - h_{\text{out}}) \tag{2.28}$$

where h is the specific enthalpy of the mixture. If the specific heat of reaction of the reactants is q_c and the mixture can be assumed to be ideal, then Eq. (2.28) becomes

$$\dot{Q} = \dot{m}\frac{q_c}{T_{\text{f}} - T_{\text{in}}}\,(T_{\text{r}} - T_{\text{in}}) \tag{2.29}$$

where T_{f} is the adiabatic flame temperature and T_r is the reactor temperature. Now the determination of the composition of the reactor and it temperature is reduced to solving N species equations and Eq. (2.29) which can be done using a number of numerical techniques [24].

Another parameter of interest in WSR studies is the residence time, τ which characterizes the amount of time a particular fluid element remains within the reactor volume. It is calculated by

$$\tau = \frac{\rho V}{\dot{m}} \tag{2.30}$$

where ρ is the mean density within in the reactor volume, V. The mixture mean density is calculated using the ideal gas equation of state and the mixture's mean molecular weight as determined by its composition.

The well-stirred nature of a reactor is estimated by comparing the representative mixing time scale to the representative chemical time scale of the reactor. This ratio, the Damköhler number Da, is useful in separating different reaction regimes. In the case of the WSR

$$Da = \frac{L/u'}{\delta/S} \tag{2.31}$$

where L is a characteristic turbulent length scale, u' is RMS velocity fluctuation which can be estimated from turbulence theory by assuming that the kinetic energy of the fluid entering the reactor is dissipated during its residence time, and $\delta/\mathrm{S_L}$ is the laminar flame thickness divided by the laminar flame speed of the mixture. For $Da \leq 0.1$ the system may be considered to operate in the distributed reaction regime and, therefore, be well-stirred [24, 95].

2.5.2 WSR Stability Theory

Static instabilities in WSR models have been related to a grouping of reactor operating conditions called a loading parameter. In their investigation of high temperature reaction rates using a WSR Longwell and Weiss related extinction to [2]

$$\frac{\dot{m}}{VP_{\mathrm{r}}^{n}} = f(\phi, T) \tag{2.32}$$

where the left-hand-side is the chemical loading parameter, P_{r} is the reactor pressure, n is an effective reaction order (1.8 for iso-octane [2], 1.25 for propane [96]) and the function on the right side is related to the efficiency of fuel consumption. The content of the reactor is a mixture of air, fuel, and product gases. For CO_2 diluted CH_4-air systems, like biogas, this function can be determined from the global reaction for fuel-lean mixtures

$$\phi\left(x_f \mathrm{CH_4} + \left(1 - x_f\right)\mathrm{CO_2}\right) + 2x_f\left(\mathrm{O_2} + 3.76\mathrm{N_2}\right) \rightarrow \phi\left(1 + x_f\left(\beta - 1\right)\right)\mathrm{CO_2} + 2\phi\beta x_f \mathrm{H_2O} + \phi\left(1-\beta\right)x_f\mathrm{CH_4} + 2\left(1-\phi\beta\right)x_f\mathrm{O_2} + 7.52x_f\mathrm{N_2} \tag{2.33}$$

where x_f is the mole fraction of CH_4 in the fuel, β is the fraction of CH_4 consumed in the reaction, and it is assumed that the CO_2 present in the biogas does not dissociate. It is important to recall that CO_2 is not inert, see Section 2.4; rather the combustion temperatures are expected to be low enough to avoid the thermal pathway to NO_x production and, therefore, below the temperatures where extensive dissociation is expected. The RHS of Eq. (2.33) represents the contents of the reactor. Following the procedure of Longwell and Weiss [2] and Ballal and Lefebvre [97], if it is assumed that the reaction is of order n, then the rate of consumption of CH_4 within the reactor is

$$\frac{\phi\beta x_f \dot{m}}{MW_{\mathrm{CH_4}} V} = A_{\mathrm{G}} T_{\mathrm{r}}^{c} \exp\left(\frac{-E_{\mathrm{a,G}}}{R_{\mathrm{u}} T_{\mathrm{r}}}\right)\left(\frac{P_{\mathrm{r}}}{R_{\mathrm{u}} T_{\mathrm{r}}}\right)^{n} \chi_{\mathrm{CH_4}}^{m} \chi_{\mathrm{O_2}}^{n-m} \tag{2.34}$$

where the subscript G indicates the global reaction, T_{r}^{c} is to compensate for the temperature dependence of A_{G}, and $\chi_{\mathrm{CH_4}}$ and $\chi_{\mathrm{O_2}}$ are the mole fractions of CH_4 and O_2 in the reactor,

respectively. From the RHS of Eq. (2.33) the mole fractions of fuel and oxidizer are

$$\chi_{\mathrm{CH_4}} = \frac{\phi x_f \left(1-\beta\right)}{\phi + 9.52 x_f} \tag{2.35}$$

and

$$\chi_{\mathrm{O_2}} = \frac{2 x_f \left(1-\beta\phi\right)}{\phi + 9.52 x_f} \tag{2.36}$$

respectively. Substituting Eq. (2.35) and Ex. (2.36) into Eq. (2.34) and rearranging yields

$$\frac{\dot{m}}{V P_{\mathrm{r}}^n} = \frac{MW_{\mathrm{CH_4}} A_{\mathrm{G}}}{R_{\mathrm{u}}^n T_{\mathrm{r}}^{n-c}} \exp\left(\frac{-E_{\mathrm{a,G}}}{R_{\mathrm{u}} T_{\mathrm{r}}}\right) \frac{\left(1-\beta\right)^m \left(2\left(1-\phi\beta\right)\right)^{n-m}}{\beta \phi^{1-m} x_f^{1-n} \left(\phi + 9.52 x_f\right)^n} \tag{2.37}$$

It has been suggested that the value of n is related to ϕ at fuel-lean extinction [20, 98].

A second expression for the loading parameter comes from the work of Lefebvre and Halls [99]

$$\frac{\dot{m}}{D^3 P^2} \tag{2.38}$$

where D is the diameter of the reactor and is characteristic of its volume. The reaction order $n = 2$ is based on an analysis that indicated that the reaction order should be between 1 (fast reactions) and 2 (fast mixing). This version of LP has also been used to correlate extinction in GT combustors to their operating conditions [8].

Conditions at extinction are useful in the determination of overall reaction order and kinetics limits for different fuels [2]. A variety of tools have been used to determine maximum combustor air flow rates in both diffusion and premixed flames at representative GT conditions. Spherical reactors intended to be kinetically controlled (i.e., approach well-stirred conditions) and thus approach the absolute extinction limits were used in the study of a

number of fuels [2, 100, 101, 102]. Other workers have used flames stabilized behind bluff bodies to more closely approximate conditions in a GT combustor [97]. In the early 1990's a series of laboratory combustors of increasing complexity were used to determine the effect of changing system back pressure on the stability of annular combustors using diffusion flames [51, 103]. Much of the work has focused on determining empirical relations useful for design.

2.5.3 Laminar Premixed Flame Speeds

Though the flow field within a WSR is highly turbulent, its stability, and the characteristics of turbulent flames in general, are often related to the laminar flame speed of a mixture. The laminar flame speed captures the effects of unburned gas temperature, stoichiometry, pressure and fuel type on the structure of a flame [24]. Along with flame thickness, the laminar flame speed may be used to determine characteristic time scales which, in turn, may be used to predict instabilities. A brief introduction to the theory and modeling of laminar flame speeds is included here.

2.5.3.1 Governing Equations

The governing equations of a laminar premixed flame propagating in a combustible mixture are broadly similar to those of the WSR. The primary differences arise from the presence of spatial gradients which account for the finite flame zone. Starting with the conservation of mass

$$\frac{\mathrm{d}\dot{m}''}{\mathrm{d}x} = 0 \tag{2.39}$$

continuing with the conservation of species

$$\dot{m}'' \frac{\mathrm{d}Y_i}{\mathrm{d}x} \frac{\mathrm{d}}{\mathrm{d}x} \left(\rho Y_i u_{i,\mathrm{dif}} \right) = \omega_i M W_i \tag{2.40}$$

where $u_{i,\mathrm{dif}}$ is the diffusional velocity of species i which may be due to gradients of concentration, temperature, pressure or body forces, [24], and finally conservation of energy

$$\dot{m}''' c_{\mathrm{P}} \frac{\mathrm{d}T}{\mathrm{d}x} + \frac{\mathrm{d}}{\mathrm{d}x} \left(-k \frac{\mathrm{d}T}{\mathrm{d}x} \right) + \sum_{i=1}^{N} \rho Y_i v_{i,\mathrm{dif}} c_{\mathrm{P},i} \frac{\mathrm{d}T}{\mathrm{d}x} = - \sum_{i=1}^{N} h_i \omega_i M W_i \tag{2.41}$$

To solve this system of equations constitutive equations for $u_{i,\mathrm{dif}}$, a kinetic mechanism (see Section 2.5.5) to determine ω_i, and species properties are required [104]. The temperature boundary conditions on Eq. 2.41

$$T\left(-\infty\right) = T_u \tag{2.42}$$

where T_u is the temperature of the unburned reactant mixture, and it is assumed the downstream boundary is located in a region where the temperature has become spatially uniform

$$\frac{\mathrm{d}T}{\mathrm{d}x}\left(\infty\right) = 0 \tag{2.43}$$

Because $u_{i,\mathrm{dif}}$ may be related to a concentration gradient, Eq. 2.40 is second-order in Y_i [24]. The mass fraction boundary conditions on Eq. 2.40 are

$$Y_i\left(-\infty\right) = Y_{i,u} \tag{2.44}$$

where $Y_{i,u}$ is the unburned mass fraction of species i, and a the downstream boundary is, again, spatially uniform

$$\frac{\mathrm{d}Y_i}{\mathrm{d}x}(\infty) = 0 \tag{2.45}$$

For freely propagating flames $\dot{m}$ is an eigenvalue of the problem. To solve the system an additional boundary condition must be specified or a degree of freedom removed. One approach is to fix the location of the flame within the domain by constraining the temperature at one point. The location must be carefully chosen to ensure that the gradients disappear near the boundaries of the domain [104].

2.5.3.2 Estimating Laminar Flame Speeds

The importance of laminar flame speeds to predicting a variety of combustion phenomena has led to the development of models and correlations for estimating their value. Based on a simplified version of the governing equations discussed above, Turns [24] suggests that the flame speed should scale as

$$S_L \propto \left(\frac{T_u + T_b}{2}\right)^{0.375} T_u T_b^{-n/2} P^{(n-2)/2} \exp\left\{\frac{-E_\mathrm{a}}{2 * R_\mathrm{u} T_b}\right\} \tag{2.46}$$

where T_b is the temperature of the product gases downstream of the flame and n is, again, the effective reaction order. It is immediately apparent that $\mathrm{S_L}$ is a strong function of temperature. If the effective reaction order is ≈ 2, then, based on Eq. (2.46), it might be concluded that pressure has little effect on $\mathrm{S_L}$. This assumption of reaction order is generally used for most simple bimolecular global reactions as well as for the WSR as discussed in Section 2.5.1. Correlations based on experimental data have generally agreed with the temperature scaling suggested by this simplified model, but they disagree with its pressure scaling.

This agreement/disagreement is borne out by the work of Andrews and Bradley [105] who examined the experimental CH_4-air data from a number of sources and developed the correlation

$$\mathrm{S_L} = 10 + 3.71 \times 10^{-4} \left(T_u\right)^2 \tag{2.47}$$

where $\mathrm{S_L}$ is in cm/s. Most experimenters have demonstrated a negative correlation between $\mathrm{S_L}$ and pressure. When comparing experiments performed at different pressures, Andrews and Bradley determined that

$$\mathrm{S_L} = 43 \left(P\right)^{-0.5} \tag{2.48}$$

where $\mathrm{S_L}$ is in cm/s and P is in atmospheres, best predicts the laminar flame speed of a mixture.

Later, the laminar flame speed of a variety of fuel-air mixtures were determined in experiments by Metghalchi and Keck. They then attempted a number of correlations before finding [106]

$$\mathrm{S_L} = S_{L,\mathrm{ref}} \left(\frac{T_u}{T_{u,\mathrm{ref}}}\right)^a \left(\frac{P}{P_{\mathrm{ref}}}\right)^b \left(1 - 2.1 Y_{\mathrm{diluent}}\right) \tag{2.49}$$

where

$$S_{L,\mathrm{ref}} = B_M + B_2 \left(\phi - \phi_M\right)^2 \tag{2.50}$$

with B_M, B_2, and ϕ_M as fuel dependent constants, $T_{u,\mathrm{ref}}$ and P_{ref} are reference conditions (298K and 1atm, respectively), a and b depend ϕ

$$a = 2.18 - 0.8 \left(\phi - 1\right) \tag{2.51}$$

$$b = -0.16 + 0.22 \left(\phi - 1\right) \tag{2.52}$$

and Y_{diluent} is the mass fraction of non-fuel and non-oxidizer species. The decrement of S_L by the presence of diluent species, in this case to compensate for any recirculated exhaust gas, is of interest in biogas flames due to the presence of CO_2 in the fuel stream.

A model of the type described by Eq.s (2.49) - (2.52) has been used by other workers to investigate a variety of fuel-air mixtures. Kobayashi et al. used such a model to describe turbulent burning velocities of methane-air flames at elevated temperatures and pressures. Using a Bunsen-type flame stabilized over different sizes of burners at $\phi = 0.9$, parameters a and b were found to be 1.9 and -0.5, respectively [107]. Cohé et al. confirmed the pressure exponent in studies of CO_2 diluted CH_4-air flames. Both the work by Cohé et al. [108] and previous work by Kobayashi et al. [109] confirmed that S_L decreases as the mole fraction of CO_2 in the reactant mixture increases. Cohé noted that the effect of CO_2 dilution was less important than that of pressure [108].

2.5.4 Laboratory WSR Designs

Various laboratory apparati have been designed to approximate the well-stirred condition. These devices have proven quite useful in the study static instabilities, high-temperature reaction kinetics, soot formation, and pollutant emissions. Four designs are described here. While others exist, these four are illustrative of the development laboratory WSRs.

2.5.4.1 Spherical WSR

The earliest effort to construct a laboratory WSR was that of Longwell and Weiss [2]. Sometimes called the 'Longwell Bomb,' it was designed for high-temperature kinetics and extinction investigations of hydrocarbon-air systems. As such, the reactor was capable of operating over a wide range of temperatures, both inlet and reactor, and pressures. Residence times

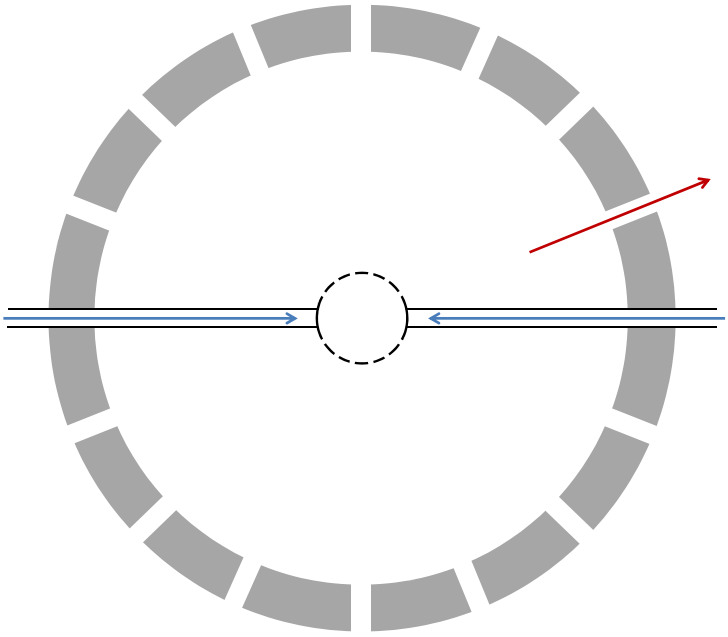

Figure 2.4: A sketch of the spherical WSR of Longwell [2], blue arrows indicate incoming fuel-air mixture and red arrows indicate exhaust ports.

could be varied from 0.1 to 15ms. The design was extremely useful in developing correlations between extinction and loading parameter. These works concluded that the pressure exponent in the loading parameter, see Eq. (2.32), should be set to 1.8 for a variety of fuels [2, 100].

Their reactor was a spherical shell, carved in two halves, of refractory brick, see Figure 2.4 for a sketch. The brick was chosen for its ability to withstand high temperatures ($\leq$ 1900K) and approach adiabatic operation. Reactor volumes ranged from 230 to 1880mL. Premixed, pre-heated fuel-air mixture was fed into the center of the reactor by a perforated spherical injection manifold. The injector had between 68 and 102 holes, drilled symmetrically, depending on reactor volume. Reactants exited the injection holes at sonic velocity. The number injection points and gas velocity was intended to yield vigorous mixing of reactants and products. Products exited through a series of symmetrically arranged ports in the re-

actor shell. The reactor was contained within a nickel shell again constructed in two halves and bolted together. The entire assembly was further enclosed in pipe sections to create a pressure vessel for elevated pressure testing. Both the pipe sections and nickel shell were manufactured with the necessary fittings and optical accesses for measurement, monitoring, and control equipment.

The major drawbacks of this design were primarily due to the insulating material and lack of conclusive evidence of homogeneity in the reactor volume. Though intended to be nearly adiabatic, there was high heat loss through the brick. Operation at near stoichiometric conditions and small residence times, i.e., high reactor loading, greatly reduced the life of the brick. At these conditions only one or two tests were possible. Lighter loading extended life. Measurements of oxygen consumption and other species made across the volume of one reactor did show that the device had time-averaged homogeneity. Though there was no evidence of non-homogeneity, the reactor could not be proven to be homogeneous.

To address some of these concerns, the spherical design was modified to determine the effect of injector geometry and pressure drop on mixing within the reactor. Initial experiments investigated changes in injector geometry by varying the body shape. The spherical shape of Longwell and Weiss was compared to cylindrical injectors with holes drilled either perpendicular to the cylindrical surface or at angled towards the center of the injector (i.e., as if the were drilled from the surface of a sphere). In blowout tests of propane-air mixtures, spherical and cylindrical with perpendicular hole injector geometries yielded similar results. It was also determined that mixing played a significant role in the conditions at blowout [101]. To determine how the number of holes and pressure drop across the injector affected the reactor's performance two additional experiments were undertaken. In the first, the pressure drop was held constant while the number of holes in a cylindrical injector was

varied from 3 to 68. It was via visualization studies with a water model that the extreme geometries, 3 and 68 holes, were associated with large scale recirculation patterns. These patterns were compared to those associated with the spherical injector of Longwell and Weiss and shown to be similar. The effect of variation in pressure drop was determined by maintaining a constant hole pattern and varying the diameter of the holes. Blowout conditions were not appreciably affected until the pressure drop reached 20% of the reactor pressure. It was concluded that flow patterns, which are dominated by reactor injector geometry, have major effects on blowout performance [102]. This was confirmed by a fluid dynamics study comparing spherical and cylindrical stirred reactors [110]. Hottel et al. showed that the shape of the jets coming from the centered injector led to the outer portion of the reactor approaching the well-stirred condition while the regions near the injector did not [111]

Building on these results, a final set of experiments attempted to determine the maximum loading of propane-air and propane-oxygen systems using a spherical reactor. It was found that at ϕ near unity the loading parameter satisfactorily predicted the blowout condition when the pressure exponent was 2 [112]. This agrees with the work of Lefebvre and Halls [99] discussed earlier.

Even with the modified injectors, the design still suffered from many of the issues related to the insulation. High heat loss through the walls and the injector were noted and treated as an equivalent loss in reactant enthalpy [2, 100, 101, 102, 112]. Though flow visualization was performed [102], there was still little evidence to prove the well-mixedness of the entire reactor volume. Work by Hottel et al. also showed that there is an optimal number of injectors to produce the best mixing in a spherical reactor. The number of holes should be that for which the jet angle matches the angle between jets on the spherical surface of the injector ball [113]. If these conditions were met, then the reactor approached well-stirred in

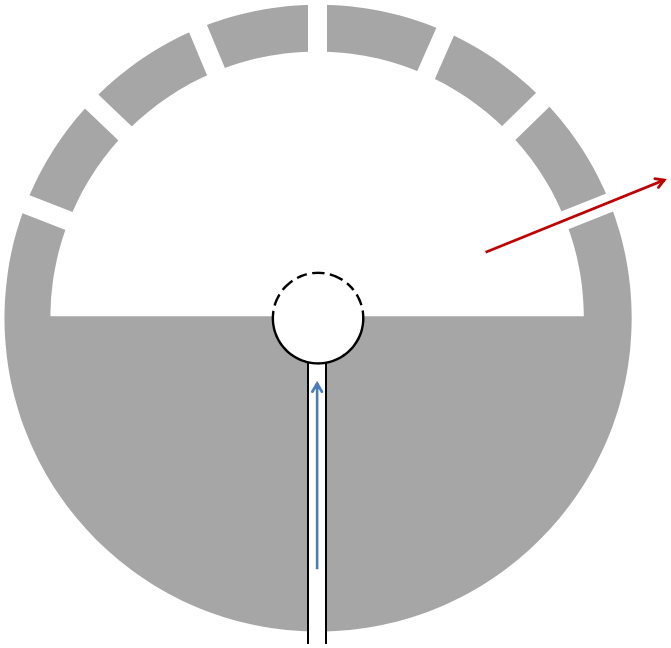

Figure 2.5: A sketch of the hemispherical WSR of Wright [3], blue arrows indicate incoming fuel-air mixture and red arrows indicate exhaust ports.

cold-flow experiments.

2.5.4.2 Hemispherical WSR

The spherical WSR was further modified by Wright to alleviate the inherent effect of the tubes feeding the injector on symmetry [3]. The reactor volume was modified by filling half with refractory to create a hemispherical reaction volume, see Figure 2.5. A single tube fed premixed, pre-vaporized fuel to to the injector through the solid half of the sphere. The injector body was spherical in shape but half buried in the refractory yielding a hemispherical injector. Product gases exited though exhaust ports in the shell of the reactor as before. The change in reactor shape led to strongly back-mixed combustion that more accurately represented the conditions in a GT combustor than other aerodynamic configurations [114, 115].

This reactor was used by several investigators to explore soot inception in back-mixed combustion and NO_x production. Early work by Wright using this reactor found that sooting in pure higher-hydrocarbon fuels was dependent on the presence of hydrocarbons in the product gases. It was also found that the sooting behavior is distinctly different for different fuels in back-mixed combustion [3]. This was confirmed by the work of Blazowski for blends of higher-hydrocarbon fuels [115, 116]. Later experiments by Wright determined that the effect of back-mixing was to dilute the combustion gases which is equivalent to lowering combustion pressure. Lower combustion pressures were associated with lower soot production when other parameters were held constant [117]. Engleman et al. used measurements from a reactor of this type to determine the accuracy of kinetics calculations for H_2, CO, and C_3H_8 flames. They found H_2 and CO models showed good agreement with WSR measurements whereas C_3H_8 models were not as accurate [118].

The hemispherical reactor overcame some of the deficits found in the spherical design but was unable to eliminate all of them. The use of a single feed line eliminated the effect of the fuel feed tubes on the reactor volume. However, the hemispherical shape also eliminated the overall symmetry present in the spherical reactor. There was still little proof of well-stirred operation [10].

2.5.4.3 Conical WSR

The spherical WSR has been further simplified to conical or truncated-conical shapes by various workers (e.g., [4, 119, 120]). Like the spherical and hemispherical designs, these reactors are constructed of refractory material or other ceramic insulators. In these reactors a single or small number of jets eject reactants from the tip towards the base of the conical reactor. There the jets impinge on the wall and are forced out and back towards the jet

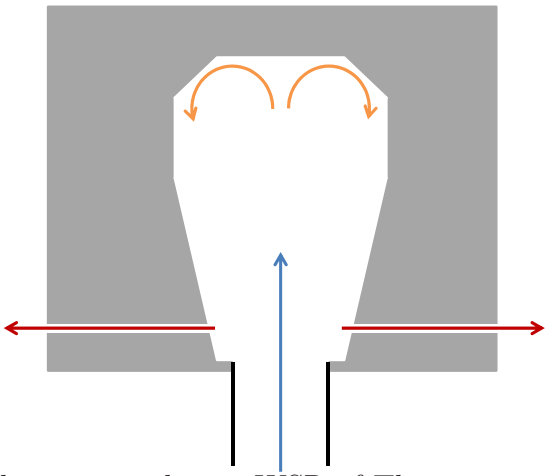

Figure 2.6: A sketch of the truncated cone WSR of Thorton et al. [4], blue arrows indicate incoming fuel-air mixture, orange arrows indicate back-mixing zones, and red arrows indicate exhaust ports.

source. Product gasses finally exit the reactor either around the outer surface of the injector or through radial ports near the tip of the cone. The net effect is back mixing of combustion products with the incoming reactants especially in the region near the base of the cone. The design is simple and easy to modify [121]. It exists in a range of reactor volumes, but based on the work on mixing in stirred reactors of Evangelista et al. [122] smaller volumes (i.e., tens of mL) are preferred.

The design of Thorton et al. [4] which was modified by Corr et al. [123] has been used extensively and warrants further description, see Figure 2.6 for a sketch. Due to the method of back mixing (i.e., impingement on the base of the cone) a high degree of erosion, similar to that found in spherical reactors, was expected if the reactor was to be constructed entirely of ceramic insulator. For experiments where this is a particular concern, the base may be replaced by high-temperature alloy to extend life. The walls are still high-temperature

refractory material (e.g., Zirconia or Alumina). In it's initial configuration, well-stirred operation was approached by using fuel-lean H_2-air combustion products as the primary inlet gas. The compound of interest was introduced to the product gases of the H_2-air combustion at levels below the flammability limit before the mixture entered the reactor. This resulted in the incoming jet having very nearly the same temperature (1000 - 1300K) as the reactor eliminating the difficulty of mixing fluids of different densities [4]. Later studies on NO_x production used cold gases and hydrocarbon-air mixtures above the flammability limits to reach temperatures sufficient to produce measurable levels of NO_x and expanded operation to elevated pressures [17, 22, 123]. When measurements are made near the base of the cone, the results are well predicted by WSR theory [17].

Like the spherical and hemispherical reactors the level of mixing within conical reactors is dependent on operating condition. When the walls are heated to make the system truly adiabatic, up to 80% of a conical reactor with a rounded base can be considered well-stirred [120]. Without heated walls reactors of this type exhibited poor mixing particularly at low loading [121]. The work of Williams et al. confirmed that the region near the base of the cone behaves as if it were well-stirred for certain conditions. They questioned whether a conical reactor would meet the well-stirred condition for methane-air combustion at elevated pressures [124].

2.5.4.4 Torroidal WSR

Another effort to improve mixing within a WSR resulted in the torroidal WSR of Nenniger [125]. In this design, the reactor volume is a torus with premixed reactants injected on the outer radius and products ejected at the inner radius. Reactants are fed into the reactor via a series of small jets angled off the radial to produce intense swirling flow. Like

the other designs the injection ring is constructed of temperature resistant metals and the reactor volume is made of ceramic insulator. Due to the angle of the jets, impingement on the reactor walls is avoided; thus, hot gas erosion is limited and reactor life is extended. A detailed description of the construction of this reactor can be found in Chapter 5.

The intense mixing found in this reactor is produced by a jet-in-crossflow flow pattern. Circulation is produced by canting the feed jets 20° off radial. This was later shown to produce sufficient jet penetration and swirling flow to create well-stirred conditions in the torus [95, 126, 127]. Reactors of this type have been used to investigate polycyclic aromatic hydrocarbon (PAH) production [125, 128, 129], pollutant emissions [127, 130, 131, 132, 133], and instabilities [130, 132, 133, 96].

2.5.5 Numerical Modeling

Numerical simulations have become increasingly popular in the early stages of the combustor design process. The simplest method of numerically simulating a GT combustor consists of using a WSR for the primary zone followed by a PFR for the remainder of the combustor [134]. As computational power has increased, the complexity of combustor models possible to simulate has followed. Many such models rely on the CHEMKIN chemical kinetics code and its updates, [135, 136, 137], to solve coupled equations describing the thermodynamics and chemistry of simple reactors. Modern techniques use a series of simple reactors to model the complex mixing and reacting zones within a combustor [138]. These techniques have become especially important in the design of LP combustors.

The PSR calculations assume perfect mixing at both the macro and micro-scales which may not always be true. Macro-scale mixing is controlled by fluid mechanical structures (i.e., jet in cross flow) whereas the micro-mixing is controlled by diffusional processes. Because

conditions within an experimental device are not perfectly mixed, many devices are simulated using a series of PSRs to simulate the different phenomena within the reactor [87]. By varying the flow split and the residence time in each reactor a range of chemistry can be investigated. The effect of imperfect micro-mixing has also been investigated with partially stirred reactor (PaSR) models. Micro-mixing is simulated using various techniques including coalescence/dispersion [139] and interaction by exchange with the mean [93].

Comparisons between the measurements made in various WSR experiments have been made to a CHEMKIN routine developed to model a PSR [140]. The relatively simple PSR model has proven useful for modeling the stability of a range of alternative low energy content fuels [141]. However, direct comparisons between emissions measurements made experimentally and simulated can be made difficult by probe effects [10, 132]. To compensate, reactor networks have been used to more accurately capture the complex interaction between fluid mechanics and chemistry found in these compound systems [138].

2.5.5.1 Chemical Kinetics Simulations with CHEMKIN

The process of simulating the chemical kinetics of combustion requires three pieces of information. First, a reaction mechanism which includes a number of reactions whose kinetics may be described by Eq.s (2.21)-(2.24) or physically equivalent methods. Second, the thermodynamic properties of all species participating in in the reaction mechanism must be specified. For reacting gasses, the thermodynamics may be described by curve-fit functions that describe the dependence of the isobaric specific heat, c_{P}, on temperature. Knowing the temperature and c_{P} allows the calculation of other important thermodynamic properties through integrals (e.g., enthalpy and entropy) and other relations (e.g., isochoric specific heat, c_{V}, and Gibbs free energy). Finally, for systems with spatial or temporal gradients,

the transport properties for all species are required.

One software that is popular for performing chemical kinetics calculations is the CHEMKIN code developed at Sandia National Lab by Kee et al. [135]. CHEMKIN was developed as a general purpose package determining thermodynamic properties and reaction rates in problems including complex chemistry. For those cases where the reactions of interest take place in a reactor alongside other physics, an supplementary piece of software is required to define and solve the additional governing equations.

Within the CHEMKIN software, chemical reactions are treated in the manner of Eq.s (2.21)-(2.22). Unless otherwise specified, the molecular concentration exponents for each reaction are assumed to be their stoichiometric coefficients. For reactions that are reversible, the constants in Eq. (2.24) are specified by the user for the forward reaction rate constant, $k_{\mathrm{f}j}$. The reaction rate constant for the reverse reaction, $k_{\mathrm{b}j}$, may be specified similarly. If the constants for $k_{\mathrm{b}j}$ are not specified, which is common in large mechanisms, then it is related to $k_{\mathrm{f}j}$ by the equilibrium constant, K_j,

$$K_j = \frac{k_{\mathrm{f}j}}{k_{\mathrm{b}j}} = \left[\frac{P}{R_{\mathrm{u}}T}\right]^{\sum_{i=1}^{N}\left(\nu''_{ji}-\nu'_{ji}\right)} \exp\left[\frac{\Delta S_j^{\mathrm{o}}}{R_{\mathrm{u}}} - \frac{\Delta H_j^{\mathrm{o}}}{R_{\mathrm{u}}T}\right] \tag{2.53}$$

where ΔS_j^o is the change in standard state entropy defined as

$$\Delta S_j^{\mathrm{o}} = \sum_{i=1}^{N}\left(\nu''_{ij} - \nu' ij\right)\int_0^{T_{\mathrm{eq}}} \frac{c_{\mathrm{P}i}}{T}\mathrm{d}T \tag{2.54}$$

ΔH_j^o is the change in standard state enthalpy

$$\Delta H_j^{\mathrm{o}} = \sum_{i=1}^{N}\left(\nu''_{ij} - \nu' ij\right)\int_0^{T_{\mathrm{eq}}} c_{\mathrm{P}i}\mathrm{d}T \tag{2.55}$$

and T_{eq} is the equilibrium temperature.

Pressure dependent unimolecular reactions may be treated using any of three different but related approaches in the CHEMKIN solver. All three are based on the assumption that the reaction rate constant at an intermediate pressure k is related to the rate constants above a high pressure limit, k_∞, and below a low pressure limit, k_0, by

$$\frac{k}{k_\infty} = \left(\frac{k_0 \left[M\right] / k_\infty}{1 + k_0 \left[M\right] / k_\infty} \right) F \tag{2.56}$$

where $[M]$ is the concentration of the mixture minus the reacting molecule and F is a function [142]. If F takes the value of unity, then Eq. (2.56) is the Lindemann-Hinshelwood model. The Troe formulation [142] of F is

$$\log F = \frac{\log F_{\text{cent}}}{1 + \left[\frac{c + \log k_0 [M]/k_\infty}{n - d(c + \log k_0 [M]/k_\infty)} \right]^2} \tag{2.57}$$

where

$$c = -0.4 - 0.67 \log F_{\text{cent}} \tag{2.58}$$

$$d = 0.14 \tag{2.59}$$

$$n = 0.75 - 1.27 \log F_{\text{cent}} \tag{2.60}$$

$$F_{\text{cent}} = (1 - a) \exp\left\{-T/T^{***}\right\} + a \exp\left\{-T/T^{*}\right\} - \exp\left\{-T/T^{**}\right\} \tag{2.61}$$

and a, T^*, T^{**}, and T^{***} are reaction specific constants which must be specified. The final approach to pressure dependent reactions supported by CHEMKIN was developed from the

Troe formulation by Stewart et al. which defines F as [143]

$$F = \left[a\exp\left\{-b/T\right\} + \exp\left\{-T/c\right\}\right]^{\left(1+\log^2 k_0[M]/k_\infty\right)^{-1}} \tag{2.62}$$

where a, b, and c are constants that must be specified. Additional flexibility is provided by modifying Eq. (2.62) with

$$F = dT^e\left[a\exp\left\{-b/T\right\} + \exp\left\{-T/c\right\}\right]^{\left(1+\log^2 k_0[M]/k_\infty\right)^{-1}} \tag{2.63}$$

where d and e must be specified. All three of the proceeding approaches may also be used to define chemically active bimolecular reactions [137].

The definition of the reactions within a mechanism results in a series of ordinary differential equations. Often the equations involve a variety of time scales due to the presence of radical species (quick reacting) and stable species (slow reacting) rendering them numerically stiff. A number of methods for solving differential equations of this type exist [94, 144].

The numerical PSR model employed in this work solves Eq.s (2.26)-(2.28). The conservation of energy, Eq. (2.28), is restated in unsteady form as

$$(\rho V)\,\bar{c}_{\mathrm{p}}\frac{dT_{\mathrm{r}}}{dt} = \dot{m}\sum_{i=1}^{N}\left(h_{i,\mathrm{in}} - h_{i,\mathrm{out}}\right) + Q + V\frac{dP_{\mathrm{r}}}{dt} \tag{2.64}$$

where $\bar{c}_{\mathrm{p}}$ is the mean isobaric specific heat of the mixture in the reactor, Q represents the heat transfer to/from the reactor and heat release from any reactions [104]. The series of stiff differential equations are solved using the DASPK algorithm of Li and Petzold [144]. This scheme uses an implicit backwards differentiation formulation to discretize the system of ODEs in time and a modified Newton's method to integrate at each time step. The details

of the DASPK technique are described in [144].

Laminar flame speed estimates made in this work are solved using packaged CHEMKIN routines. A computational domain, whose size is specified by the user, is discritized using a finite difference scheme where the number of cells is also set by the user. The grid is non-uniform becoming finer in regions of higher gradients. Two dicretization options are available. The first is a first-order in space windward method. This method is less dependent on the initial guess but introduces artificial diffusion in the regions of coarser mesh. A second-order in space central difference method is also available. The central difference method is more accurate but prone to convergence issues [104]. The second derivatives of the governing equations are discretized using central difference schemes where the coefficients within the derivatives are evaluated as averages between grid points points. Diffusional velocities are evaluated in a similar way [104].

2.5.5.2 Reaction Mechanisms

A number of global, quasi-global, and detailed reaction mechanisms have been suggested in the literature for CH_4-air combustion. Global and quasi-global mechanisms sacrifice accuracy for reduced computational intensity. As such, they are popular for use in conjunction with CFD for modeling GT combustors. Detailed mechanisms include too many individual reactions to be solved efficiently along with the equations governing the turbulent flow in combustors. However, they make more accurate predictions of minor species which are important to meeting modern emissions standards.

Global mechanisms and quasi-global reactions attempt to predict the rates of production of the major species (i.e., Fuel, Oxidizer, CO_2, and H_2O) in a single reaction or small number of reactions. Single-step global mechanisms, like those of Bradley et al. [145] and

Westbrook and Dryer [146, 147], usually have a limited range of applicability in terms of reaction temperature, pressure, and stoichiometry. Often, such mechanisms are focused on matching experimental measurements of specific combustion properties [146]. In quasi-global mechanisms, a single-step reaction of the type

$$C_xH_y + O_2 \leftrightarrows CO + H_2 \tag{2.65}$$

is followed by a set of reactions describing the oxidation of CO and H_2 to CO_2 and H_2O [146]. The constants used to describe the reaction rates (i.e., A, β, E_a and the species concentration exponents) are chosen to best match aspects of experimental measurements (e.g., laminar flame speed, ignition delay, species profiles). Mechanisms including just a single additional reaction, called a 2-step, like that of Westbrook and Dryer [146], or multiple steps involving other minor species like the 4-step mechanism of Jones and Lindstedt [148] and the 21-step mechanism of Westbrook and Dryer [146]. These larger mechanisms offer better matching to experimental data at the cost of additional computational requirements.

Detailed combustion mechanisms attempt to be more complete in their description of the elementary reactions that take place during the combustion process than is possible in global and quasi-global mechanisms. They can contain many hundreds or thousands of reactions depending on the fuel species considered. The size and complexity of detailed mechanisms has led to a number of methods of construction having been sought. The Gas Research Institute (GRI) has developed, via funding several researchers, a series of detailed mechanisms that describe natural gas combustion with a focus on the oxidation of CH_4. The most recent version, GRI-Mech 3.0, consists of 325 elementary reactions considering 53 species [149]. Most reactions have been studied individually to provide accurate reaction rates. Not all of

the reactions or species included are relevant to all CH_4 combustion problems, but they are included for completeness and flexibility. The mechanism developed at University of California San Diego (235 reactions including 46 species) was built up from simple mechanisms adding complexity only as necessary. The resulting mechanism combines the influence of many elementary reactions into single steps. This limits the applicability of the mechanism to certain conditions and phenomena, but it also reduces the sources of uncertainty by reducing the number of reaction parameters [150]. The mechanism of Glarborg and Bentzen, developed based on experiments in environments containing high concentrations of CO_2, consists of 424 reactions involving 60 species. It is an example of a mechanism made up of sub-mechanisms (i.e., detailed mechanisms describing simpler processes like CO or CH_3OH oxidation). In this case, the sub mechanisms were previously described by the authors. To fit the problem of interest the combined mechanism was 'tuned' with special emphasis on reactions involving CO_2 [151].

A compromise between detailed and quasi-global mechanisms are the reduced mechanisms. The goal in developing the smaller mechanisms from larger mechanisms is to reduce the computational intensity while maintaining the accuracy, to a certain extent. There are a number of methods for reduction (e.g., approximation of partial equilibrium, lumping, and response modeling) which result in varying levels of simplification and accuracy [152, 153]. Many reductions aim to create mechanisms that are computationally better suited to specific problems. One such reduced mechanism that is used in CH_4 combustion is the reduced version of GRI-Mech 1.2 which was developed to maintain some of the capabilities, particularly predictions of ignition delay and laminar flame speeds, of the full GRI-Mech 1.2 (117 reactions, 32 species). The result is a mechanism consisting of 84 reactions involving 22 species that is able to replicate the predictions, within 11%, of the full mechanism over

a range conditions [154]. Care must be taken when applying these reduced mechanisms to problems for which they were not designed due to the nature of the reduction process [152].

Simulations using detailed kinetic mechanisms in different computational models have been used to investigate the effect of various combustion phenomena on chemistry. Sturgess used a stirred reactor model to approximate fuel-lean extinction in various commercial aero-GT diffusion flame combustors. As the combustors approached fuel-lean extinction, the flames lifted from the fuel nozzles leading to zones premixing of reactants and products before combustion. Using CFD and empirical correlations, Sturgess was able to identify a portion of the primary zone that could be reasonably modeled as a WSR. The WSR predictions, made using a variety of chemical kinetic mechanisms, agreed satisfactorily with measurements [155]. In their work suggesting a mechanism for dynamic instabilities in LP combustors, Lieuwen et al. developed an unsteady PSR model using a single-step propane mechanism to investigate the role of chemical kinetics. They determined that the amplitude of the dynamic instability in reaction-rate, forced by oscillations in ϕ, increases by two orders of magnitude as average magnitude of ϕ decreases to 0.75 from unity [55]. A similar technique was used by Lilleberg et al. to investigate the effect of different forcing amplitudes, parameters (reactor loading, ϕ, and inlet temperature) and kinetic mechanisms on the reaction rates for various species. They found that increasing the amplitude of the forcing function led to a linear increase in the amplitude of the oscillation in reaction rate. This was true for all forcing parameters. The effect of decreasing ϕ on the reaction rate was species dependent with CO_2 and OH increasing, CO and H_2 decreasing, and H_2O not changing significantly. Additionally, when the fuel and oxidizer concentration exponents in global reaction mechanism have a non unity value, the mechanism can force the amplitude of the oscillations in reaction rate to increase with decreasing ϕ. This is true even under

conditions where the amplitude increase is not seen when using detailed mechanisms [156].

2.6 Summary & Conclusion

In this chapter the necessary theory and applicable previous work has been discussed. A number of conclusions can be formed from this research:

- Governmental and social pressure has forced manufacturers power generation systems to develop low pollutant emissions options
- Gas turbine manufacturers have found several possible paths to reducing pollutant emissions among them the fuel-lean premixed combustion approach
- Combustion systems operating in the fuel-lean premixed regime are susceptible to combustion instabilities which may lead to extinction or mechanical failure
- Fluctuations in the global energy market and social pressures have lead to interest in alternative fuels such as biogas
- Variability in the species constituency of a fuel like biogas alters the combustion chemistry and stability characteristics of a GT combustor
- WSR models, both experimental and numerical, have been developed to attempt to characterize combustion processes, stability and pollutant emissions of GT combustors
- There have been only very limited applications of the WSR model to the investigation of the effect of alternative fuels like biogas on the stability of modern fuel-lean premixed GT combustors. Those limited studies focused mostly on pollutant emissions.

Chapters 3 and 4 of this work are dedicated to the description of a series of investigations into the effect of CO_2 dilution of the fuel stream, like that seen in biogas, on the stability of CH_4-air combustion systems.

Chapter 3

Predicting Laminar Flame Speeds of Biogas-Air Flames

Previous workers have noted the effect of diluents on laminar flame speeds [106, 108, 109]. In their numerical investigations biogas flames, Jahangirian and Engeda pointed to the lack of correlations to predict the laminar flame speed in biogas-air mixtures [157]. The work of Cohé et al. has partially filled this deficit [108]. This chapter expands on these previous results and attempts to develop a more comprehensive correlation.

3.1 Methods

Laminar flame speeds were investigated using CHEMKIN's PREMIX algorithm [158, 104] solved using CHEMKIN 10101 (Reaction Design, San Diego, Ca) software. This one-dimensional algorithm solves the governing equations outlined in Section 2.5.3. For these simulations the GRI mechanism version 3.0 for natural gas was employed. This mechanism has been used previously to investigate the effect of kinetics on laminar flame speeds of biogas mixtures [157, 108]. Other workers have indicated that earlier versions the GRI mechanism, particularly 2.11, are better at predicting laminar flame speeds at pressures above 5 bar [109, 107]. This work is focused on conditions found in micro-GT combustors which operate in conditions near or below 5 bar. The 3.0 version of the mechanism is chosen

to be consistent with the work of Jahangirian and Engeda [157].

The conditions simulated were chosen to represent those found in micro-GT combustors with varying levels of recuperation burning biogas. The combustor operating conditions are tabulated in Table 3.1. Different reactant mixes are chosen to represent the range of fuels produced by anaerobic digestion of organic materials from low heating contents typical of sanitary landfill gas to higher quality gas produced by well controlled digesters. Pure methane is included for a reference. Diluents are modeled as CO_2 only. Previous workers have linked its effect on kinetics to be more influential than that of N_2 [79]. The range of fuels tested are tabulated in Table 3.2. Due to convergence issues that occurred as the level of dilution increased, the first-order windward scheme was employed to solve the governing equations.

Table 3.1: Conditions used in laminar flame speed calculations

V (L)	T_{in} (K)	P_{r} (atm)	ϕ
0.25	$300 - 900$	$1 - 4$	$0.5 - 1.0$

Table 3.2: Fuel Compositions used in laminar flame speed calculations

Mix No.	Fuel Composition (By Vol.)	WI (kJ/kg)
1	100% CH_4 - 0% CO_2	$70,621$
2	80% CH_4 - 20% CO_2	$46,056$
3	70% CH_4 - 30% CO_2	$37,922$
4	60% CH_4 - 40% CO_2	$30,790$
5	50% CH_4 - 50% CO_2	$24,435$
6	40% CH_4 - 60% CO_2	$18,696$

The fit method of Metghalchi and Keck [106] was chosen as the basis for the results presented here. Though based on experiments with higher hydrocarbon and blended fuels, this method was chosen because it was originally formulated to include diluents (simulated combustion products 85% N_2 and 15% CO_2). However, the diluent term is modified here to better reflect the effect of pure CO_2 dilution of CH_4-air combustion

$$\mathrm{S_L} = S_{L,\mathrm{ref}} \left(\frac{T_u}{T_{u,\mathrm{ref}}} \right)^a \left(\frac{P}{P_{\mathrm{ref}}} \right)^b \left(c - d \ln \chi_f \right) \tag{3.1}$$

where the exponents a and b, $S_{L,\mathrm{ref}}$ and χ_f are defined as before. The constants in this equation have been modified to better fit the biogas flames simulated here.

3.2 Results & Discussion

The fit scheme was divided into two sections due to an apparent change in behavior with increasing ϕ. This effect has been noted by others in CH_4-air flames [159]. Though both regions can be predicted well by the type of model described in Eq. (3.1), the constants take different values. The best point to split the data was around $\phi = 0.6$. In the regions above and below this ϕ, the dependence on pressure and diluent were similar. Indeed, the effect of diluent is nearly identical. The influence of temperature, though of similar form, was markedly different. Also $S_{L,\mathrm{ref}}$ behaved differently above and below this dividing line. The values of all of the constants and those in Eq. (3.1) are in Table 3.3.

The exponents for the influence of temperature and pressure take similar forms to those of Metghalchi and Keck [106] (see Eq.s (2.51) and (2.52))

$$a = a_1 + a_2 \left(\phi - 1 \right) \tag{3.2}$$

and

$$b = b_1 + b_2 (\phi - 1) \tag{3.3}$$

where a_1, a_2, b_1, and b_2 differ between the two regions.

The influence of temperature in these CO_2 diluted mixtures is more dependent on ϕ than found by Metghalchi and Keck in mixtures diluted by a combination of CO_2 and N_2 especially at lower values of ϕ. Above $\phi = 0.6$ the offset coefficient found here is similar to that found by Metghalichi and Keck (2 compared to 2.18); whereas below $\phi = 0.6$ the offset is smaller here (1.51 compared to 2.18). Both above and below $\phi = 0.6$ the slope of the exponent term is larger in magnitude. The magnitude is approximately twice as large here above $\phi = 0.6$ (1.5 compared to 0.8) and over five times larger below $\phi = 0.6$ (4.3 compared to 0.8) [106].

The reference laminar flame speed is predicted in a similar manner to that suggested by Metghalchi and Keck [106], see Eq. (2.49), where B_M, B_2 and ϕ_M vary between the two regions. The reference flame speeds (fuel was assumed to be pure CH_4) were determined using the same CHEMKIN model as the rest of the data presented here. The ϕ modifier, ϕ_M, is only different by 2% where as the two other constants are 80% larger for $\phi \leq 0.6$.

Table 3.3: Constants used in the proposed model to predict the laminar flame speed of biogas-air mixtures

ϕ	a_1	a_2	b_1	b_2	B_M	B_2	ϕ_M	c	d
≥ 0.60	2.00	−1.50	−0.30	0.30	0.38	−0.65	1.25	1.00	0.45
< 0.6	1.51	−4.30	−0.30	0.25	0.21	−0.36	1.22	1.00	0.45

Plots of the fit model's predictions versus the flame speeds calculated by the detailed kinetic model are shown in Figures 3.1 and 3.2. Agreement in both ranges is generally

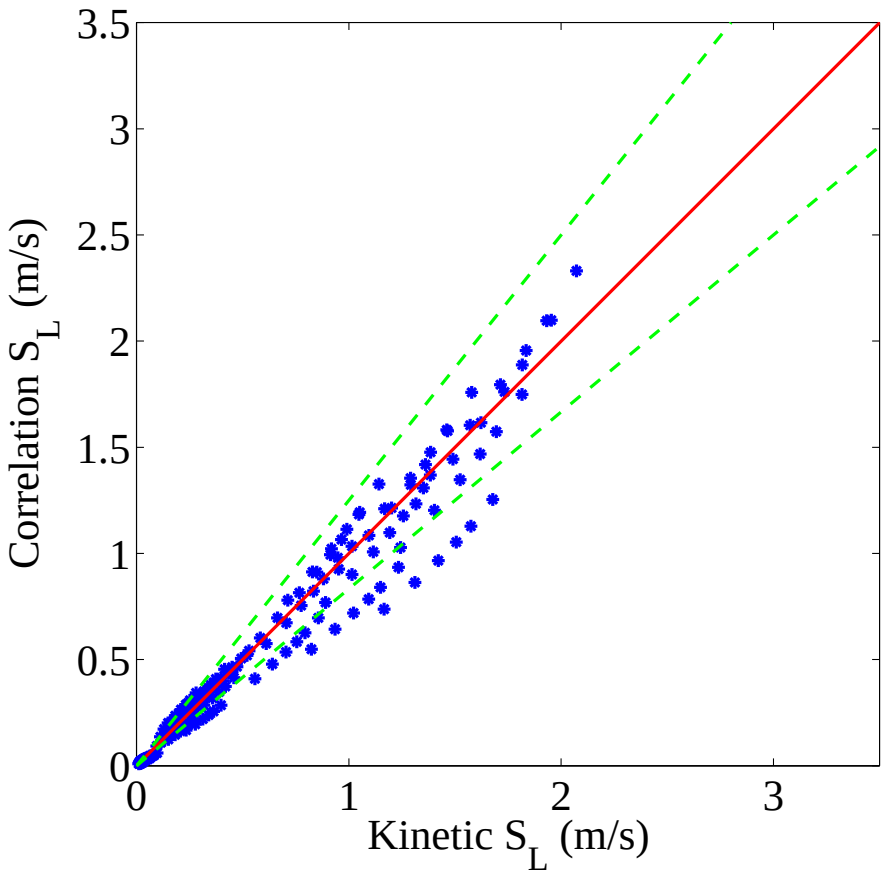

Figure 3.1: A plot of the laminar flame speed as predicted by the model vs. the laminar flame speed predicted by the detailed kinetics simulations for $\phi < 0.6$. The green dashed lines indicate deviation of 20% from the kinetics simulation.

good. The RMS error between the correlation and the predicted flame speeds is 19.5% below $\phi = 0.6$ and 20.6% above $\phi = 0.6$. Figures 3.1 and 3.2 include lines indicating $\pm 20\%$ deviation from the flame speeds calculated using detailed kinetic, green dashed lines. Most of the error occurs at low flame speeds where dilution is high. As pressure increases the scheme becomes more accurate as noted by Metghalchi and Keck [106].

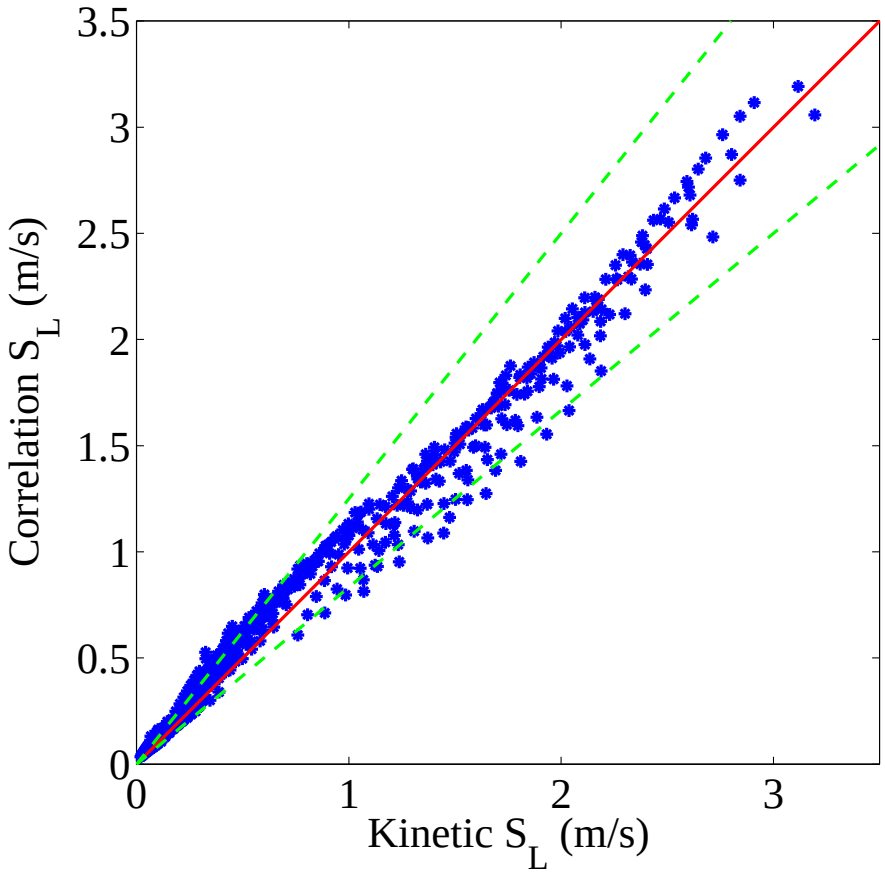

Figure 3.2: A plot of the laminar flame speed as predicted by the fit vs. the laminar flame speed predicted by the detailed kinetics simulations for $\phi > 0.6$. The green dashed lines indicate deviation of 20% from the kinetics simulation.

3.3 Conclusions

In this chapter the laminar flame speeds of CO_2 diluted CH_4-air mixtures have been simulated over a range of conditions similar to those found in small GT combustors. The fuel mixtures approximate the content of biogas from a variety of sources or the effect of EGR into fully premixed combustion system. Two fit models of the type proposed by Metghalchi and Keck [106] were established to predict the laminar flame speed of these mixtures. These fits, split around $\phi = 0.6$, adequately predict value of S_L over the range of conditions simulated. Fits of this type can be useful as components of methods for predicting a variety of combustion phenomena including both static and dynamic instabilities.

Chapter 4

Static Instability Simulations using Detailed Chemical Kinetics

4.1 Purpose of Experiments

Kinetic modeling of fuel-lean static stability limits of the combustion of biogas type fuels in a model of an ideal primary zone of a GT combustor is presented here. In this study, CH_4 is diluted with CO_2 to simulate a range of gases representative of the products of anaerobic digestion of organic materials from different sources (e.g., landfill and animal waste digester). Fuels of this type are of interest for use in small gas turbines in distributed generation applications. Predictions made by two detailed mechanisms (GRI-Mech 3.0 and San Diego) and one reduced mechanism (GRI-Mech 1.2, reduced) are employed to investigate the underlying kinetics near fuel-lean extinction. Approximate correlations to predict fuel-lean extinction are extracted from these results and compared to those of other fuels.

The WSR is an established tool for evaluating combustion kinetics through measurements made at extinction. From these experiments useful correlations relating fuel-lean blowout to combustor loading have been established for a variety of fuels [2, 100, 101, 96]. As outlined in Section 2.5.1 and following the work of Longwell and Weiss [2] and Ballal and Lefebvre [97], a set of fuel-lean stability curves for simulated biogas with varying CO_2 content have been made. Any variation in ϕ and reactor chemical loading parameter at blowout with CO_2

content will be correlated to important physical parameters and boundary conditions of the reactor.

4.2 Methods

It has been suggested that the value of the reactor order n is related to ϕ at blowout, ϕ_{LE} [98, 20]. As an example, from investigations into the stability limits of propane-air flames Ballal and Lefebvre [97] showed that ϕ_{LE} at blowout is predicted by

$$\phi_{\mathrm{LE}} = \left[\frac{\dot{m}}{CVP_{\mathrm{r}}^{1.25}\exp\left(T_{\mathrm{in}}/150\right)}\right]^{0.16} \tag{4.1}$$

where $\dot{m}$ is the mass flow rate of air and C is determined empirically.

Following the work of Jahangirian and Engeda [157], three different mechanisms were compared in this investigation. The first is the GRI-Mech 3.0 detailed mechanism. This mechanism includes 325 elementary reactions and thermodynamic and transfer properties of 53 species including NO_x formation chemistry [149]. The second detailed mechanism is the San Diego mechanism [150] (release 2009/11/22) including the NO_x mechanism (release 2004/12/9 (2)). This mechanism includes 46 species and 235 reactions. Finally, a reduced mechanism developed from GRI-Mech 1.2 [154] which does not include nitrogen chemistry is used for comparison. This mechanism includes 19 reacting species, inerts N_2 and Ar, and 84 reactions.

The governing equations for the unsteady PSR model, see Sections 2.5.1 and 2.5.5, are solved using CHEMKIN 10101 (Reaction Design, San Diego, Ca) software assuming an adiabatic, fixed volume reactor operating at constant pressure. Five levels of CO_2 diluted

CH_4 and one blend of CH_4, CO_2, H_2O, and N_2 were investigated in these simulations. See Table 4.1 for the different fuel mixes. Air was modeled as a mixture of 21% O_2 and 79% N_2, by volume. In each simulation, the reactions were initiated by assuming an elevated reactor temperature (1800K) and a LP in the stable region. Conditions within the reactor were then allowed to stabilize before LP was increased gradually while ϕ was held constant. Extinction was determined by a sharp decrease in reactor temperature. The conditions in the reactor were chosen to simulate those found in micro-GT combustors with varying levels of recuperation, and the reactor size was chosen to be consistent with previous experimental studies from other investigators [2], [96], [131], see Table 4.2.

Table 4.1: Fuel Compositions used in kinetics simulations

Mix No.	Fuel Composition (By Vol.)	WI (kJ/kg)
1	80% CH_4 - 20% CO_2	46,056
2	70% CH_4 - 30% CO_2	37,922
3	60% CH_4 - 40% CO_2	30,790
4	50% CH_4 - 50% CO_2	24,435
5	40% CH_4 - 60% CO_2	18,696
6	50% CH_4 - 16.6% CO_2 - 16.6% N_2 - 16.6% H_2O	27,927

Table 4.2: Conditions used in kinetics simulations

V (L)	T_{in} (K)	P_{r} (atm)	ϕ
0.25	$300-900$	$1-4$	$0.5-0.8$

4.3 Results & Discussion

4.3.1 Simulated Lean Extinction

Lean extinction points as calculated by the three different mechanisms for Mix 3 are shown in Fig. 4.1. An effective reaction order $n = 1.75$ has been chosen for these plots. The units of LP ($\mathrm{mol/s\,L\,atm^n}$) are chosen to be consistent with previous work from others [2], [96]. All three mechanisms predict similar extinction points over the range of temperatures, pressures, and fuel mixes simulated here. The reduced GRI-Mech 1.2 mechanism tends to predict extended fuel-lean extinction limits. This effect increases with P_r. The prediction of extended stability is due to the reduced mechanism's prediction of higher concentrations of minor species, specifically H radicals which are important in the breakdown of CH_4, as seen in previous studies [157]. The GRI-Mech 3.0 mechanism is the most conservative predictor of extinction (*i.e.*, highest ϕ_LE for a fixed reactor LP) with the San Diego mechanism generally falling between the two other mechanisms. Results presented from here on will be based on the predictions of GRI-Mech 3.0.

The effects of P_r and T_in on simulated fuel-lean extinction for three different fuel mixes, are shown in Fig. 4.2. As LP increases so does ϕ_LE in a manner that indicates a power law relation similar to Eq. (4.1). The slope of the relation seems to change around a ϕ_LE of 0.6. Increasing T_in causes ϕ_LE to decrease for a given reactor loading. This effect is consistent across the range of fuel mixes tested. The influence of P_r is smaller than that of T_in which is similar to the work of Ballal and Lefebvre [97]. Across the range of fuel mixes the effect of increased P_r is to increase ϕ_LE.

The effect of fuel CH_4 content on ϕ_LE is illustrated in Fig. 4.2 and Fig. 4.3. Lowering the CH_4 content of the fuel increases ϕ_LE for a fixed LP, compare (a) and (b) of Fig. 4.2.

When the diluent is a mixture of species, as in Mix 6, ϕ_{LE} for a fixed LP is lower than that for a fuel with similar CH_4 content mixed only with CO_2, Mix 4, confirming the role of CO_2 is not limited to that of an inert diluent near fuel-lean extinction, compare (b) and (c) of Fig. 4.2. In Fig. 4.3 three fuel mixes (1, 3, and 4) are compared to Mix 6 at three different levels of T_{in} and P_{r}. Mix 1 and Mix 6 have similar ratios of CO_2 to CH_4. Mix 4 and Mix 6 have identical CH_4 content but different diluents. A comparison of the extinction curves for this combination of Mixes elucidates the effect of CO_2 and other diluents on fuel-lean extinction. The extinction curve of Mix 1 is shifted towards lower ϕ_{LE} compared to that of Mix 6 confirming that the effect of the other diluents in Mix 6 is to reduce the fuel-lean extent stable operating range. If the CO_2 was playing no role kinetically it would be expected that the extinction curves for Mix 4 and Mix 6 would be identical. However, replacing a portion of the CO_2 with other diluents shifts the extinction curve for Mix 6 towards lower ϕ_{LE}. The fuel mix which matches best with Mix 6 is Mix 3 which has a higher CH_4 content. Thus, the effect of replacing 2/3 of CO_2 in the diluent with other species is akin to increasing the CH_4 content of the fuel indicating a kinetically active role for CO_2.

For two fuel mixes with the same ϕ_{LE} but different levels of CH_4, the presence of radical species necessary for the continuation of combustion is decreased in two ways. First, dilution of the combustion mixture causes reduced concentrations and lower reaction temperatures; thus, reducing reaction rates. Second, when CO_2 is the diluent, as in fuel Mixes 1-5 of this work, there is a competition for H radicals between the reaction $CO_2 + H \rightleftharpoons CO + OH$ and chain branching reactions [160]. To show this Fig. 2.1 is plots of reactor temperature and mole fractions of H, O and OH versus LP at a fixed inlet ϕ of 0.65 and Tin of 300K for Mix 3, Mix 4, Mix 6 and a mix where the H_2O in Mix 6 is replaced by N_2. Extinction occurs near 1500K for all four fuel mixes. As LP increases the fraction of H, O, and OH increase

until near extinction for all four fuel mixes, and all three species fractions fall off before extinction is indicated by the T_r profile. The H_2O in Mix 6 increases the hydrogen content of the fuel stream to be similar to that of Mix 4. Reactor temperatures are below those at which a large percentage of the H_2O in the fuel stream would be expected to dissociate to add additional H radicals to the reaction. However, both Mix 4 and Mix 6 have similar species profiles, compare Fig. 2.1(a) and Fig. 2.16(c). Eliminating the water from the diluent mix and replacing it with N_2, shown in Fig. 2.16(d), produces a similar mole fraction of H in the reactor and extends the LP at extinction relative to Mix 6. The increased H content of the reactor is more a function of the reduced CO_2 content in the fuel rather than of the additional H provided by the H_2O.

4.3.2 A Correlation to Predict Lean Extinction

When generating the curve fits for qualitatively predicting fuel-lean extinction the focus was on micro-GT applications. Mixes 15 plus simulations of 100% CH_4 are used, because the fuel is often dried before combustion to avoid condensation in the fuel system. Additionally, fitting focused on combinations of T_{in} and P_r that are practical (e.g., at elevated P_r fitting focused on higher T_{in} due to heat of compression or recuperation). The method presented here follows the work of Longwell and Weiss, [2], and Ballal and Lefebvre, [97], by relating LP and ϕ_{LE}. Other methods such as those that use Damkhler number relations like that of Amato et al. [77], based on laminar flame speed like that recommended by Lafay et al. [80] or other methods like those reviewed by Hoffmann et al. [161] are also possible.

Based Fig. 4.2, Fig. 4.3 and Eq. (4.1) two fits were made due to an apparent change in slope near ϕ_{LE} 0.6. Above this point extinction behavior was generally similar for all fuels and operating conditions. Below ϕ_{LE} 0.6 the behavior was more strongly dependent on fuel

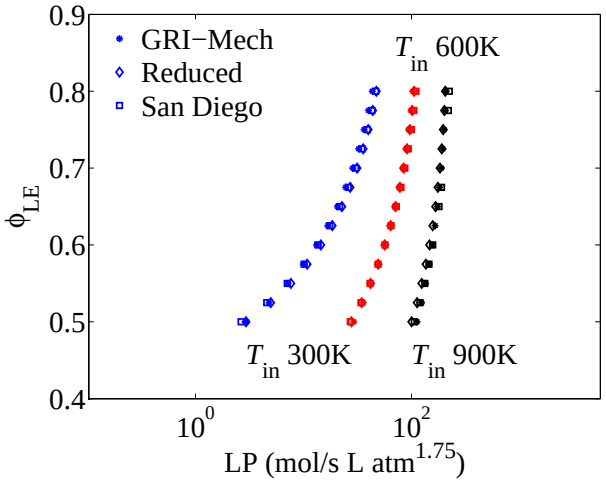

(a) 1atm

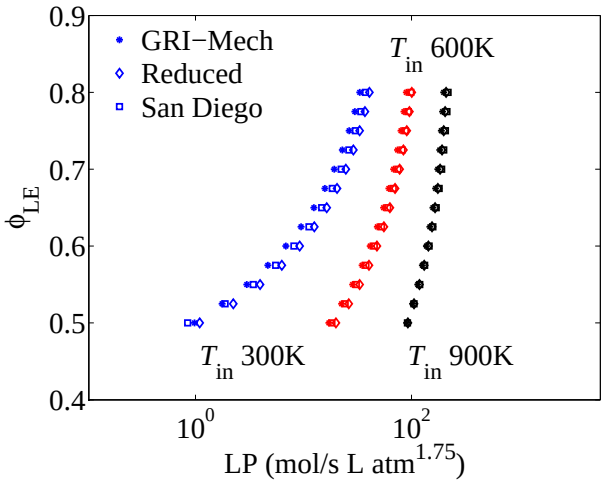

(b) 2atm

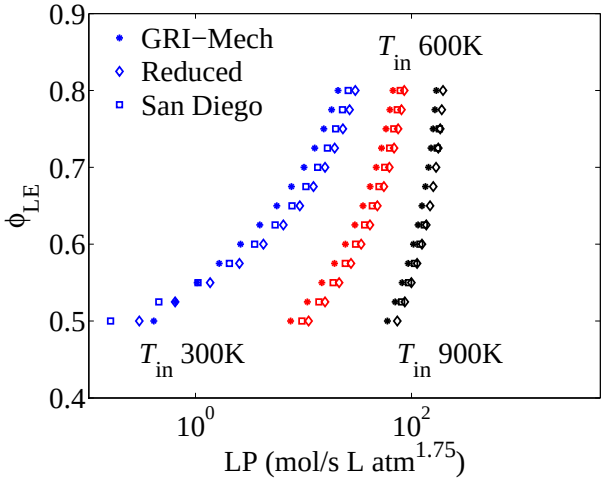

(c) 4atm

Figure 4.1: ϕ_{LE} versus LP as computed by three mechanisms (stars GRI-Mech 3.0, diamonds GRI-Mech 1.2 reduced, squares San Diego) at three different Tin (blue 300K, red 600K, black 900K) and three different operating pressures for Mix 3: (a) 1atm, (b) 2atm, and (c) 4atm.

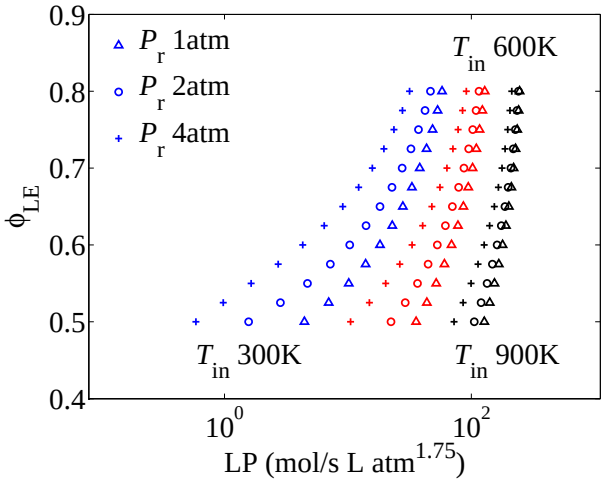

(a) Mix 1

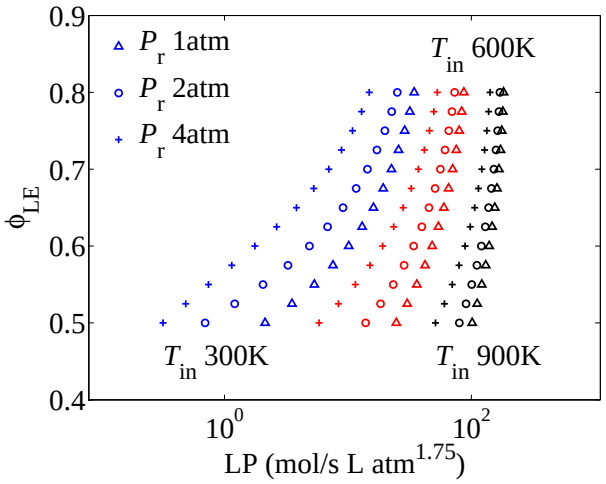

(b) Mix 4

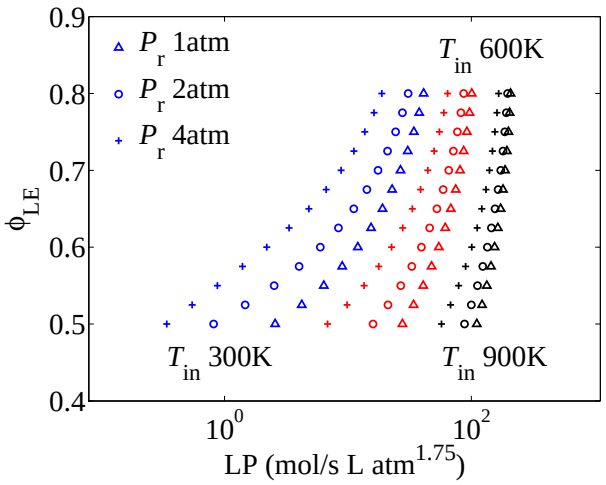

(c) Mix 6

Figure 4.2: ϕ_{LE} versus LP as computed by three mechanisms (stars GRI-Mech 3.0, diamonds GRI-Mech 1.2 reduced, squares San Diego) at three different $T_{mathrmin}$ (blue 300K, red 600K, black 900K) and three different operating pressures for Mix 3: (a) 1atm, (b) 2atm, and (c) 4atm.

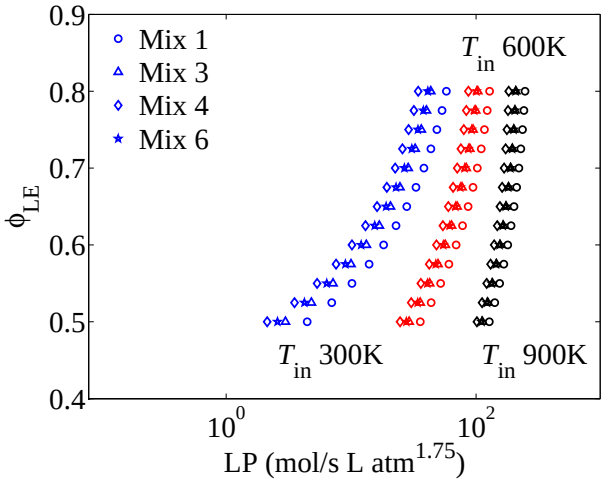

(a) 1atm

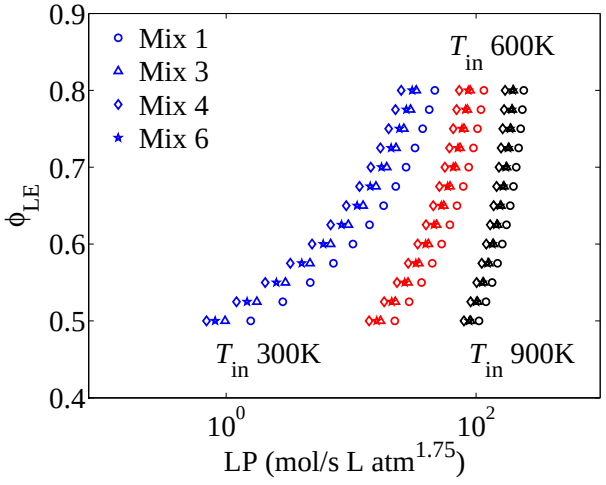

(b) 2atm

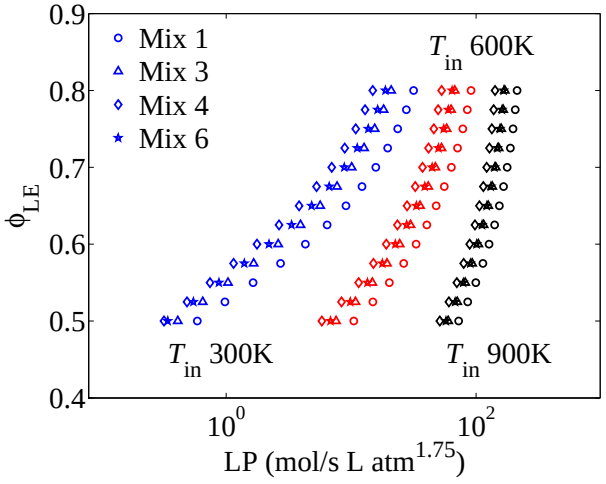

(c) 4atm

Figure 4.3: ϕ_{LE} versus LP as computed by the GRI-Mech 3.0 mechanism, at three different T_{in} in (blue 300K, red 600K, black 900K) comparing three mixes to Mix 6 at three operating pressures: (a) 1atm, (b) 2atm, and (c) 4atm.

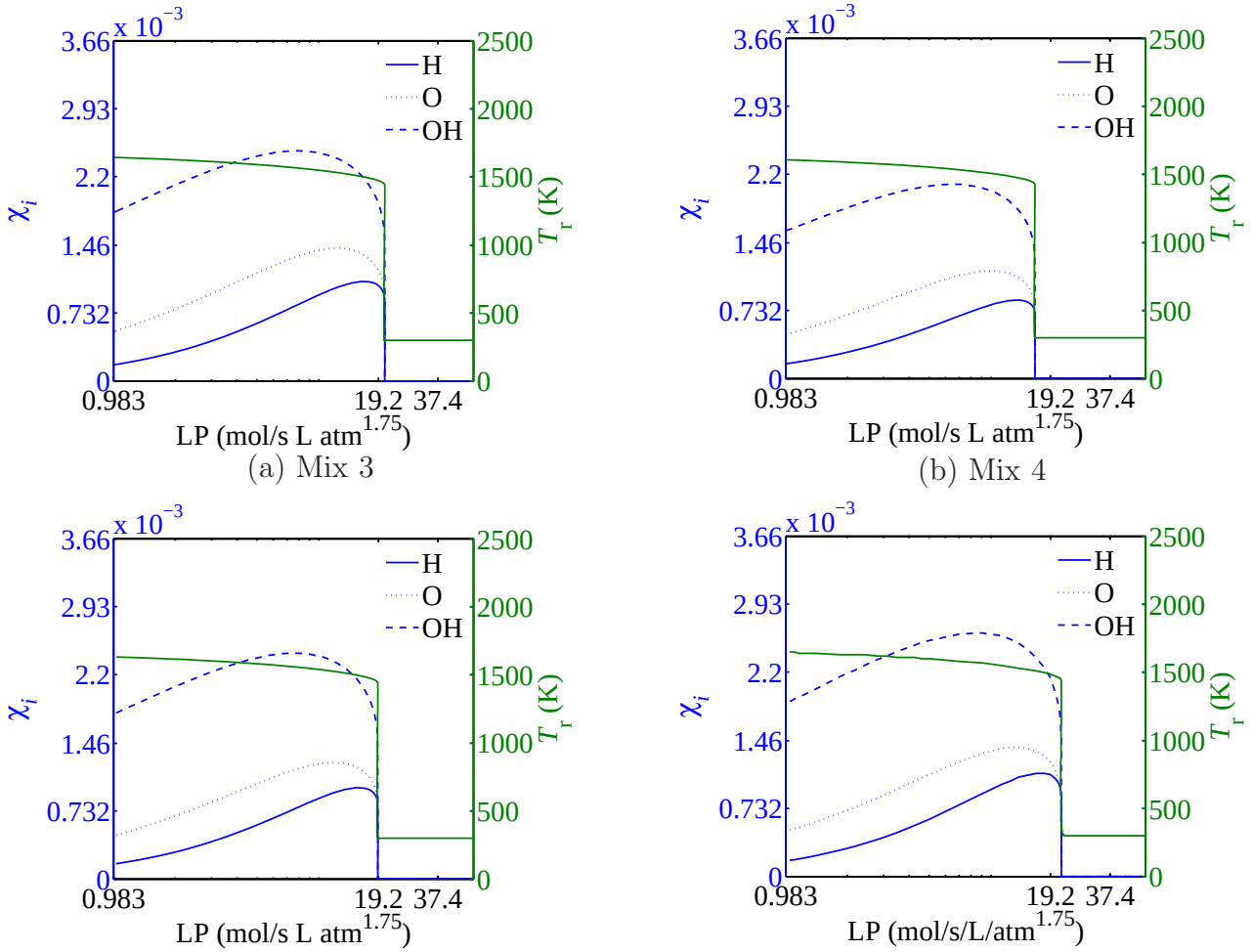

(a) Mix 3

(b) Mix 4

(c) Mix 6

(d) 50% CH_4, 16.6% CO_2, 33.4% N_2

Figure 4.4: Mole fraction of three radical species and Tr versus LP as computed by GRI-Mech 3.0 at $P_r = 1$atm, $\phi = 0.65$, $T_{in} = 300$K for three different mixes: (a) Mix 3, (b) Mix 4, (c) Mix 5, and (d) 50% CH_4, 16.6% CO_2, 33.4% N_2.

content and pressure. This change in behavior is similar to that seen in the laminar flame speed study presented in Chapter 3 though speed was affected more by temperature below this limit. For consistency both fits have the same form

$$\frac{\dot{N}}{VP_{\mathrm{r}}^{n}} = C_1 \exp\left\{C_2 T_{\mathrm{in}}\right\} \phi^{z} \tag{4.2}$$

where the values of C_1, C_2 and z are different for the two fits. The dependence of fuel-lean extinction on fuel content is approximately logarithmic, so C_1 is a function of the form

$$C_1 = C_3 \ln x_{\mathrm{f}} + C_4 \tag{4.3}$$

See Table 4.3 for the values of C_2, C_3 and C_4. The term that makes up z is more complex and contains two functions of the form of Eq. (4.1) where both terms include a temperature correction. A further pressure correction was also necessary to improve fit. For $\phi_{\mathrm{LE}} < 0.6$, z is

$$z\left(\phi_{\mathrm{LE}} < 0.6\right) = \left(\frac{P_{\mathrm{r}}}{101325}\right)^{-0.38} \left(\left(0.0007 T_{\mathrm{in}} - 0.542\right) \ln x_{\mathrm{f}} + 1\right) \left(\ln x_{\mathrm{f}} + 16\right) \exp\left\{-0.0025 T_{\mathrm{in}}\right\} \tag{4.4}$$

And for $\phi_{\mathrm{LE}}\, 0.6$, z is

$$z\left(\phi_{\mathrm{LE}} > 0.6\right) = \left(\frac{P_{\mathrm{r}}}{101325}\right)^{-0.38} \left(\left(0.0011 T_{\mathrm{in}} - 0.942\right) \ln x_{\mathrm{f}} + 1\right) \left(\ln x_{\mathrm{f}} + 6.5\right) \exp\left\{-0.002 T_{\mathrm{in}}\right\}$$

The temperature and pressure dependence of z is not seen in similar expressions describing fuel-lean extinction for pure fuels [97]. These dependencies may be due to the kinetic

influence of CO_2 and require further investigation.

Table 4.3: Conditions used in kinetics simulations

	$\phi_{LE} < 0.6$	$\phi_{LE} > 0.6$
$C_1\,(C_3)$	515	74.25
$C_1\,(C_4)$	1000	113
C_2	-0.0075	0.0013
n	1.975	1.75

As noted by Zelina and Ballal in their work with propane, the value of n changes with ϕ_{LE}. These simulations suggest that n varies from 1.75 to 1.975 as ϕ_{LE} decreases whereas Zelina and Ballal indicate that n varies linearly from 1 to 1.25 with ϕ_{LE} [96]. The value of n for all values of ϕ_{LE} is consistent with that predicted by Longwell and Weiss (1.8, [2]).

It is important to note that the method presented here to predict fuel-fuel-lean extinction is limited to CO_2 diluted CH_4-air flames. The presence of other diluents will affect the extinction point as shown earlier. The results of the fit are plotted with the results of some representative simulations in Fig. 4.5. The value of n in Fig. 4.5 changes at ϕ_{LE} of 0.625 from 1.975 to 1.75 to be consistent with the curve fits. Fuel-lean extinction points for conditions similar to those found in micro-GT combustors (P_r 2atm-4atm and Tin 600K-900K) shows good qualitative agreement between predictions and simulations. The most accurate fits are made for ϕ_{LE} ¿ 0.6 due to the more comparable behavior for these extinction points across the range of temperatures, pressures and fuel mixes simulated. For cases where ϕ_{LE} falls below 0.6, the Tin dependence was closer to quadratic than it was to exponential as suggested by Eq. (4.1). This leads to increasing error at the extreme values of Tin where the divergence from exponential behavior is greatest. Lower mole fractions of CH_4 in the

fuel (e.g., Mix 5 in Fig. 4.5(c)) are also less accurate due to deviation from the logarithmic dependence on CH_4 mole fraction at low T_{in}.

4.4 Conclusions

In this work a series of detailed chemical kinetics simulations using a perfectly-stirred reactor model to investigate the effect of different of fuel dilution on fuel-lean extinction limits were performed. The fuel, CH_4, and diluent, CO_2 or a mixture of CO_2, H_2O, and N_2, mixtures were chosen to be representative of the alternative fuel biogas from different sources. Reactor operating conditions were chosen to simulate conditions within the combustor of a micro gas-turbine for use in a distributed generation application. It was found that increasing the diluent content of the fuel increases ϕ_{LE} for a fixed LP (i.e., reduces the fuel-lean extent of the stability loop) across the range of operating conditions simulated. Increasing inlet temperature decreases ϕ_{LE} for a fixed LP (i.e., expands the fuel-lean extent of the stability loop) for all fuel mixtures. By comparing two fuel mixtures with similar CH_4 contents but different diluent constituents, it was determined that pure CO2 dilution reduces the mole fraction of H radicals present in the reactor. Replacing the CO_2 with a mixture of CO_2, H_2O and N_2 increases the mole fraction of H in the reactor which is consistent with previous work from others [160]. The effect of the increased mole fraction of H as well as other radicals due to reduced CO_2 content is to reduce ϕ_{LE} at a fixed LP.

A set of equations to predict LP at fuel-lean extinction for dry fuel mixes of CH_4 diluted with CO_2 were developed. They suggest that reactor loading has a power law relation with ϕ_{LE}, the influence of fuel CH_4 mole fraction is logarithmic, and the dependence on inlet temperature is exponential. The fit was broken into two ranges around a ϕ_{LE} of 0.6 based

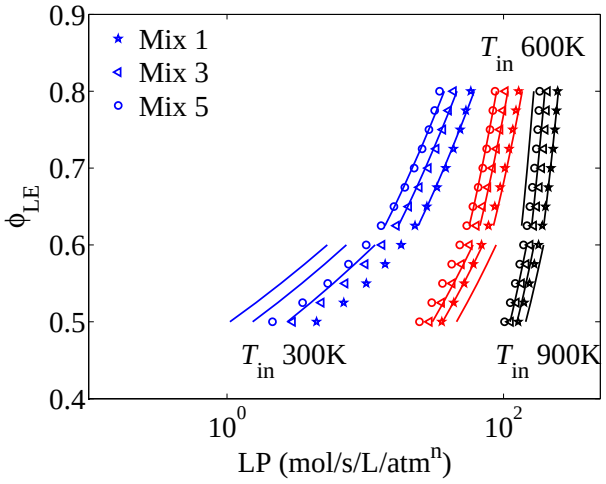

(a) 1atm

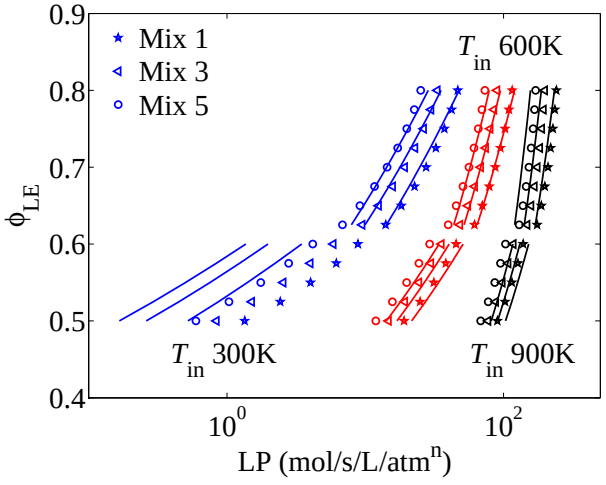

(b) 2atm

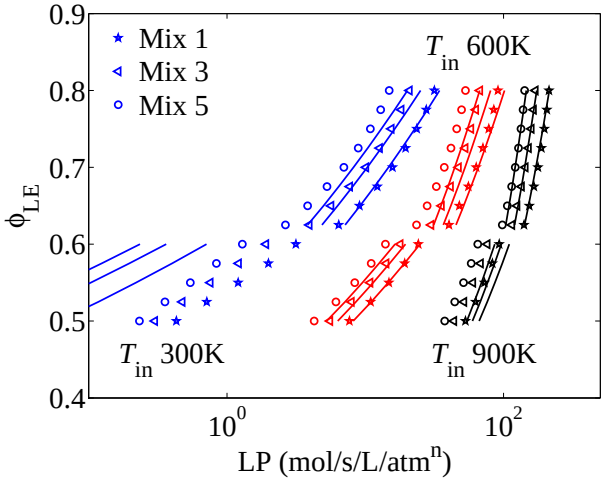

(c) 4atm

Figure 4.5: ϕ_{LE} versus LP as computed by three mechanisms (stars GRI-Mech 3.0, diamonds GRI-Mech 1.2 reduced, squares San Diego) at three different Tin (blue 300K, red 600K, black 900K) and three different operating pressures for Mix 3: (a) 1atm, (b) 2atm, and (c) 4atm.

on an apparent change in the relation between ϕ_{LE} and LP at this point. Above ϕ_{LE}=0.6, the fuel-lean extinction points behaved in a similar fashion over the range of reactor conditions tested than it did below. The influence of inlet temperature and pressure are consistent with previous experimental work by others, [2], [96], and [131]. The dependence on fuel CH_4 mole fraction as well as the exponent of ϕ_{LE} requires experimental validation. Expansion of the method to include other diluents is also recommended.

Chapter 5

A Test Facility for WSR Experiments

The operation of a WSR requires several layers of precision equipment. A facility capable of safely and accurately operating a WSR for future alternative fuels research at MSU would be of great use in this important field. This chapter describes a facility currently under construction including the reactor design, safety equipment, and the emissions measurement and sampling systems.

5.1 WSR Design

As discussed in Chapter 2.5, the primary goal of the laboratory-scale, practical WSR is to achieve a state of near uniformity with in the reactor volume. The aim of this facility is to simulate the conditions in the primary-zone of a micro-GT combustor. After careful evaluation of the designs found in the archival literature, it was decided that the toroidal design is best suited for this application. Its toroidal flow pattern is similar to that caused by the combination of induced axial swirl and a sudden increase in flow area found in many modern fuel-lean premixed GT combustors. This reactor has also been shown to approach a well-stirred state over a substantial portion of its volume [10].

The reactor design chosen for this facility is identical to that designed by Nenniger [125] and modified by Zelina [10] and later by Stouffer [129]. The basic design features a ceramic 250 cm^3 torroidal reactor cast in two halves, shown pictorially in Figure 5.1 and schematically

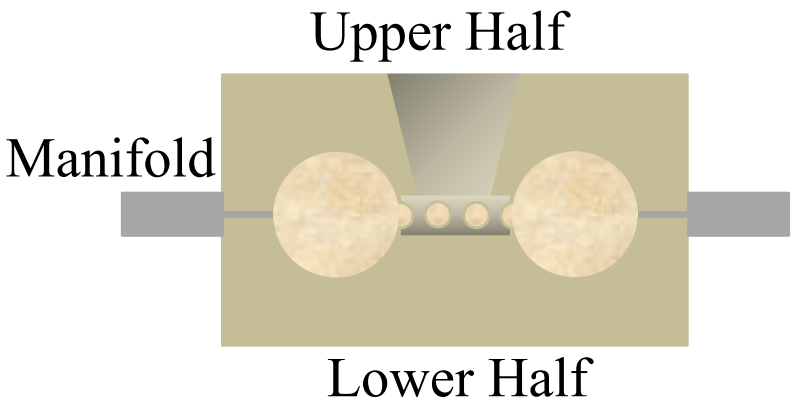

Figure 5.1: A cut view schematic of the assembled WSR with components identified.

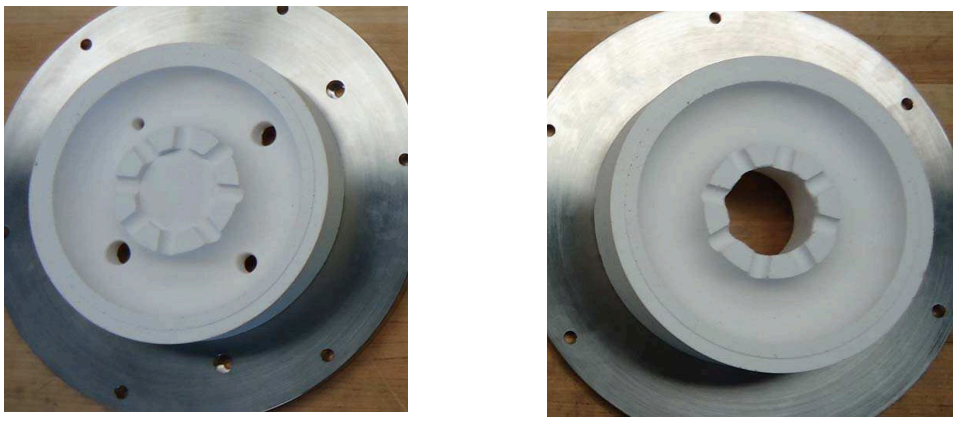

Figure 5.2: An image of the ceramic halves of the toroidal WSR.

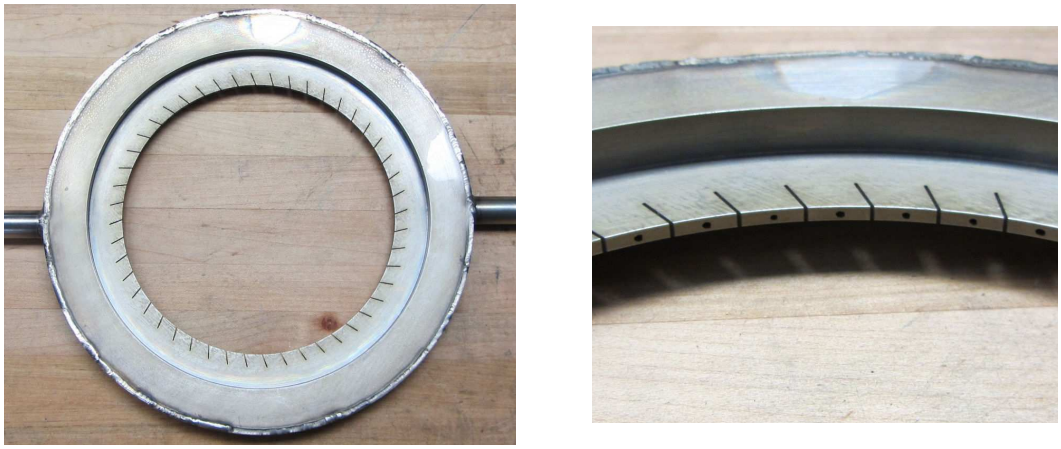

Figure 5.3: An image of the fuel-air manifold and jet ring showing the injection nozzles.

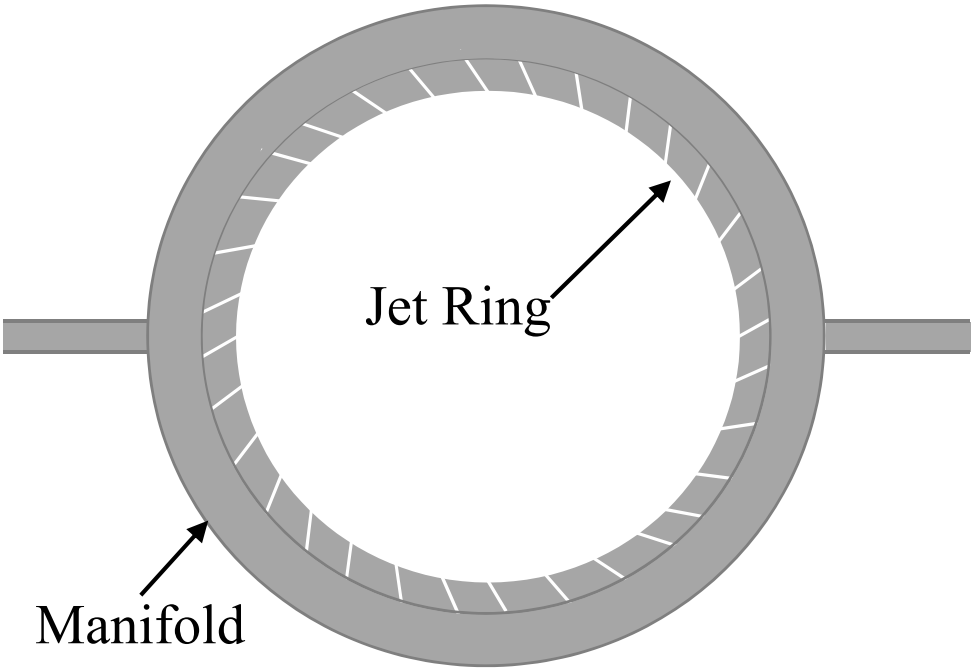

Figure 5.4: A schematic of the fuel/air manifold and jet ring.

in Figure 5.2. The lower half has four access ports along its center-line for an ignition source and temperature, pressure, and emissions measurement equipment. The upper half has an exhaust port at it's center. Sandwiched between the two reactor halves is the fuel-air manifold and jet ring, see Figure 5.3. Fresh fuel-air mixture is fed to the reactor through the jet ring. Within the reactor the fresh mixture is rapidly mixed with product gases. The high temperature product gases provides the necessary energy to initiate the combustion of the fresh mixture. Product gases are exhausted through eight ports at the center of the torus. This process is shown schematically in Figure 5.5.

Special materials are required for the manufacture of the reactor halves due to the extreme conditions at which they are expected to operate. To maintain the conditions stipulated for

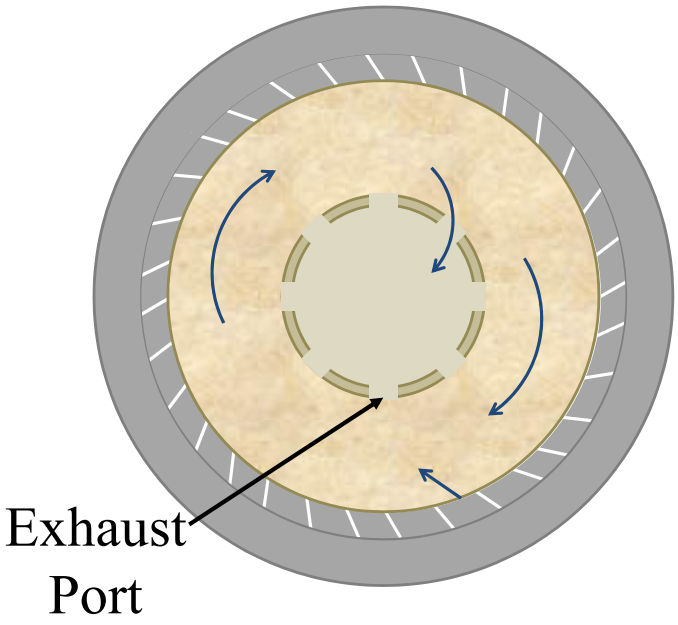

Figure 5.5: A schematic the mixing of product and reactant gases.

well-stirred operation, the reactor must be nearly adiabatic. It must also be able to survive some thermal cycling and extended periods of elevated temperature conditions. Finally, the reactor must withstand the frictional forces associated with the high speed flows necessary to maintain well-stirred conditions.

Reactors constructed of two materials. The first is an alumina ceramic. This material is commonly used in high temperature applications. Alumina is somewhat delicate and prone to cracking and is intended for use in less demanding tests (i.e., those without fast thermal cycling). For more extreme experiments, a reactor cast of silica-carbide is available. This material withstands cycling better than the alumina but is also more expensive.

Uniform delivery of the premixed fuel and air is of paramount importance to maintaining well-stirred conditions. The fuel-air manifold and jet ring, shown schematically in Figure 5.4,

are constructed of nickel alloys and provide the high velocity inflow condition necessary to maintain well-stirred operation. The reactant mixture enters through the two feed tubes and is exhausted into the WSR by forty-eight jets of 1 mm inner diameter. The jets are angled 20° off radial which promotes efficient mixing [95]. High velocity is achieved by maintaining a sufficient pressure drop across the jets to guarantee a sonic or near sonic exit condition. To prevent autoignition in the manifold, it is cooled by impinging flows of nitrogen from above and below.

Assembly of the WSR is a straight forward process. The jet ring is first aligned and sandwiched between the two reactor halves. To prevent catastrophic failure of the reactor, both halves are wrapped in thin steel bands. This assembly is held together by two steel plates tethered by threaded rods. The lower plate has access ports and plumbing connections which align with those in the lower reactor half. Once the end plates are in place the WSR is ready to be lowered into its containment vessel.

5.2 Housing and Exhaust

The containment vessel is made of welded steel flanges and pipe designed to hold the WSR and provide connection points to the required feed and monitoring systems. The vessel is manufactured from 0.925 cm thick and 30 cm inner diameter steel pipe. Like the reactor, the vessel consists of two parts. The lower part has connections for the fuel-air feed system, nitrogen cooling system and access to the ports on the lower steel plate of the WSR assembly. The upper part has a flange for mating to the exhaust section. At this point the containment vessel is not designed to be gas tight. initially all experiments envisioned for the facility are to be conducted at atmospheric pressure. Thus, the vessel does not need to be sealed. This

further reduces the risk of catastrophic failure of the vessel. In the future if high pressure experiments are desired, the vessel may be modified in a manner similar to that used by Stouffer et al. in their development of a high pressure WSR facility.

The exhaust section varies depending on the experiment to be performed, generally consists of a 15 cm inner diameter steel pipe lined with alumina sleeves. The sleeves reduce its inner diameter to the desired test section for a plug flow reactor (PFR) or the diameter of the exhaust port of the WSR (5 cm). Its purpose is to direct the effluent of the WSR into the facilities ventilation system as well as provide additional residence time to complete combustion. The exhaust is transformed into a PFR with the addition of a flow straightener in the exhaust port of the WSR. Specialized sections can be added to provide connections for air and water (for cooling, combustion completion in high ϕ experiments) as well as adapters for measurement probes.

5.3 Facility

All experiments are carried out in the Turbomachinery Research Laboratory in the Engineering Building at Michigan State University. A combination of standard building systems and custom built equipment supply the facility. Compressed air and cold water are supplied by building systems. The supplied air is filtered (0.01 μm) and dried to a dew point no greater than 275K before being fed into the metering and control system. Fuel, diluents and nitrogen are supplied from bottles through custom manifolds. The fuel, air and, nitrogen piping systems are shown schematically in the Appendix.

Experimental conditions are set using LabView (National Instruments) control system (DAQ and VI) which monitors the fuel and air handling systems. Air flow rate is controlled

by a Brooks thermal mass flow controller (SLA5853) capable of controlling flow between 100 and 1100 SLPM with an accuracy of 1% of full scale. The fuel is metered through a Dwyer thermal mass flow controller (GFC-1144) capable of supplying 0 to 500 SLPM at an accuracy of 1.5% of full scale. A rotometer and needle valve are in-line with the flow controller for calibration. Diluents are metered by a similar Dwyer thermal mass flow controller to that used in the fuel system. Flow measurements are corrected for temperature and pressure variations in real time using T-type thermocouples and pressure transducers in the piping system.

To operate in well-stirred conditions, the fuel and air are required to completely premixed and at a controlled temperature before entering the reactor. Prior to mixing with the fuel, the air is heated to simulate the temperature conditions leaving the compressor of a GT. This is accomplished by a 3 kW electric heater (WatLow). Air temperature upstream and downstream of the heater is monitored by thermocouples to detect conditions that may cause damage to the heating element. A PID temperature controller (Love Controls Series 16c) is used to hold desired temperature conditions at a thermocouple placed in the stream after fuel is mixed. Mixing of the fuel and air is ensured by flowing through a static mixer.

The fuel and air systems are capable of feeding the reactor over a wide range of operating conditions. Residence times can be varied from 2.5 to 23ms and inlet temperatures up to 450K are possible. This allows for a range of reactor loading levels to be investigated while operating at the relatively safer condition of atmospheric pressure. Equivalency ratios can be varied from fuel-lean extinction to $\phi = 2$.

Safety systems are multi-layered and located through out the facility. Product gases are removed by a ventilation system capable of exhausting 42,500 SLPM. A positive flow switch is used to indicate sufficient exhaust flow to the control system. Emergency shut-off

switches as well as hazardous gas monitors are located throughout the facility. Fuel flow is automatically ceased by activation of any of the switches, an alarm from the gas monitor, a low flow rate condition in the ventilation system or a loss of power to the facility. Experiments are monitored from a control room located a safe distance from the reactor assembly.

5.4 Emissions Analyzers

Two VA-3000 series (Horiba) emissions systems containing a total of 5 analyzer modules are available for use in experiments. The five modules are: VA-3111 CO_2 $0 - 25\%$, VA-3111 CO 0-10000ppmV, VA-3111 CH_4 0-10000ppmV, VA-3012 NO_x 0-2000ppmV, and VA-3012 SO_2 0-2000ppmV. Emissions samples are prepared in a pair of Horiba VS-3000 series sample conditioners (VS-3001 for the VA-3111 and VS-3003 for the VA-3012) each drawing 500 mL per minute. To prevent condensation, emissions are fed from the sampling probe to the sample conditioners in a heated sample line maintained above 328 K.

The analyzers measuring CO_2, CO, CH_4, and SO_2 rely on the non-dispersive infrared (NDIR) technique. Gases absorb and emit light in specific spectra depending on their constituents. The NDIR detector uses an infrared light source tuned to the spectra of a specific species which is directed through the measurement cell to a detector. Modulation via a chopper wheel is used to offset thermal background signals. When the sample gas flows into the measurement cell, it absorbs the light proportional to the concentration of the species of interest altering the intensity of the light reaching the detector. A reference gas, in this case N_2, flows through a second chamber to provide a baseline signal.

Measurement of NO_x concentrations is made using the chemilluminescence principle. Within the sample conditioning unit (VS-3003) any NO_2 is converted to NO and ozone (O_3)

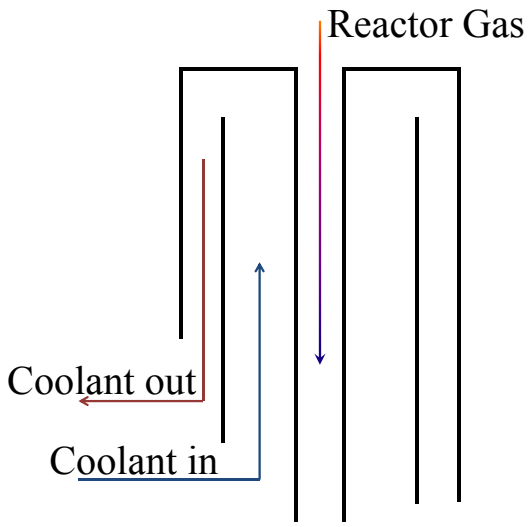

Figure 5.6: Schematic of the emissions sampling probe.

is generated. These two streams are fed to the detector unit in which the following reaction occurs:

$$NO + O_3 \rightarrow NO_2{}^* + O_2 \tag{5.1}$$

where the $NO_2{}^*$ molecules are in an excited state. As they return to the ground state they release energy according to

$$NO_2{}^* \rightarrow NO_2 + hv \tag{5.2}$$

where h is Planck's constant and v is the frequency of the emitted light. The intensity of the emitted light, detected and amplified by a photomultiplier, is proportional to the concentration of NO before the reaction. Because the NO_2 in the sample was converted to NO in the conditioner, the measurement representative of the NO_x in the sample.

5.5 Sample Probe

To withdraw gas from the WSR an oil-cooled stainless steel sample probe was designed following the work of Blust et al. [162]. The probe consists of three concentric stainless steel tubes, see Figure 5.6. The innermost tube conveys the sampled gas through the probe to the sample line. The two larger tubes are designed to allow a pathway for the cooling oil to pas. Oil heated to 425 K by a MOKON HTF 350 is used to cool the probe and quench any reactions.

5.6 Conclusion

This chapter has described a WSR facility designed for installation in the Turbomachinery Research Laboratory at MSU. The initial construction of the facility has been completed. Much of the necessary infrastructure including the fuel, reactor and cooling air, and auxiliary cooling system has been finished. Preliminary work on the control and pollutant emissions measurement equipment has also been completed. The remainder of the work to be done has been described here in a manner to allow completion by future workers.

Chapter 6

Combined Cycle Steam Power Generation and Cooling

The benefits offered by using GT engines in power generation at small scales also apply to medium (¡10MWe) and large scales. These larger turbines, which are now used for both peaking and base load, have higher air flow rates and exhaust temperatures due to their use of simple Brayton cycle architectures. This excess energy can be used to generate steam for a Rankine cycle plant that increases overall system fuel efficiency. In a distributed generation system, combined-cycle plants can be used to provide clean, fuel flexible base load near large population or manufacturing centers. In this chapter a background review of combined-cycles, their uses and the need for advances in cooling technology are discussed.

6.1 Combined Cycles

To further increase the fuel efficiency of GT engines used in electric power generation, they may be grouped with a water vapor cycle to produce additional power. The aggressive, high temperature environment that the hot-sections of GT engines are designed to survive make ideal hot gas generators. However, GTs are limited by the exit pressure which must remain in a range dictated by the surge limit of the compressor and the pressure drop of the exhaust system. The high exhaust temperature ($\approx$ 800K) caused by the exhaust gas pressure

considerations limits the possible thermal efficiency of the Brayton cycle. The Rankine cycle is well suited to take advantage of the exhaust temperatures from the GT. Fuel efficiency is increased by using the exhaust in a heat recovery steam generator. Efficiency gains are increased by the condenser of the Rankine cycle which lowers the minimum temperature of the combined cycles. The different temperature regimes lead to the GT being referred to as the topping cycle and the steam system being referred to the bottoming cycle. The two cycles may be linked on a single shaft, both cycles power the same electric generator, or multi-shaft arrangements where each cycle powers its own electric generator.

6.1.1 Topping Cycle

The simple, open Brayton cycle was described generally in Chapter 1 and ideally consists of isentropic compression, isobaric combustion and isentropic expansion stages, an example T-s diagram is in Figure 6.1. In Large industrial turbines, compression (station 1t to station 2t) is accomplished by multiple stages of axial or centrifugal compressors and power extraction/expansion (station 3t to station 4t) by multiple stages of axial turbines. Combustion systems are similar to those described in Chapters 1 and 2. Recuperation is difficult at this scale due to the size of the heat exchanger required.

The topping cycle's primary levers to increase the fuel efficiency of the combined cycle are compressor pressure ratio and turbine inlet temperature. The cycle efficiency of the topping cycle may be written as

$$\eta_{\mathrm{t}} = \frac{\dot{W}_{3\mathrm{t}-4\mathrm{t}} - \dot{W}_{2\mathrm{t}-1\mathrm{t}}}{\dot{Q}_{3\mathrm{t}-2\mathrm{t}}} \tag{6.1}$$

assuming a cold air-standard cycle with constant specific heats and negligible fuel flow

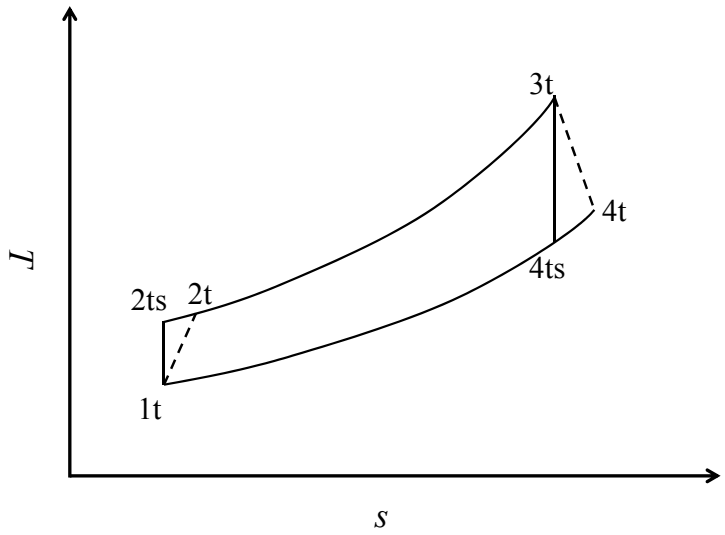

Figure 6.1: A T-s diagram of the simple, open Brayton cycle.

compared to air flow, Eq. 6.1 may be rewritten as [163]

$$\eta_{\mathrm{t}} = 1 - \frac{1}{\left(\frac{P_{2\mathrm{t}}}{P_{1\mathrm{t}}}\right)^{\frac{\gamma-1}{\gamma}}} \tag{6.2}$$

Increasing pressure ratio will increase topping cycle efficiency when turbine inlet temperature is fixed. Similarly, increasing the turbine inlet temperature increases the fuel efficiency of the topping cycle for a fixed pressure ratio through increasing the Carnot efficiency. Maximum compressor pressure ratios are limited by footprint and shaft dynamics considerations. Aero-derivative GT engines traditionally have higher pressure ratios than other types of industrial turbines owing to their initial design operating environment of the upper troposphere. Turbine inlet temperatures are limited by available hot-section materials for all GT engines. The development of thermal barrier coatings and film cooling of high pressure turbine stages have progressively increased temperatures. However, life and system complexity considerations limit turbine inlet temperature to about 1200K. Improved high temperature

material properties is an area of intense research.

6.1.2 Bottoming Cycle

The hot gas exiting the topping cycle at 4t is used as the heat source for the bottoming cycle shown in Figure 6.2. A simple Rankine cycle is shown here as an illustration, but more complex cycles can be used. Water is pumped up to operating pressure (stations 1b to 2b) before being fed to the boiler. The boiler (stations 2b to 3b') in combined cycle plants is a heat recovery steam generator placed in the exhaust stream of the topping cycle. It may include an economizer and superheater depending on the final application of the steam. In electrical power production both are usually used. The expansion of the steam (stations 3b' to 4b) is accomplished through a steam turbine (for mechanical drive or electricity generation) or other equipment depending on application (e.g., absorption chiller, district heating system, etc.). Steam condensation is accomplished between stations 4b and 1b. Because the bottoming cycle uses the waste heat from the topping cycle, its major influence on the efficiency of the plant is through the condenser.

Like the topping cycle, efficiency gains to the combined cycle are made through the heat exchangers. The efficiency of the bottoming cycle may be written as

$$\eta_{\mathrm{b}} = \frac{\dot{W}_{3\mathrm{b}\prime-4\mathrm{b}} - \dot{W}_{2\mathrm{b}-1\mathrm{b}}}{\dot{Q}_{3\mathrm{b}\prime-2\mathrm{b}}} \tag{6.3}$$

Several studies of full scale steam power plants, without topping cycles, have indicated that the boiler and condenser are the primary sources of energy escape [164, 165, 166]. For a combined-cycle plant the boiler is using waste heat from the topping cycle. If no additional heat input is necessary for super-heating, then there are no additional combustion losses in

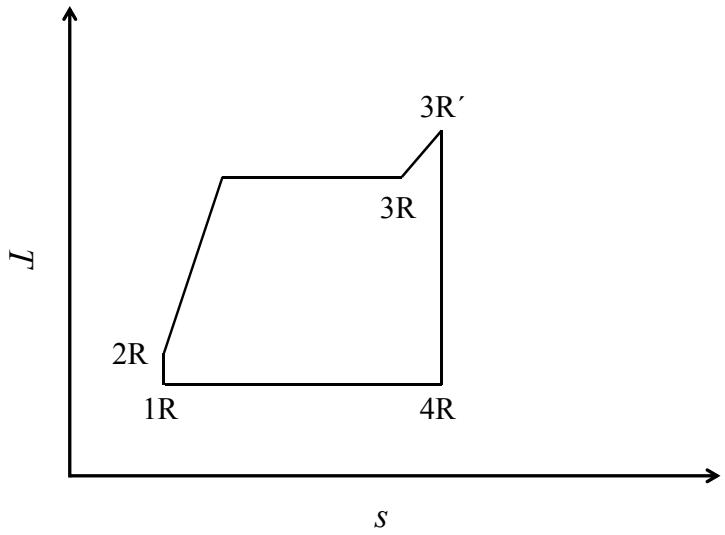

Figure 6.2: A T-s diagram of the Rankine cycle with superheat.

the bottoming cycle. Looking more specifically at the turbine

$$\eta_{\mathrm{b,turb}} = \frac{h_{4\mathrm{b}} - h_{3\mathrm{b}\prime}}{h_{4\mathrm{bs}} - h_{3\mathrm{b}\prime}} \tag{6.4}$$

The condenser is a lever to adjust combined cycle plant fuel efficiency by changing the bottoming cycle temperature at station 4b. Lowering this temperature, thus increasing the pressure drop across the turbine for the same boiler temperature, increases the work output of the plant and increases its efficiency for the same heat input [167, 168]. The focus of the remainder of this work is a method of lowering bottoming cycle condenser pressure and reducing its seasonal variability.

6.2 Use of Combined Cycle Power Plants in Distributed Generation

Industrial and dense population centers are better suited to large power generating stations. In a distributed power generation system these areas could be powered by medium to large scale combined-cycle plants. Unlike the micro-GTs discussed previously, the large industrial GTs used in the combined-cycle plants will likely be sited near more traditional fuel sources like natural gas pipe lines. These sources are commonly available near industrial and population centers. The choice of the cooling source for the bottoming-cycle is a primary concern when siting a large combined-cycle or steam power plant power plant near its load. However, condenser cooling options may be limited by climate or regulatory factors.

6.2.1 Cooling Cycles

The combined-cycle's low temperature is usually dictated by one of three cooling cycles currently in use for steam condensing: single pass, closed loop and dry cooling. Shell and tube condensers are most common for the wet methods with the coolant flowing through the tube side and the steam through the shell side. Dry cooling systems use different heat exchanger geometries. The amount of possible cooling from these methods is dependent to some extent on the ambient conditions. Hybrid systems, combining closed loop and dry cooling, attempt to minimize the variability by changing the cooling technique depending on the season.

Single pass cooling systems use large quantities of water making a single transit through the condenser before being discharged. The total flow of water is dictated not only by cycle requirements but also by local regulations which limit temperature rise in the coolant

source. Maximum temperature rise limitations (e.g., The Clean Water Act of 1972) have been enacted to reduce or eliminate the effect on aquatic species of thermal plumes resulting from the discharge of cooling water. In addition, these limit reduce water consumption by the condensers by limiting evaporation. These limits increase the flow of water required. The regulations also place restrictions on cooling water inlet construction to ensure sufficiently low inlet velocities to avoid ingestion of fish, shell fish and aquatic plants. Steam condenser operating temperatures for single pass systems are limited by the water source's temperature which in most cases is seasonably variable [14].

Closed-loop cooling systems use less water than open-loop systems but consume more through evaporation. The heat absorbed from the steam by the coolant is released through direct contact with atmospheric air in a cooling tower. Rather than passing through the condenser a single time, the water continuously circulates between the condenser and the cooling tower. Make up water is added to the loop to replace that lost through evaporation. Minimum cycle temperatures in the steam cycle are dictated by the wet bulb temperature of the air entering the cooling tower.

Water consumption and usage is reduced or eliminated in dry and hybrid cooling systems. In dry cooling the water in the steam loop is cooled by indirect contact with air in a cooling tower. Minimum cycle temperature varies with ambient temperature and humidity limiting the utility of dry cooling systems in hot, arid environments. Hybrid cooling systems use cooling towers equipped for both dry and closed loop cooling. The system in use depends changes seasonally with ambient conditions to minimize water consumption.

Population growth and changes in climate have led to concern over the management of limited water resources. In regions located far from ocean coasts, steam condenser cooling may compete with agricultural and domestic uses for fresh water. Some municipalities now

mandate that a certain percentage of cooling water used in steam condensers be reclaimed (i.e., treated sewage) to reduce the consumption of potable water [11]. Recent heat waves in western Europe led to output reductions and shutdown at a number of plants due to insufficient cooling. Drought conditions have exacerbated the issue by reducing the quantity of cooling water available [169]. Dry cooling systems, despite the additional capital costs associated with them, have received more interest to eliminate the need for cooling water to avoid these power reductions/shutdowns [170].

6.2.2 Alternative Cooling Approaches

A group of alternative cooling techniques using ammonia in addition to water are under investigation. One proposed alternative uses a phase change ammonia loop to augment a wet-dry hybrid cooling system. The addition of the ammonia loop reduces the capital costs of a dry cooling system by 25 to 45% [171]. In a similar system proposed by Goswami et al. , the working fluid is a binary mixture of ammonia and water which is used to produce shaft power, through a turbine, and refrigeration (tri-generation). The binary vapor mixture leaving the turbine is sufficiently cool to chill water through transfer of sensible heat. The mixture then passes through a water cooled absorber to condense [172]. This system was proposed to use low temperature heat sources like solar and geothermal.

A second proposed system uses excess power available during off peak load hours to charge a cooling storage system with a hybrid cooling system. Two turbines are cooled by a dry cooling system, first turbine, and a closed-loop wet cooling system, second turbine. Power from the second turbine is used to drive a refrigeration system for the cooling storage or directly cool the wet condenser. Warm water leaving the wet cooling system passes through the cold storage system rather than a cooling tower to reject the absorbed heat. Depending

on configuration, the output of the plant can be increased by up to 33% at 50°C [173]. This design was modified to include two refrigeration systems and three modes of operation. When grid demand is small enough to drive the first refrigeration system with the excess available power, the condenser water is cooled directly by refrigeration. If enough excess power is available to drive both refrigeration systems, the second refrigeration system is used to charge the cooling storage system. Finally, at peak demand the condenser is cooled using the cooling storage system. This modification to the cycle further increases the plant's power output at peak demand [174].

6.3 Conclusions

In this chapter the design and application of combined cycle power plants has been discussed. Focus was on the limits placed on the steam condenser of the bottoming cycle by both environmental and regulatory changes. From this review the following conclusions were drawn:

- Combined cycle power plants use the best features of the Brayton (topping) and Rankine (bottoming) cycles to increase overall plant efficiency
- The efficiency of the combined cycles is limited by operating temperature of the steam condenser in the bottoming cycle
- Most current cooling technologies, both wet and dry, cause condenser operating temperature to be seasonally variable
- Governmental and environmental pressures are limiting the water available for wet condenser cooling

- Dry cooling systems add up to 15% to the cost of electricity generation
- Alternative cooling approaches based on refrigeration technology are a promising path to reducing or eliminating water usage and stabilizing plant efficiency

Chapter 7 discusses the design and preliminary testing of a proof of concept test rig for a VCRS cooled steam condenser. A condenser of this type would have applications in larger combined cycle power plants as a part of a more distributed electrical generation system.

Chapter 7

Refrigerant Cooled Steam Condenser

Here we investigate using a vapor-compression refrigeration system (VCRS) to cool a steam condenser. Both well documented in literature and commercially viable, a VCRS offers an intriguing solution to steam condenser cooling issues. There is no requirement for cooling water unlike wet cooling systems, though water may be used to cool the condenser of the VCRS. Additionally, refrigerants offer better heat transfer rates and lower operating temperatures compared to water or air. Unlike dry cooling, VCRS operating temperatures would not depend on the local dry bulb temperature. In this chapter we discuss different cooling cycles, the development of a novel, reduced-scale experimental model of a VCRS cooled steam condenser and some preliminary results of experiments conducted with R-410a as a steam condenser coolant.

7.1 Cooling Fluids and Coolant Cycles

A number of refrigerant cycles may be integrated into the bottoming cycle of a combined-cycle plant for condenser cooling. All will be a parasitic load on the plant. In many cases it may be preferable to use these mechanical cooling systems to augment traditional condenser cooling approaches rather than as stand alone systems. Optimization of the cooling cycle is beyond the scope of this work.

Excess heat from either the topping cycle or bottoming cycle could be used to drive a

vapor absorption chiller. The heat source may come from a bleed off either the GT exhaust gas entering the heat recovery steam generator (HRSG) or the steam generated. Such a system is similar to the hybrid power-cooling systems described earlier [171, 172]. The work input required by an absorption chiller system would be less than that required by a similarly sized VCRS. The trade-off is a lower COP compared to a VCRS and a required secondary cooling source to maintain a suitable absorber temperature.

A Brayton refrigeration cycle implemented between the steam condenser (cold region) and the ambient environment (hot region) is a possible solution in warmer climates. Similar systems, on smaller scales, are used in aircraft cabin cooling applications. Other than for start up, a Brayton refrigeration system would be minimally parasitic to the combined-cycle plant unlike an absorption chiller or VCRS. However the cycle does not include a phase change of the refrigerant; thus, it is less efficient than a VCRS or absorption chiller. To compensate, larger mass flows of coolant would be required resulting in a larger footprint and more expensive turbomachinery.

Recent work has investigated, in more detail, the specifics of integrating a VCRS into a vapor power generation loop. An analytic study has compared water to R-134a for condenser cooling. The authors found that R-134a outperforms water [175]. In a continuation of the study, R-134a was compared to several other commercial refrigerants. Of the refrigerants studied, R-410a performed the best due to its higher operating pressure and heat transfer properties [176]. As noted in Chapter 6 the work of Hegazy has identified potential methods of integrating a VCRS cooled steam condenser into a standard steam power plant [173, 174].

7.2 A Refrigerant Cooled Steam Condenser Test Rig

To perform proof-of-concept testing for a VCRS cooled steam condenser, a novel reduced-scale model of the system has been constructed. The facility is located in the Turbomachinery Research Laboratory at Michigan State University. All utilities are provided by building connections. The initial design consisted of a commercially available steam generator, domestic air conditioner condenser unit and a commercial ASME 150lb rated shell and tube steam condenser. A three-loop system, including a chilled water loop, was ultimately necessary for safety and economic reasons, see Figure 7.1 for a schematic and Figure 7.2 for photos. The additional chilled water loop is an intermediate step that is convenient for experiments. A commercial system would eliminate this loop.

The first loop in the system was the open steam loop. Steam was supplied by a 9kW commercial steam generator (CMB-9A, Chromalox, Pittsburgh, PA). The heat rate was fixed and steam was supplied in a saturated condition. Consequently, steam mass flow rate is dictated by the temperature set point and inlet water temperature. The water level in the boiler was maintained at a safe level by a boiler-feed-water valve. Practically, the maximum saturation temperature was limited by water feed pressure. The system was capable of producing steam at a pressure of up to 68.9 kPa less than feed pressure (377.1 kPa in this facility). For safety reasons pressure was ultimately limited by a 790.8 kPa pressure relief valve. The steam ran in an open loop from the building water supply through the steam generator and the shell side of the steam condenser (SX2000U, Standard-Xchange, Buffalo, NY) to a building drain. A thermostatic condensate valve and water column were used to maintain pressure inside the steam condenser. The capabilities of the condensate valve limit the minimum steam condenser pressure to -30.500 kPa. Condensate flow rates were

measured by using a graduated tank installed between the exit of the condenser and the drain and hand operated timer.

Due to a lack of commercially available shell an tube heat exchangers rated for the high pressures necessary for R-410a use in a vapor-vapor exchanger, an intermediate, closed chilled-water loop was added. This loop used a commercially available R-410a-water shell and tube heat exchanger, intermediate heat exchanger (IHX), (SST-200A, Standard Refrigeration, Wood Dale, IL) as a link to the VCRS loop and the ASME rated shell and tube steam condenser as a link to the open steam loop. The water flows through the tube side of the steam condenser and the tube side of the water chiller. Water is circulated through the system by a variable speed pump. Safety in this loop is provided by a high pressure switch, a low temperature switch, to prevent freezing, and a pressure relief valve. System performance measurements are made in this loop due to the relative safety of pressurized water compared to refrigerant or steam. Water flow rate is measured by a rotameter (FLD107, Omega Engineering, Inc., Stamford, CT), temperature is measured by T-type thermocouples and pressure is measured by bourdon gauges. Operating conditions in this loop are listed in Table 7.1.

The VCRS loop was based on a commercially available domestic air conditioner condenser charged with R-410a. The condenser unit (Dayton 3.0 Ton 14.5 SEER, Grainger, Chicago, IL) and the steam generator were matched in power consumption. Chilled water temperature was adjusted by the refrigerant charge and pressure. A pressure relief valve and high pressure switch were used to maintain safe operation of the system. Short cycling of the AC compressor is prevented by a pressure regulator that smoothly loads the system. A pair of filter/driers in the liquid and vapor lines kept debris out of the thermal-expansion valve and refrigerant compressor, respectively. An accumulator tank and a section of heated

tubing ensured that only refrigerant vapor is fed to the compressor. Heat from the refrigerant condenser is rejected to the room where building systems are used to remove it from the area.

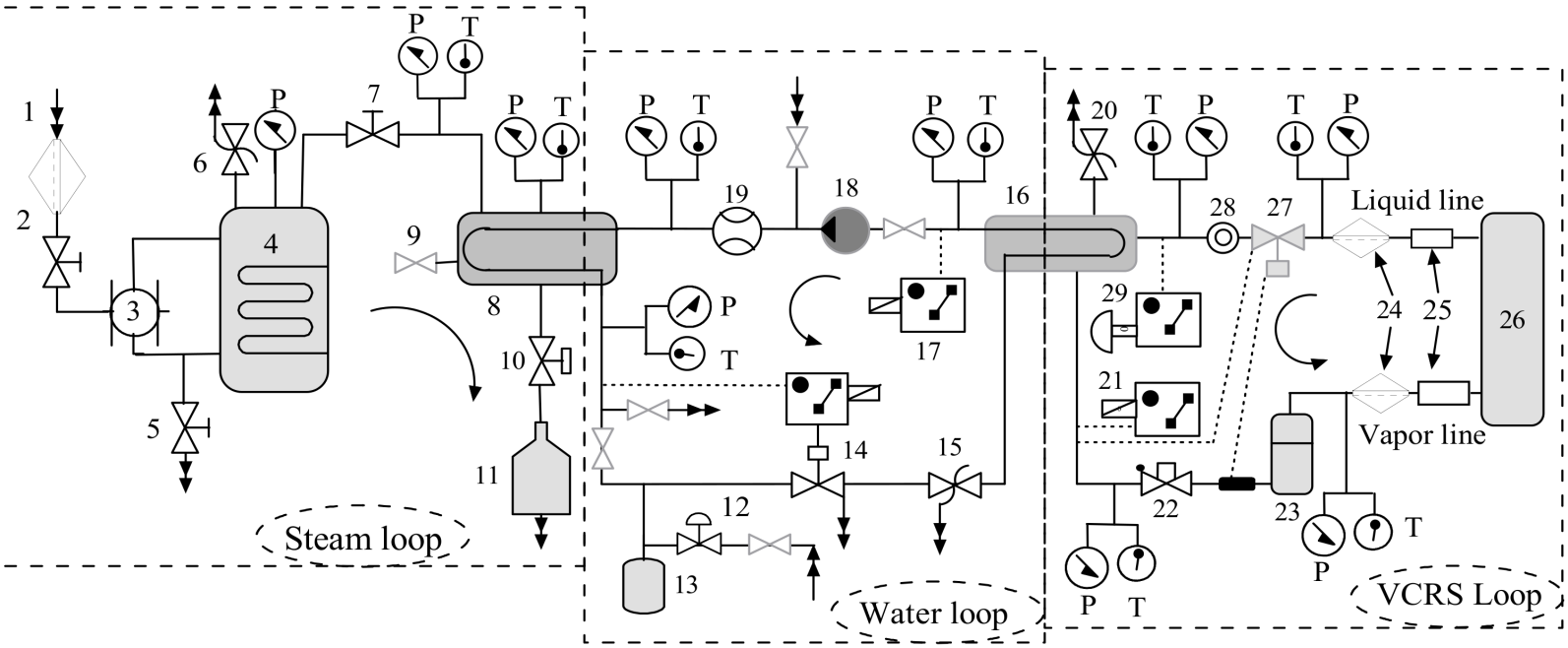

Figure 7.1: Experimental layout: Steam loop: 1-Water source, 2- filter and ball valve, 3-Float control valve, 4-Boiler, 5-Drain valve, 6-Pressure relief valve, 7-Steam outlet valve, 8-Condenser, 9-Air vent valve, 10-Thermostatic check valve, 11-Graduated tank; Water loop: 12-Pressure reducing valve, 13-Thermal expansion tank, 14-high pressure switch, 15-pressure relief valve, 16-Intermediate heat exchanger, 17-low temperature switch, 18-Circulator pump, 19-Rotameter; VCRS loop: 20-pressure relief valve, 21-low pressure switch, 22-pressure regulator, 23-accumulator, 24-filter driers, 25-Vibration absorber, 26-AC unit, 27-TXV, 28-Glass Screen, 29-high pressure switch.

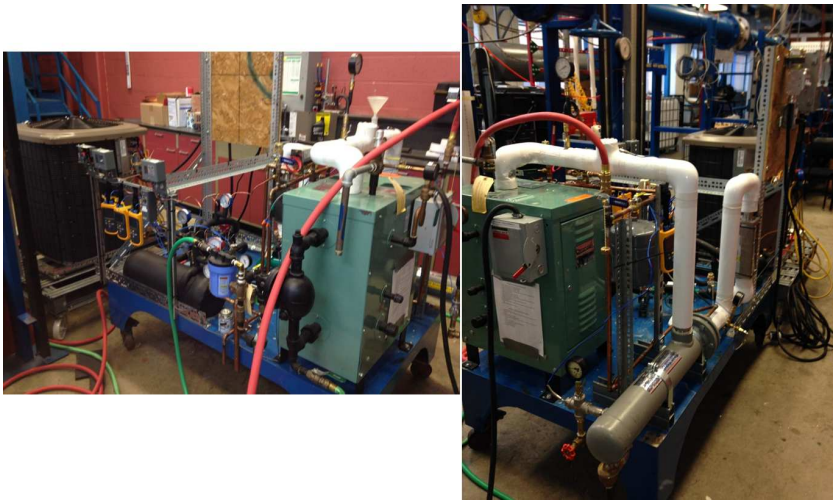

Figure 7.2: Photo of the assembled reduced scale refrigerant cooled steam condenser.

To ensure safe operation of the entire test system, experiments were carried out in a manner that kept the VCRS loop within design constraints. The steam loop and chilled water loops were started first to provide a heat load to the VCRS loop. Once an adequate load was established, the VCRS was brought on line and allowed to stabilize. Settings in the steam and chilled water loops were adjusted to meet intended operating conditions once the VCRS was stable. Heat losses in the steam system required the saturation temperature set point to be about 1°C above that required by the desired condenser pressure. Refrigerant pressures were closely monitored at all times. Test conditions were chosen to best match the power output from the steam condenser to that absorbed by the VCRS loop. This minimized safety risks.

System performance measurements are made once a safe, stable operating point has been established. Equilibrium was determined to be when system temperatures varied by less than the accuracy of the measurements, see Table 7.2, for six minutes. At each operating point fluid temperatures and pressures in all three loops and input voltage and current to the VCRS condenser unit were measured. The VCRS power measurement includes both the

compressor and condenser cooling fan loads. The duration of each measurement was 3 to 5 minutes. Variations in water loop pressure had a negligible effect on system operation and is ignored here. The heat rejected by the steam condenser was calculated by

$$\dot{Q} = \dot{m}_{\mathrm{cw}} c_{\mathrm{P\,cw}} \left(T_{\mathrm{cw,out}} - T_{\mathrm{cw,in}} \right) \tag{7.1}$$

where the condenser is assumed to be adiabatic due to the insulation. In all equations in this chapter subscript cw refers to the cooling water and subscript R is refrigerant. Similarly the flow rate of refrigerant is calculated based on the heat balance between the VCRS and chilled water loops across the IHX

$$\dot{m}_{\mathrm{R}} \left(c_{\mathrm{PR,vap}} T_{\mathrm{R,out}} - c_{\mathrm{PR,liq}} T_{\mathrm{R,in}} \right) = \dot{m}_{\mathrm{cw}} c_{\mathrm{P\,cw}} \left(T_{\mathrm{cw,out}} - T_{\mathrm{cw,in}} \right) \tag{7.2}$$

VCRS COP is calculated using

$$\mathrm{COP} = \frac{\dot{m}_{\mathrm{cw}} \left(T_{\mathrm{cw,out}} - T_{\mathrm{cw,in}} \right)}{(VI)_{\mathrm{AC}}} \tag{7.3}$$

Finally, the overall heat transfer coefficient U_{o} is calculated from

$$U_{\mathrm{o}} = \frac{\dot{m}_{\mathrm{cw}} \left(c_{\mathrm{P}} T_{\mathrm{cw,out}} - T_{\mathrm{cw,in}} \right)}{A_{\mathrm{o}} \mathrm{LMTD}} \tag{7.4}$$

where A_{o} is the outer surface area of the condenser tubes and LMTD is calculated with

$$\mathrm{LMTD} = \frac{\left(T_{\mathrm{cw,out}} - T_{\mathrm{cw,in}} \right)}{\ln \frac{T_{\mathrm{sat}} - T_{\mathrm{cw,in}}}{T_{\mathrm{sat}} - T_{\mathrm{cw,out}}}} \tag{7.5}$$

These relations, COP and U_{o}, will be used to evaluate the condenser test rig.

The data collected from the new test rig can also be used to investigate different proposed empirical correlations for the Nusselt number of film condensation for a R-410a cooled condenser. Models of this type were first developed by Nusselt. He assumed that the wall of the tubes were at constant temperature, the condensate film was laminar, the thickness of the film was small compared to the tube diameter, heat transfer in the film was limited to conduction only, the temperature distribution inside the film is linear and that all properties are constant. This resulted in the well known relation [177]

$$\bar{\mathrm{Nu}} = 0.728 \left(\frac{\rho_{\mathrm{cond}}^2 g h_{\mathrm{fg}} D^3}{\mu_{\mathrm{cond}} k_{\mathrm{cond}} \bar{\Delta T}} \right)^{0.25} = 0.728 \left(F \tilde{Re}^2 \right)^{0.25} \tag{7.6}$$

where $F = \dfrac{g D_{\mathrm{o}} h_{\mathrm{fg}} \mu_{\mathrm{cond}}}{k_{\mathrm{cond}} \Delta T u_{\infty}}$, $\tilde{\mathrm{Re}} = \dfrac{\rho_{\mathrm{cond}} u D_{\mathrm{o}}}{\mu_{\mathrm{cond}}}$ is the two-phase Reynolds number, $\bar{\Delta T}$ is calculated by

$$\Delta T = T_{\mathrm{sat}} - T_{\mathrm{w}} \tag{7.7}$$

$$T_{\mathrm{w}} = \frac{T_{\mathrm{cw,in}} + T_{\mathrm{cw,out}}}{2} \tag{7.8}$$

and all condensate properties are calculated at $T^* = \dfrac{2}{3} T_{\mathrm{w}} + \dfrac{1}{3} T_{\mathrm{sat}}$. Shekriladze and Gomerlauri [178] took vapor shear into account by assuming the cylinder wall was isothermal, the condensate film is laminar and boundary layer separation can be neglected. Their derivation resulted in

$$\bar{\mathrm{Nu}} \tilde{\mathrm{Re}}^{-0.5} = 0.64 \left(1 + (1 + 1.69F)^{0.5} \right)^{0.5} \tag{7.9}$$

Butterworth adapted for pure vapors Eq 7.9 by taking into account low vapor velocities [179]

$$\bar{\mathrm{Nu}} \tilde{\mathrm{Re}}^{-0.5} = 0.416 \left(1 + (1 + 9.47F)^{0.5} \right)^{0.5} \tag{7.10}$$

Rose further modified Eq 7.9 to

$$\bar{\mathrm{Nu}}\tilde{\mathrm{Re}}^{-0.5} = \frac{0.9 + 0.728F^{0.5}}{\left(1 + 3.44F^{0.5} + F\right)^{0.25}} \tag{7.11}$$

Fujii et al. performed a series of experiments on low pressure steam condensation through tube banks of different arrangements. This experimental data was correlated by [180]

$$\bar{\mathrm{Nu}}\tilde{\mathrm{Re}}^{-0.5} = 0.96F^{0.2} \tag{7.12}$$

Lakshmi et al. developed a mathematical model for the condensation of turbulent films flowing both parallel and normal to horizontal condenser tubes. It was assumed constant heat flux at the tube wall. They concluded that condenser pressure and steam approach velocity have a significant effect on the heat transfer coefficient. The following correlation was proposed [181]

$$\bar{\mathrm{Nu}}_{\mathrm{t}}\tilde{\mathrm{Re}}^{-0.5} = 0.8732\frac{\varphi^{0.3124}}{(FS)^{0.03376}\ q^{0.1306}} \tag{7.13}$$

$$\bar{\mathrm{Nu}}_{\mathrm{l}}\tilde{\mathrm{Re}}^{-0.5} = 0.4103\frac{(FS)^{1/3}}{q^{1/3}} \tag{7.14}$$

$$\bar{\mathrm{Nu}}^3 = \bar{\mathrm{Nu}}_{\mathrm{t}}^3 + \bar{\mathrm{Nu}}_{\mathrm{l}}^3 \tag{7.15}$$

These empirical formulations will be compared to the present experimental data to determine the best fit for the VCRS cooled steam condenser.

Table 7.1: Operating conditions of the three-loop VCRS cooled steam condenser test rig

$\dot{m}_{\mathrm{H_2O}}$	Condenser $\mathrm{H_2O}$ T_{in}	Condenser P
56 to 131 g/s	9 to 32°C	−30.5 to 0 kPa

Table 7.2: Estimated experimental measurement error for experiments with the three-loop VCRS cooled steam condenser

Device	Measurement	Error
Rotameter	Water Volume Flow Rate	±3% of full scale
Thermocouple	Fluid Temperature	±0.3°C
Condensate Collector	Condensate Volume Flow Rate	±3.3%
Calculated Parameter	Coolant Water Mass Flow Rate	±3.01%
–	Heat Rejection	±3.9%
–	LMTD	±2.59%
–	COP	±4.42%
–	U_o	±4.15%
–	Refrigerant Mass Flow Rate	±4.32%
–	$\tilde{Re}$	±5.1%
–	F	±4.30%
–	$\tilde{Nu}$	±0.34%
–	$\bar{Nu}\tilde{Re}$	±3.06%

7.3 Preliminary Experimental Results

Figure 7.3 shows the effect of inlet coolant water temperature on the condensate and refrigerant mass flow rates. Decreasing the coolant water temperature increases the rate of steam condensation due to the increased temperature difference between steam and coolant, similar trends were observed by [182]. For the same inlet coolant temperature, when water flow rate increases the condensation and refrigerant mass flow rates also increase. Figure 7.3 can be used for selection of the required R-410a mass flow to condense 1 kg of steam at a design condition.

The effect of changes in R-410a mass flow rate on heat rejected to the ambient and COP of the VCRS is shown in Figure 7.4. Decreasing inlet coolant temperature, which increased the rate of condensation and refrigerant mass flow rate, increased the heat rejection. Similarly, increasing cooling water flow rate also increased heat rejection. Trends of this type have been

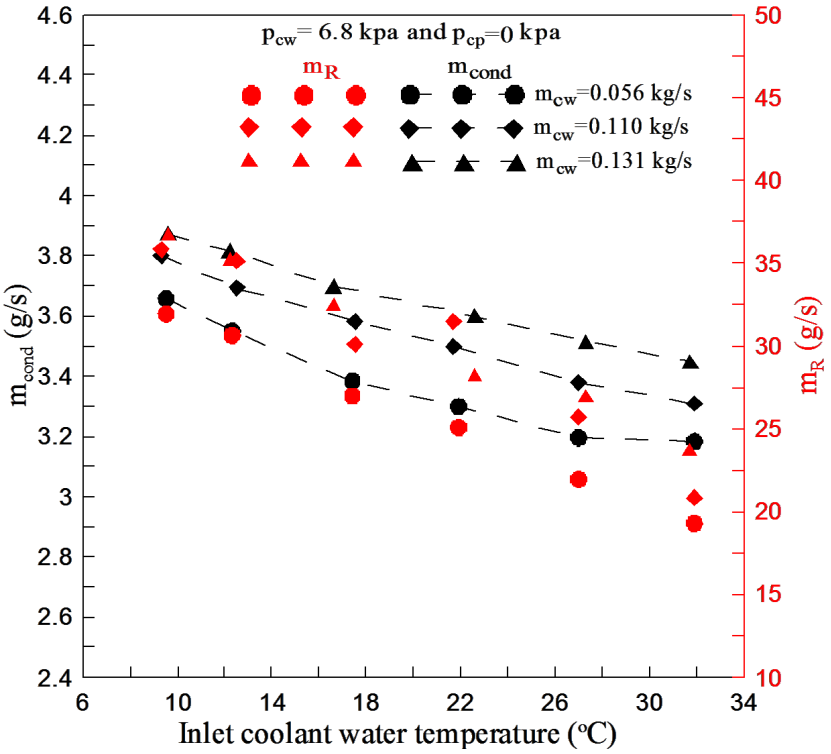

Figure 7.3: Condensation rate and R-410a mass flow rates at p_{cw}=6.8kPa and p_{cp}=0kPa.

identified by other investigators [168], [182], [183]. The variation of COP with inlet coolant temperature is also shown in Figure 7.4. The COP of the VCRS increased with chilled water flow rate and decreased inlet coolant water temperature. Increasing COP by decreasing chilled water temperature increases the overall steam power plant efficiency by decreasing the power demand of the VCRS and reducing the temperature of the steam condenser.

The effect of inlet coolant temperature and water mass flow rate on U_o is depicted in Figure 7.5. Decreasing inlet coolant temperature enhances U_o below 22°C. Above this temperature little change with inlet water temperature is noted. The trend with water mass flow rate is different than that seen in Figure 7.3 and Figure 7.4. This may be attributed to the reduction of outlet coolant temperature with increasing its mass flow rate. The result is a rate of increase of coolant heat rejection by less than the rate of increasing LMTD when

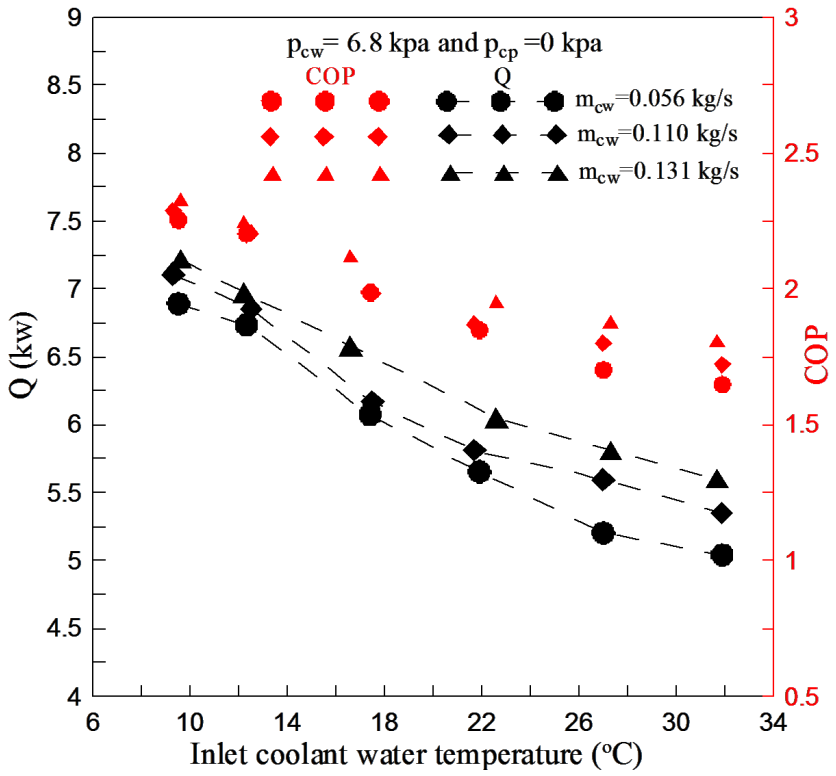

Figure 7.4: Heat rejection and COP at p_{cw}=6.8kPa and p_{cp}=0kPa.

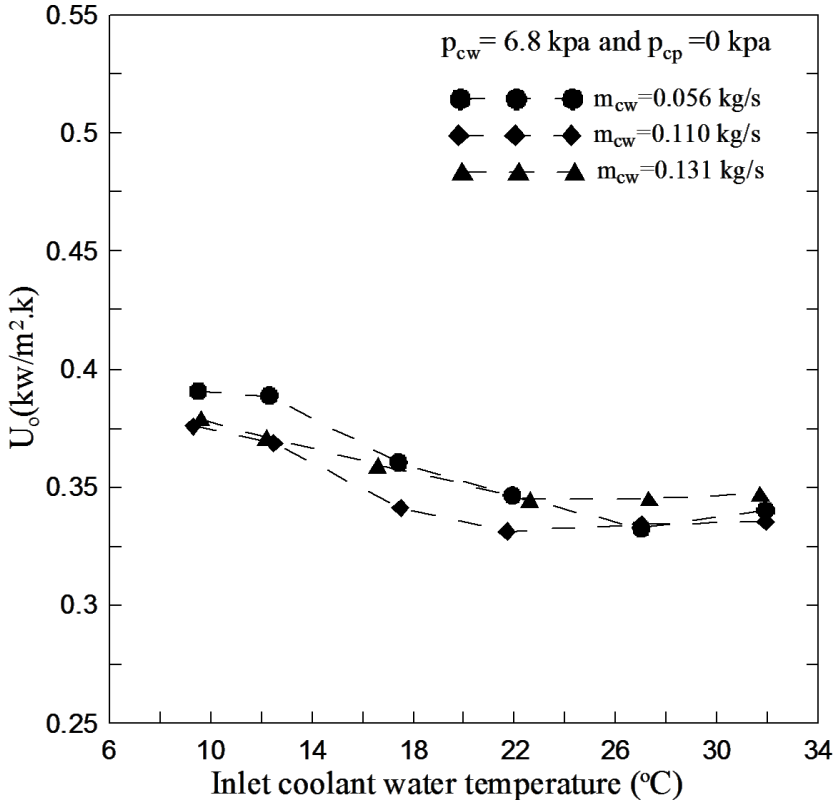

Figure 7.5: Overall heat transfer coefficient at $p_{cw} = 6.8$ kPa and $p_{cp} = 0$ kPa.

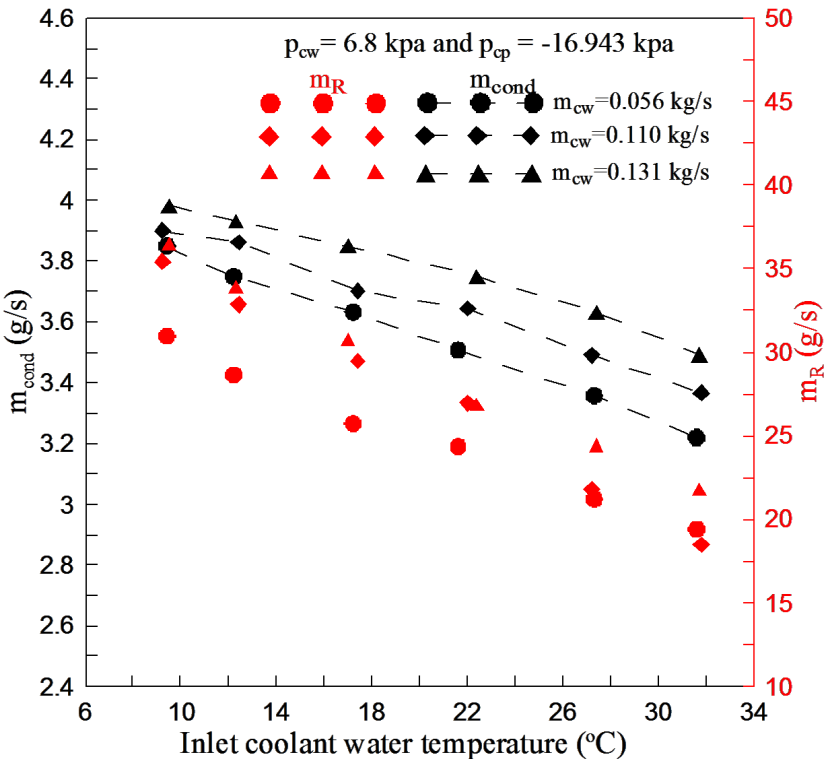

Figure 7.6: Condensation rate and R-410a mass flow rates at p_{cw} = 6.8 kPa and p_{cp} = −16.943 kPa.

the coolant temperature increases and coolant mass flow rate decreases.

Trends of condensation rate, refrigerant mass flow rate, heat rejection, COP and U_o are shown in Figures 7.6, 7.7 and 7.8, at $P_{cp} = -16.943$ kPa, and Figures 7.9, 7.10 and 7.11, at $P_{cp} = -30.500$ kPa. When comparing Figures 7.3, 7.6 and 7.9, it is evident that increased levels of vacuum result in higher rates of condensation and refrigerant mass flow. The rate of increase in the condensation rate is higher than the rate of increase in the refrigerant flow rate as condenser pressure decreases. That means that operating the steam condenser under vacuum will be more efficient for the VCRS when used in condenser cooling applications. This lower operating pressure enhances steam condenser performance and the overall steam cycle efficiency and decreases the condenser total temperature difference as reported elsewhere [167], [168].

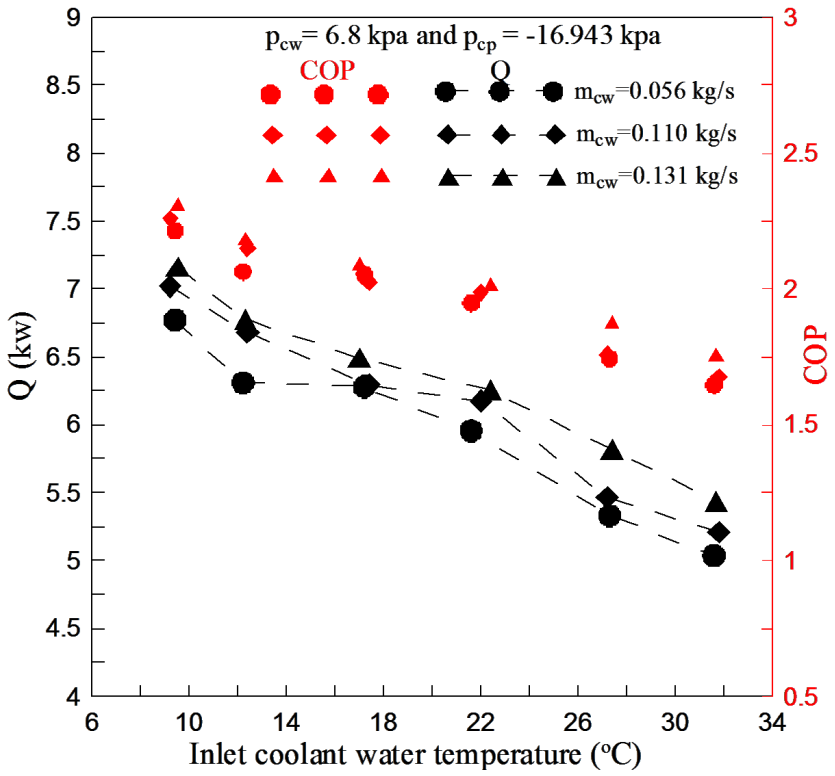

Figure 7.7: Heat rejection and COP at $p_{cw} = 6.8$ kPa and $p_{cp} = -16.943$ kPa.

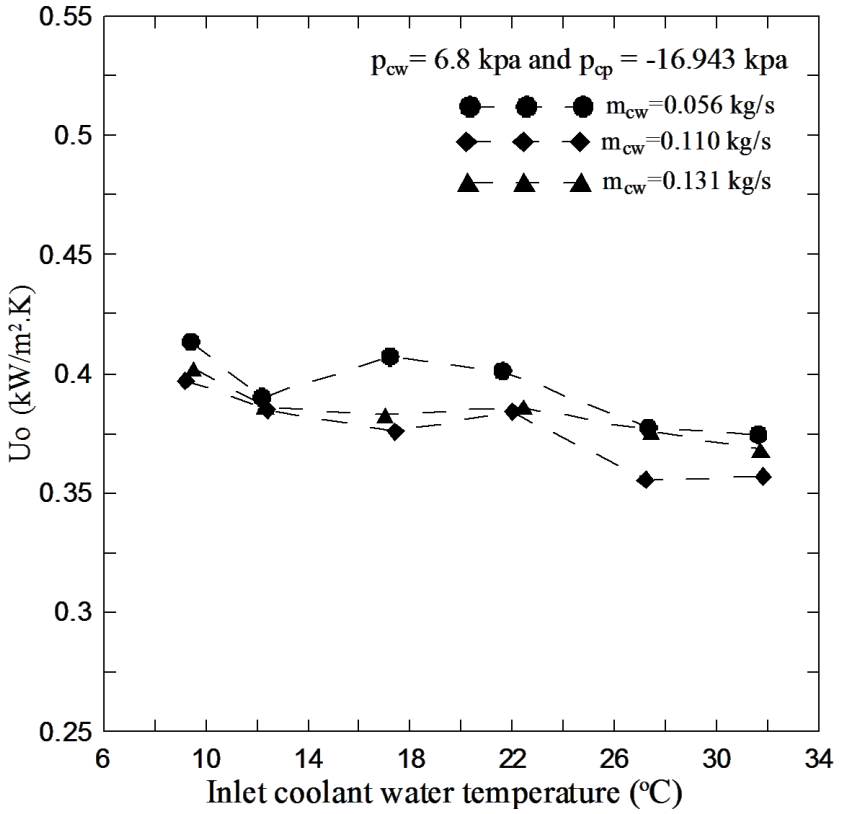

Figure 7.8: Overall heat transfer coefficient at $p_{cw} = 6.8$ kPa and $p_{cp} = -16.943 kpap$.

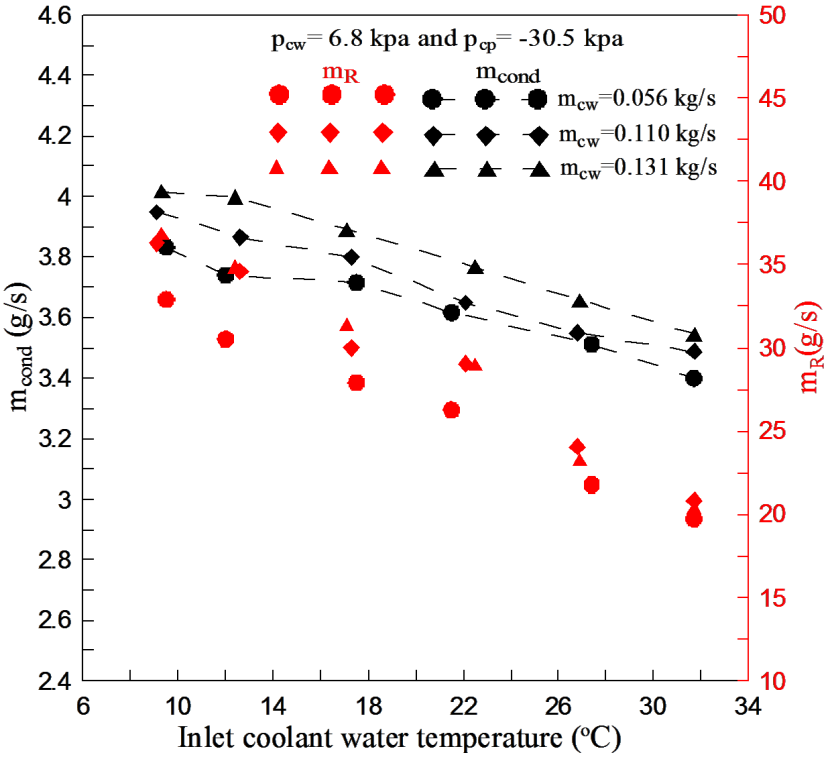

Figure 7.9: Condensation rate and R-410a mass flow rates at $p_{cw} = 6.8$ kPa and $p_{cp} = -30.5$ kPa.

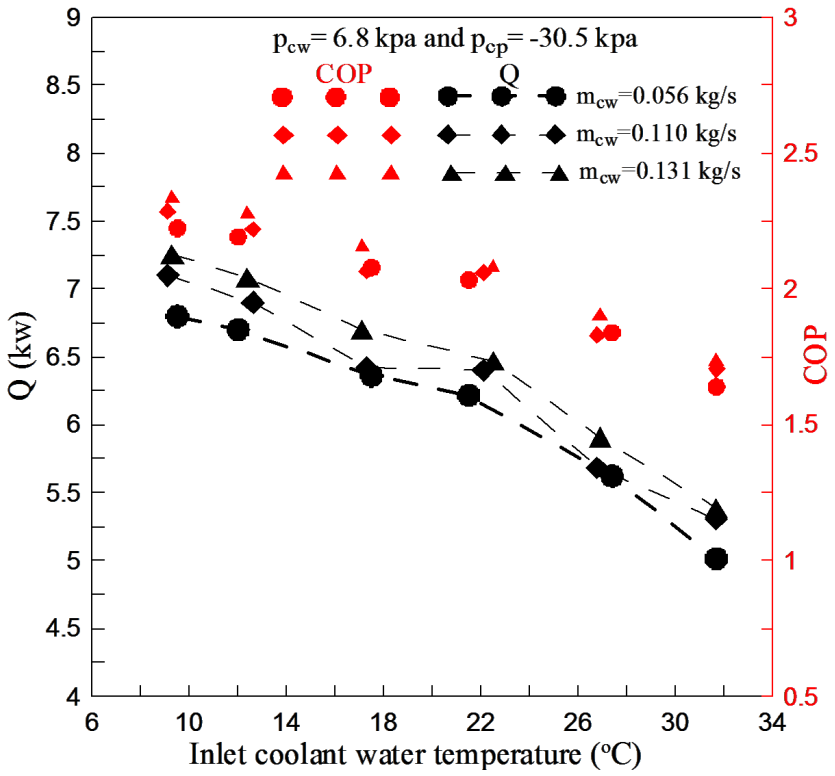

Figure 7.10: Heat rejection and COP at $p_{cw} = 6.8$ kPa and $p_{cp} = -30.5$ kPa.

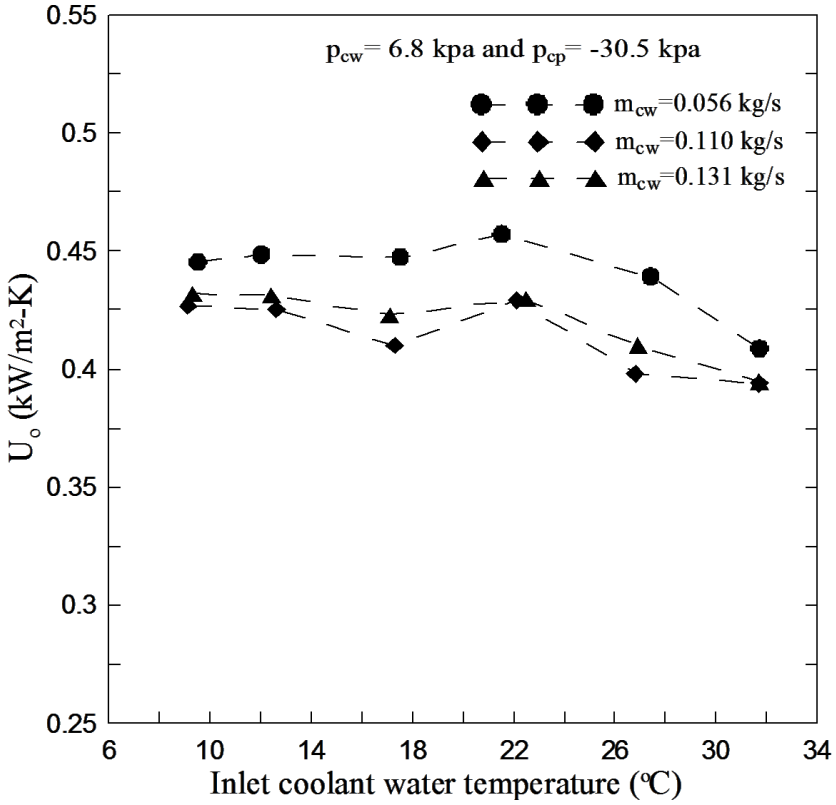

Figure 7.11: Overall heat transfer coefficient at $p_{cw} = 6.8$ kPa and $p_{cp} = -30.5$ kPa.

Comparing the corresponding Figures 7.4, 7.7 and 7.10 reveals that COP and heat rejection increase when both steam condenser pressure and inlet coolant water temperature decrease. Best performance occurs at $P_{\mathrm{cp}} = -30.500$ kPa and $\dot{m}_{\mathrm{cw}} = 0.131$kg/s as will be discussed later, see Table 7.3. Reducing the condenser pressure enhances U_{o} especially at $\dot{m}_{\mathrm{cw}} = 0.056$kg/s as evidenced on comparison of Figures 7.5, 7.8 and 7.11. A similar effect was documented by [184] that local heat transfer coefficient decreases with higher steam pressures. This may be attributed to the dependence of U_{o} on LMTD which depends on outlet coolant temperatures as discussed earlier.

The percentage variations of $\dot{m}_{\mathrm{cond}}$, Q, COP, $\dot{m}_{\mathrm{R-cw}}$, and U_{o} from a reference condition are tabulated in Table 7.3. The reference values are calculated at a coolant temperature of 31.9°C and condenser pressure of 0.000 kPa. At $\dot{m}_{\mathrm{cw}} = 0.056$kg/s by decreasing the coolant temperature from 31.9°C to 9.6°C results in enhancements of the condensation rate, heat rejection, COP, mass ratio and U_{o} of 14.94%, 36.66%, 36.61%, 44.05% and 14.92%, respectively. If in addition to reducing the coolant temperature from 31.9°C to 9.6°C, the condenser pressure is also reduced from $p_{\mathrm{cp}} = 0$ to -16.943 kPa, the levels of improvement changed to be 20.96%, 34.28%, 34.24%, 32.68% and 21.77%, respectively. Further, decrease of condenser pressure yields more improvement in performance as shown at $p_{\mathrm{cp}} = -30.500$ kPa in Table 7.3.

Similar trends are seen using the same calculation procedures at $\dot{m}_{\mathrm{cw}} = 0.11$ and 0.131kg/s. It may be inferred from Table 7.3 that working under more vacuum in the steam condenser increases the possible quantity of condensate. Moreover, it widens the pressure difference across the turbine which increases the work output. Both the decrease of $\dot{m}_{\mathrm{R-cw}}$ and increase of COP lead to a reduction in power consumption by the AC unit which increases system efficiency. The enhancement percentage ratio for U_{o} at $\dot{m}_{\mathrm{cw}} = 0.056$kg/s. As

U_o increases from 14.92% to 31% at $\dot{m}_{cw} = 0.056$kg/s while it increases from 9.1% to 24.4% at $\dot{m}_{cw} = 0.131$kg/s. The smaller levels of enhancement in U_o with increasing coolant mass flow rate at the same condenser pressure may be related to the outlet coolant temperature effect as discussed earlier.

Table 7.3: Percentage variations of condensation rate, heat rejection, COP, ratio of refrigerant to condensate mass flow rates and U_o compared to calculated values at a coolant temperature of 31.9°C and $p_{cp} = 0$kPa.

p_{cp} (kPa) \ $\dot{m}_{cw}$ (kg/s)		0.056	0.110	0.131
0	$\dot{m}_{cond}$ %	14.94	14.82	12.32
	Q %	36.66	32.84	28.81
	COP %	36.61	32.80	28.81
	$\dot{m}_{R-cw}$ %	44.05	49.52	38.34
	U_o %	14.92	12.24	9.10
−16.943	$\dot{m}_{cond}$ %	20.90	17.84	15.46
	Q %	34.28	31.16	27.83
	COP %	34.24	31.17	27.84
	$\dot{m}_{R-cw}$ %	32.68	44.17	33.60
	U_o %	21.77	18.57	15.80
−30.500	$\dot{m}_{cond}$ %	20.42	19.37	16.44
	Q %	34.84	32.67	29.46
	COP %	34.79	32.65	29.47
	$\dot{m}_{R-cw}$ %	41.51	45.80	33.54
	U_o %	31.00	27.47	24.40

The results of the present study fall within the scatter of the data collected by Fujii [180] for horizontal tube condensers. This is expected based on the geometry of the condenser used in the test system. The correlations proposed by Nusselt Eq (7.6), Shekriladze and Gomelauri Eq (7.9), Butterworth Eq (7.10), Rose Eq (7.11), Fujii et al. Eq (7.12) and Lakshmi et al. Eq (7.15) have all been compared to the present data. The Butterworth correlation [179] and the related Lakshmi correlation [181] best predict the results reported

here. To improve the accuracy of the prediction, the leading coefficient of Eq 7.10 is modified

$$\bar{\mathrm{Nu}}\tilde{\mathrm{Re}}^{-0.5} = 0.4415\left(1+(1+9.47F)^{0.5}\right)^{0.5} \tag{7.16}$$

This modification agrees with the present data with a mean error of 4.43%.

7.4 Conclusions

Alternatives for water based steam power plant cooling are becoming necessary due to environmental and regulatory pressures. The use of refrigeration cycles to provide enhanced cooling for steam plants has been investigated here. An experimental model of a steam power plant has been designed to investigate the potential for a vapor compression refrigeration cycle to cool a steam condenser. The system consists of three interconnected loops: an open-loop steam condenser, an intermediate closed-loop chilled water circuit and a closed loop vapor compression refrigeration system. The links be tween the loops are two heat-exchangers. Experimental performance measurements indicate that the refrigeration cooled condenser is capable of delivering sufficient cooling to, at least, offset water consumption. Further the power consumption of the refrigeration system is reduced as the coolant temperature is reduced and condensate flow rates increase. This increases the efficiency of the Rankine power cycle and the COP of the refrigeration system.

Chapter 8

Conclusions and Future Work

This work has investigated two potential hurdles to a modern distributed electrical generation grid. The first is the adaption of small gas turbine engines to alternative fuels. A particular focus was on fuels from anaerobic digestion of organic materials as a source of renewable energy. There are a few commercially available engines that operate on fuels of this type, but a foundation of the operating limits of these fuels is lacking in the archival literature. To this end, a series of investigations into the effect of dilution on flame speeds and extinction limits have been reported. In an effort to expand on this research a test facility has been described and is under construction. The second avenue of investigation involves larger power plants intended for large population centers and industrial facilities. Due to the increased power demands and potential uses for steam, combined-cycle plants are of interest at these sites. The population growth in arid climates in the U.S. and global warming concerns has brought cooling of steam condensers to interest. A method of reducing the reliance of steam power cycles on natural water sources for cooling of steam condensers by using vapor compression refrigeration has been proposed. To investigate the effectiveness of such a system, a novel test rig has been designed. Initial results from this model have shown the promise of this method. This chapter is divided into two sections to describe the future of the research presented here.

8.1 Alternative Fuels for Small Gas Turbines

Two drivers have emerged to increase interest in micro-GT engines for small scale power production. The first is a push for industrial facilities to control their electrical energy supply. In some parts of the world this is due to inadequate or unreliable electrical grids. In the U.S. the desire for control is due to both volatility in energy prices and state incentive programs that rebate much of the initial capital investment (e.g., California's Self-Generation Incentive Program). The second driver is increasing regulatory pressure to limit the emissions of pollutants and reduce flaring of waste gases. Many states are investigating legislation to limit flaring to locations where there are no other economically viable alternatives. At remote oil and gas production sites the most logical use for the waste gas is electrical generation to power the site. Both drivers lead back to small fuel flexible GT engines as potential solutions.

Though recent discoveries of large, domestic natural gas reserves and advances in fossil fuel production methods have lessened the immediate need for alternative fuels, many drill sites are in remote locations where grid power is not initially available. Using Diesel fueled generators can be cost prohibitive due to the expense of shipping fuel. The available fuel stream from the producing wells is not always of pipeline quality. Heating contents can vary widely from site to site. Thus, fuel flexibility is a major concern for power generation equipment which may be moved between sites.

In this work we have investigated some of the limiting phenomena associated with diluted fuels. Previous work by Jahangirian and Engeda [157] pointed to a need for a study of laminar flame speeds of CO_2 diluted CH_4 fuels. This work has partially filled that void by proposing a correlation to predict the flame speed of a fuel based on content. Using an established

numerical model, the lean extinction limits in an ideal lean-premixed gas turbine have been explored. Based on this data a model for predicting limits based on operating conditions and fuel content was proposed. These two correlations may be used by future combustor designers to better predict the effect of fuel changes on combustor stability.

To expand on the alternative fuels research presented here, an experimental facility has been proposed and construction initiated. The well-stirred reactor is based on a design that has been used before with success to simulate conditions in a gas turbine combustor. The facility was designed with the goal of validating some of the lean-extinction work presented here. There is the opportunity to expand the facility for high pressure experiments to validate the pressure dependence suggested here. The well-stirred reactor facility is the most direct extension of this work.

8.2 Alternative Cooling Strategies for Future Large Power Plants

The other end of the size scale was covered by the second part of this work. Large combined-cycle plants are well suited for clean generation of electricity for large industrial facilities or population centers. Though they would run primarily on standard fuels like pipeline quality natural gas, the cooling of the steam condensers in the bottoming cycle is an area of concern. Large scale use and consumption of natural water supplies by steam power plants is facing increasing regulatory and environmental pressure. Alternative methods of condenser cooling will be necessary in the near future.

In this work we discuss the potential for applying vapor compression refrigeration systems to steam condenser cooling. Recent work by other investigators has pointed to potential

methods of integrating a refrigeration system in to a water vapor power cycle [173, 174]. To further advance this approach an experimental facility has been designed and constructed. This facility uses commercial 'off the shelf' components to model a reduced scale steam condenser cooled by a refrigeration system charged with R-410a. Initial results from the novel test setup described here indicate that the system becomes more efficient as the operating pressure in the steam condenser decreases. This is true for both the vapor power cycle and the refrigeration system.

The next step in this investigation would be to modify the test rig to eliminate the intermediate water loop. This moves the system closer to the intended application. The correlation to predict the Nusselt number in the condenser recommended here can be used to design the new system. This new system should be used to explore lower operating pressures in the steam condenser. Further testing in varying ambient conditions should also be undertaken to understand the effect of climate on the efficiency of the proposed system. These investigations will be necessary before a large scale refrigerant cooled steam condenser can be made commercially viable.

APPENDIX

APPENDIX: PIPING DIAGRAMS

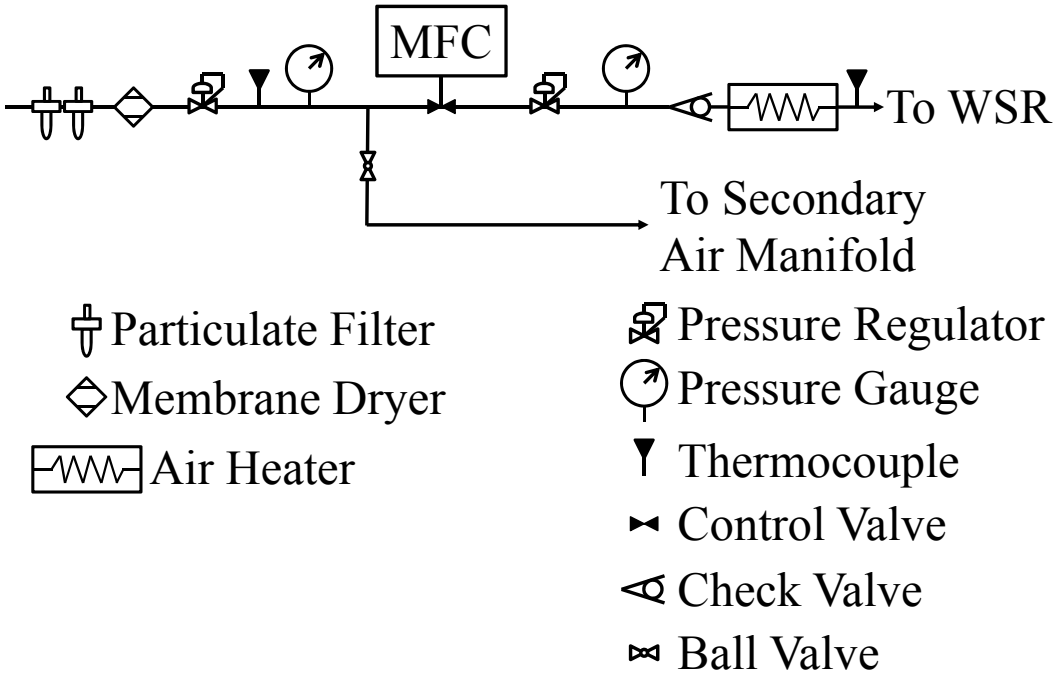

Figure A.1: Piping schematic of the air feed system to the WSR.

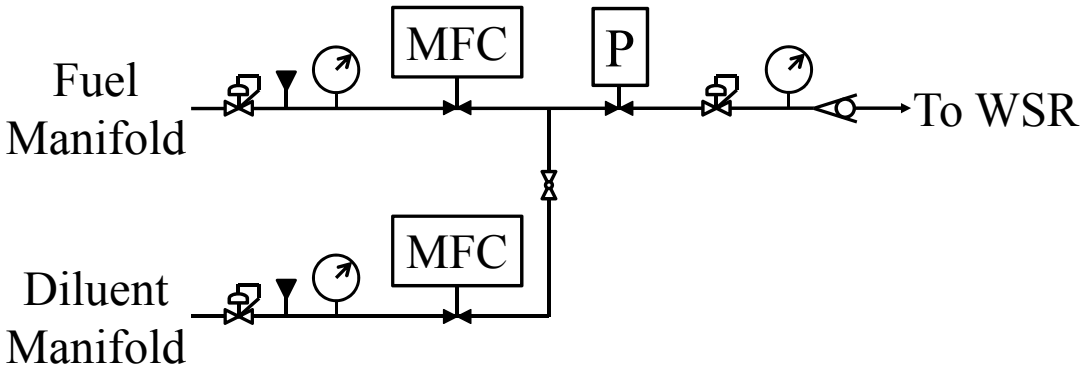

Figure A.2: Piping schematic of the fuel feed system to the WSR.

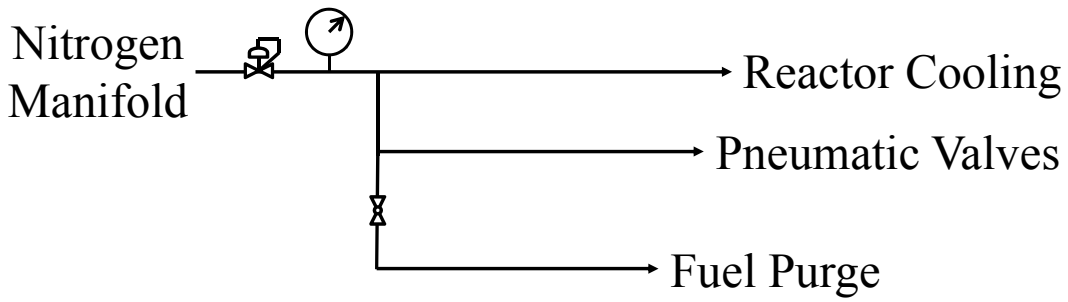

Figure A.3: Piping schematic of the nitrogen feed system to the WSR.

BIBLIOGRAPHY

BIBLIOGRAPHY

[1] T. Lieuwen, V. McDonnel, E. Petersen, and D. Santavicca, "Fuel flexibility influences on premixed combustor blowout, flashback, autoignition, and stability," *Journal of Engineering for Gas Turbines and Power*, vol. 130, p. 011506, 2008.

[2] J. P. Longwell and M. A. Weiss, "High temperature reaction rates in hydrocarbon combustion," *Industrial and Engineering Chemistry*, vol. 47, pp. 1634–1643, 1955.

[3] F. J. Wright, "The formation of carbon under well-stirred conditions," in 12^{th} *Symposium (International) on Combustion*, pp. 867–875, 1968.

[4] M. M. Thorton, P. C. Malte, and A. L. Crittenden, "A well-stirred reactor for the study of pyrolysis and oxidation kinetics: Carbon monoxide and n-pentane oxidation," *Combustion Science and Technology*, vol. 54, pp. 275–297, 1987.

[5] America's Climate Choices: Panel on Advancing the Science of Climate Change; National Research Council, "Advancing the science of climate change," 2010.

[6] M. Moliere, "Expanding fuel flexibility of gas turbines," *Proceedings of the Institution of Mechanical Engineers, Part A: Journal of Power and Energy*, vol. 219, pp. 109–119, 2002.

[7] C. Rodgers, J. Watts, D. Thoren, K. Nichols, and R. Brent, *Distributed Generation: The Power Paradigm for the New Millennium*, ch. Microturbines, pp. 119–150. CRC Press, 2001.

[8] A. H. Lefebvre, *Gas Turbine Combustion*. McGraw-Hill, 1983.

[9] J. Odgers, I. White, and D. Kretschmer, "The experimental behavior of premixed flames in tubes," *Journal of Engineering for Power*, vol. 102, pp. 422–426, 1980.

[10] J. Zelina, *COMBUSTION STUDIES IN A WELL-STIRRED REACTOR*. PhD thesis, University of Dayton, 1995.

[11] J. A. Veil, "Use of reclaimed water for power plant cooling," Tech. Rep. ANL/EVS/R-07/3, U. S. Department of Energy, National Energy Technology Laboratory, August 2007.

[12] W. C. Micheletti and J. M. Buns, "Emerging issues and needs in power plant cooling systems," in *Proceedings of Water Issues in Fossil Energy Workshop*, 2002.

[13] N. Madden, A. Lewis, and M. Davis, "Thermal effluent from the power sector: an analysis of once-through cooling system impacts on surface water temperature," *Enviornmental Research Letters*, vol. 8, p. 035006, 2013.

[14] J. S. Maulbetsch, "Comparison of alternate cooling technologies for California power plants: economic, environment and other tradeoffs," final report, EPRI and California Energy Comission, February 2002.

[15] L. J. Muzio and G. C. Quartucy, "Implementing NO_x control: Research to application," *Progress in Energy and Combustion Science*, vol. 23, pp. 233–266, 1997.

[16] Y. B. Zel'dovich, "The oxidation of nitrogen in combustion and explosions," *Acta Physiochem, USSR*, vol. 21, pp. 577–628, 1946.

[17] D. G. Nicol, R. C. Steele, N. M. Marinov, and P. C. Malte, "The importance of the nitrous oxide pathway to NO_x in lean-premixed combustion," *ASME Journal of Gas Turbines for Power*, vol. 117, pp. 100–111, 1995.

[18] T. Sattlemayer, W. Polifke, D. Winkler, and K. D$\acute{}$obbeling, "NO_x-apatement potential of lean-premixed GT combustors," *ASME Journal of Gas Turbines for Power*, vol. 120, p. 48, 1998.

[19] C. P. Fenimore, "Formation of nitric oxide in premixed hydrocarbon flames," in 13^{th} *Symposium (International) on Combustion*, (Pittsburgh), pp. 373–380, 1971.

[20] I. Glassman, *Combustion*. Academic Press, 3^{rd} ed., 1996.

[21] R. B. Edelman, O. Fortune, and G. Wellerstein, "Coupled mixing and kinetics," in *Emissions from Continuous Combustion Systems* (W. Cornelius and A. G. Agnew, eds.), 1972.

[22] R. C. Steele, A. C. Jarrett, P. C. Malte, J. H. Tonouchi, and D. G. Nicol, "Variables affecting NO_x formation in lean-premixed combustion," *Journal of Engineering for Gas Turbines and Power*, vol. 119, pp. 102–107, 1997.

[23] S. M. Correa, "A review of NO_x formation under gas-turbine combustion conditions," *Combustion Science and Technology*, vol. 87, pp. 329–362, 1992.

[24] S. R. Turns, *An Introduction to Combustion: Concepts and Applications*. McGraw-Hill, 2000.

[25] A. H. Lefebvre, "The role of fuel preparation in low-emission combustion," *Journal of Engineering for Gas Turbines and Power*, vol. 117, pp. 617–154, 1995.

[26] G. A. Richards, M. M. McMillian, R. S. Gemmen, W. A. Rogers, and S. R. Cully, "Issues for low-emission, fuel-flexible power systems," *Progress in Energy and Combustion Science*, vol. 27, pp. 141–169, 2001.

[27] I. G. Rice, "Steam-injected gas-turbine analysis: Steam rates," *Journal of Engineering for Gas Turbines and Power*, vol. 177, pp. 347–353, 1995.

[28] M. Feigl, G. Myers, S. R. Thomas, and R. Smith, "7H^{tm} combustion system performance with fuel moisturization," in *ASME Turbo Expo 2006*, no. GT2006-90281, 2006.

[29] W. S. Y. Hung, "Accurate method of predicting the effect of humidity or ingected water on NO_x emissions from industrial gas turbines," Tech. Rep. 74-WA/GT-6, ASME, 1974.

[30] J. P. Claeys, K. M. Elward, M. J. Mick, and R. A. Symonds, "Combustion system performance and fuel test results of the MS7001F gas turbine," *Journal of Engineering for Gas Turbines and Power*, vol. 115, pp. 537–546, 1993.

[31] M. Flamme, "New combustion systems for gas turbines (NGT)," *Applied Thermal Engineering*, vol. 24, pp. 1551–1559, 2004.

[32] A. T. Evulet, A. M. ELKady, A. R. Brand, and D. Chinn, "On the performance and operability of GE's dry low NO_x combustors utilizing exhaust gas recirculation for post-combustion carbon capture," *Energy Procedia*, vol. 1, pp. 3809–3816, 2009.

[33] R. A. Dalla Betta, "Catalytic combustion gas turbine systems: The preferred technology for low emissions electric power production and co-generation," *Catalysis Today*, vol. 35, pp. 129–135, 1997.

[34] A. Schlegel, P. Benz, T. Griffin, W. Weisenstein, and H. Bockhorn, "Catalytic stabalization of lean premixed combustion: Method for improving NO_x emissions," *Combustion and Flame*, vol. 105, pp. 332–340, 1996.

[35] F. D'Alessandro, G. Pacchiarotta, A. Rubino, M. Sperandio, P. Villa, A. M. Carrera, R. Fakhrai, G. Marra, and A. Congiu, "Lean catalytic combustion for ultra-low emis-

sions at high temperature in gas-turbine burners," *Energy & Fuels*, vol. 25, pp. 136–143, 2011.

[36] W. F. Domeracki, T. E. Dowdy, and D. Bachovchin, "Development of topping combustor for advanced concept pressurized fluidized bed combustion," in *Proceedings of Advances in IGCC and PFBC '94 Review Meeting*, 1994.

[37] J. H. Bowen, A. S. Feitelberg, S. L. Hung, and M. A. Lacey, "Perfromance of low Btu fuel gas turbine combustors," in *Proceedings of the Advanced Coal-Fired Power Systems '95 Review Meeting*, 1995.

[38] A. S. Feitelberg and M. A. Lacey, "The GE rich-quench-lean gas turbine combustor," *Journal of Engineering for Gas Turbines and Power*, vol. 120, pp. 502–508, 1998.

[39] L. L. Smith, H. Karim, M. J. Castaldi, S. Etemad, W. C. Pfefferle, V. Khanna, and K. O. Smith, "Rich-catalytic lean-burn combustion for low-single-digit NO_x gas turbines," *Journal of Engineering for Gas Turbines and Power*, vol. 127, pp. 27–35, 2005.

[40] A. J. Fiorentino, W. Greene, J. C. Kim, and E. J. Mularz, "Variable geometry, lean, premixed, pre-vaporized fuel combustor conceptual design," *Journal of Engineering for Power*, vol. 102, pp. 896–902, 1980.

[41] V. M. Sood and J. R. Shekleton, "Ongoing development of a low emission industrial gas turbine combustion chamber," *Journal of Engineering for Power*, vol. 102, pp. 549–554, 1980.

[42] R. K. Lyon, "The NH_3-NO-O_2 reaction," *International Journal of Chemical Kinetics*, vol. 8, pp. 315–318, 1976.

[43] L. J. Muzio, J. K. Arand, and D. P. Teixeira, "Gas phase decomposition of nitric oxide in combustion products," in 16^{th} *Symposium (International) on Combustion*, pp. 199–208, 1977.

[44] K. Skalska, J. S. Miller, and S. Ledakowicz, "Trends in NO_x abatement: A review," *Science of the Total Environment*, vol. 408, pp. 3976–3989, 2010.

[45] L. B. Davis and R. M. Washam, "Development of a dry low NO_x combustor," in *IGTI*, no. 89-GT-255, 1989.

[46] C. T. Bowman, "Control of combustion-generated nitrogen oxide emissions: Technology driven by regulation," in 24^{th} *Symposium (International) on Combustion*, pp. 859–878, 1992.

[47] V. McDonnell, *Lean Combustion: Technology and Control*, ch. Lean Combustion in Gas Turbines, pp. 121–162. Academic Press, 2008.

[48] D. Bradley, *Lean Combustion: Technology and Control*, ch. Fundamentals of Lean Combustion, pp. 19–53. Academic Press, 2008.

[49] T. F. Fric, "Effects of fuel-air unmixedness on NO_x emissions," *Journal of Propulsion and Power*, vol. 9, pp. 708–713, 1993.

[50] L. J. Spadaccini and M. B. Colket III, "Ignition delay characteristics of methane fuels," *Progress in Energy and Combustion Science*, vol. 20, pp. 431–460, 1994.

[51] G. J. Sturgess, D. G. Sloan, A. L. Lesmerises, S. P. Heneghan, and D. R. Ballal, "Design and development of a research combustor for lean blow-out studies," *Journal of Engineering for Gas Turbines and Power*, vol. 114, pp. 13–19, 1992.

[52] J. M. Beér and N. A. Chigier, *Combustion Aerodynamics*. John Wiley & Sons, Inc., 1972.

[53] T. Lieuwen, H. Torres, C. Johnson, and B. T. Zinn, "A mechanism of combustion instability in lean premixed gas turbine combustors," *Journal of Engineering for Gas Turbines and Power*, vol. 123, pp. 182–189, 2001.

[54] B. T. Zinn, *Advanced Combustion Methods*, ch. 2 Pulsating Combustion, pp. 113–182. Academic Press, 1986.

[55] T. Lieuwen, Y. Neumeier, and B. T. Zinn, "The role of unmixedness and chemical kinetics in driving combustion instabilities in lean premixed combustors," *Combustion Science and Technology*, vol. 135, pp. 193–211, 1998.

[56] M. P. Auer, C. Hirsch, and T. Sattelmayer, "Influence of the interaction of equivalence ratio and mass flow fluctuations on flame dynamics," in *Proceedings of the ASME Turbo Expo*, 2005.

[57] K. T. Kim, J. G. Lee, B. D. Quay, and D. A. Santavicca, "Spatially distributed flame transfer functions for predicting combustion dynamics in lean premixed gas turbine combustors," *Combustion and Flame*, vol. 157, pp. 1718–1730, 2010.

[58] T. Lieuwen, *Combustion Instabilities in Gas Turbine Engines*. AIAA, 2006.

[59] J. G. Meier, W. S. Y. Hung, and V. M. Sood, "Development and application of industrial gas turbines for medium-Btu gaseous fuels," *Journal of Engineering for Gas Turbines and Power*, vol. 108, pp. 182–190, 1986.

[60] R. M. Flores, V. G. McDonnel, and G. S. Samuelsen, "Impact of ethane and propane variation in natural gas on the performance of a model gas turbine combustor," *Journal of Engineering for Gas Turbines and Power*, vol. 125, pp. 701–708, 2003.

[61] S. Rasi, A. Veijanen, and J. Rintala, "Trace compounds from different biogas production plants," *Energy*, vol. 32, pp. 1375–1380, 2007.

[62] A. D. Cuéellar and M. E. Webber, "Cow power: The energy and emissions benefits of converting manure to biogas," *Enviornmental Research Letters*, vol. 3, pp. 1–8, 2008.

[63] G. Maschio, A. Lucchesi, and G. Stoppato, "Production of syngas from biomass," *Bioresource Technology*, vol. 48, pp. 119–126, 1994.

[64] A. Kumar, D. D. Jones, and M. A. Hanna, "Thermochemical biomass gasification: A review of the current status of the technology," *Energies*, vol. 2, pp. 556–581, 2009.

[65] A. J. Minchener, "Coal gassification for advanced power generation," *Fuel*, vol. 84, pp. 2222–2235, 2005.

[66] M. P. Boyce, *Gas Turbine Engineering Handbook*. Gulf Professional Publising, 2$^{\text{nd}}$ ed., 2001.

[67] E. Wheless and D. Gary, "Siloxanes in landfill and digester gas," in *SWANA Conference*, (Monterey, CA), 2002.

[68] C. K. Law, *Combustion Physics*. Cambridge University Press, 2006.

[69] J. Kubesh, S. R. King, and W. E. Liss, "Effect of gas composition on octane number of natural gas fuels," Tech. Rep. SAE 922359, Society of Automotive Engineers, 1992.

[70] R. L. Hack and V. G. McDonnel, "Impact of ethane, propane, and diluent content on the performance of a commercial microturbine generator," *Journal of Engineering for Gas Turbines and Power*, vol. 130, pp. 011509–1–7, 2008.

[71] E. C. Price and P. N. Cheremisinoff, *Biogas Production & Utilization*. Ann Arbor Science Publishers, Inc., 1981.

[72] P. N. Cheremisinoff and A. C. Morresi, *Energy From Solid Wastes*. Polution Engineering and Technology, Marcel Dekker, Inc., 1976.

[73] D. A. Tillman and N. S. Harding, *Fuels of Opportunity: Characteristics and Uses in Combustion Systems*, ch. Chapter 7: Gaseous and Liquid Opportunity Fuels, pp. 265–304. Elsevier, 2004.

[74] J. O. Leckie, J. G. Pacey, and C. Halvadakis, "Landfill management with moisture control," *ASCE Journal of The Environmental Engineering Division*, vol. 105, pp. 337–355, 1979.

[75] J. D. Murphy, E. McKeogh, and G. Kiely, "Technical/economic/envionmental analysis of biogas untilisation," *Applied Energy*, vol. 77, pp. 407–427, 2004.

[76] D. M. Wicksall and A. K. Agrawal, "Effects of fuel composition on flamibility limit of a lean premixed combustor," in *ASME Turbo Expo 2001*, no. GT2001-0007, 2001.

[77] A. Amato, B. Hudak, P. D'Carlo, D. Noble, D. Scarborough, J. Seitzman, and T. Lieuwen, "Methane oxycombustion for low CO_2 cycles: Blowoff measurements and analysis," *Journal of Engineering for Gas Turbines and Power*, vol. 133, p. 061503, 2011.

[78] Y. Ju, G. Masuya, and P. D. Ronney, "Effects of radiative emission and absorption on the propagation and extinction of premixed gas flames," in 27^{th} *Symposium (International) on Combustion*, pp. 2619–2626, 1998.

[79] D. Yossefi, S. J. Ashcroft, J. Hacohen, M. R. Belmont, and I. Thorpe, "Combustion of methane and ethane with CO_2 replacing N_2," *Fuel*, vol. 74, pp. 1061–1071, 1995.

[80] Y. Lafay, B. Taupin, G. Martins, G. Cabot, B. Renou, and A. Boukhalfa, "Experimental study of biogas combustion using a gas turbine configuration," *Experiments in Fluids*, vol. 43, pp. 395–410, 2007.

[81] D. Bohn and J. Lepers, "Effects of biogas combustion on the operation characteristics and pollutant emissions of a micro gas turbine," in *Proceedings of the ASME Turbo Expo*, no. GT-2003-38767, (Atlanta), ASME, 2003.

[82] J. A. Lycklama à Nijeholt, E. M. J. Komen, A. J. L. Verhage, and M. C. van Beek, "First assessment of biogas co-firing on the GE MS9001FA gas turbine using CFD," in *Proceedings of ASME Turbo Expo*, no. GT-2003-38791, (Atlanta), ASME, 2003.

[83] E. J. Dolak and J. P. Armstrong, "The correlation of IR microturbine combustion performance while burning diluted gaseous fuel supplied by a fuel mixing facility," in *Proceedings of GT2005*, no. GT2005-68610, (Atlanta), ASME, 2005.

[84] E. Wheless and G. Wiltsee, "Demonstration test of the Capstone microturbine on landfill gas," in *SWANA* 24^{th} *Annual Landfill Gas Symposium*, 2001.

[85] M. McDannel, E. Wheless, and J. Stahl, "First year performance and lessons learned for a digester gas-fired microturbine and a digester gas-fired fuel cell," in *POWER-GEN Renewable Energy Conference*, 2006.

[86] W. Qin, F. N. Egolfopoulos, and T. T. Tsotsis, "Fundamental and environmental aspects of landfill gas utilization for power generation," *Chemical Engineering Journal*, vol. 82, pp. 157–172, 2001.

[87] K. B. Fackler, M. F. Karalus, I. V. Novosselov, J. C. Kramlich, and P. C. Malte, "Experimental and numerical study of NO_x formation from the lean premixed combustion of CH_4 mixed with CO_2 and N_2," in *Proceedings of ASME Turbo Expo 2011*, no. GT2011-45090, (Vancouver, Canada), ASME, 2011.

[88] F. Sander, R. Carroni, S. Rofka, and E. Benz, "Flue gas recirculation in a gas turbine: Impact on performance and operational behavior," in *Proceedings of ASME Turbo Expo 2011*, no. GT2011-45608, (Vancouver, BC, Canada), June 2011.

[89] O. Bolland and S. Sæther, "New concepts for natural gas fired power plants which simplify the recovery of carbon dioxide," *Energy Conservation Management*, vol. 33, pp. 467–475, 1992.

[90] P. E. Røkke and J. E. Hustad, "Exhaust gas recirculation in gas turbines for reduction of CO_2 emissions: Combustion testing with focus on stability and emissions," *International Journal of Thermodynamics*, vol. 8, pp. 167–173, 2005.

[91] A. M. ElKady, A. Evulet, A. Brand, T. P. Ursin, and A. Lynghjem, "Exhaust gas recirculation in DLN F-Class gas turbines for post-combustion CO_2 capture," in *Proceedings of ASME Turbo Exp 2008: Power for Land, Sea and Air*, no. GT2008-51152, 2008.

[92] D. Winkler, P. Müller, S. Reimer, T. Griffin, A. Burdet, J. Mantzaras, and Y. Ghermay, "Improvement of gas turbine combustion reactivity under flue gas recirculation condition with in-situ hydrogen addition," in *Proceedings of ASME Turbo Expo 2009*, no. GT2009-59182, (Orlando, FL, USA), June 2009.

[93] C. A. Bass and R. B. Barat, "Simulation of a toroidal jet-stirred combustor using a partially stirred reactor model with detailed kinetic mechanisms," *Combustion and Flame*, vol. 135, pp. 249–259, 2003.

[94] K. K. Kuo, *Principles of Combustion*. John Wiley & Sons, Inc., 2^{nd} ed., 2005.

[95] J. P. Longwell and E. Bar-Ziv, "Modeling of inhomogeneities in the toroidal jet-stirred reactor," *Combustion and Flame*, vol. 78, pp. 99–119, 1989.

[96] J. Zelina and D. R. Ballal, "Combustor stability and emissions research using a well-stirred reactor," *Journal of Engineering for Gas Turbines and Power*, vol. 119, pp. 70–75, 1997.

[97] D. R. Ballal and A. H. Lefebvre, "Weak extinction limits of turbulent flowing mixtures," *Journal of Engineering for Power*, vol. 101, pp. 343–348, 1979.

[98] D. Kretschmer and J. Odgers, "Modeling of gas turbine combustors - a convenient reaction rate equation," *Journal of Engineering for Power*, vol. 94, pp. 173–180, 1972.

[99] A. H. Lefebvre and G. A. Halls, *AGARD Advanced Aero Engine Testing*, ch. Some Experiences in Combustion Scaling, pp. 177–204. Pergamon, 1959.

[100] M. A. Weiss, R. L. Lang, and J. P. Longwell, "Combustion rates in spherical reactors: Effects of inlet temperature and fuel type," *Industrial and Engineering Chemistry*, vol. 50, pp. 257–264, 1958.

[101] A. E. Clarke, A. J. Harrison, and J. Odgers, "Combustion stability in a spherical combustor," in 7^{th} *Symposium (International) on Combustion*, pp. 664–673, 1959.

[102] A. E. Clarke, J. Odgers, and P. Ryan, "Further sudies of combustion phenomena in a spherical combustor," in 8^{th} *Symposium (International) on Combustion*, pp. 982–984, 1960.

[103] G. J. Sturgess, R. G. McKinney, and S. A. Morford, "Modification of combustor stoichiometry distribution for reduced NO_x emissions from aircraft engines," *Journal of Engineering for Gas Turbines and Power*, vol. 115, pp. 570–580, 1993.

[104] Reaction Design, *CHEMKIN/CHEMKIN-PRO Theory Manual*. Reaction Design, San Diego, 2012.

[105] G. E. Andrews and D. Bradley, "The burning velocity of methane-air mixtures," *Combustion and Flame*, vol. 19, pp. 275–288, 1972.

[106] M. Metghalchi and J. C. Keck, "Burning velocities of mixtures of air with methanol, isooctane, and indolene at high pressure and temperatures," *Combustion and Flame*, vol. 48, pp. 191–210, 1982.

[107] H. Kobayashi, K. Seyama, H. Hagiwara, and Y. Ogami, "Burning velocity correlation of methane/air turbulent premixed flames at high pressure and high temperature," in *Proceedings of The* 30^{th} *Symposium (International) on Combustion*, pp. 827–834, 2005.

[108] C. Cohé, C. Chauveau, I. Gökalp, and D. F. Kurtuluş, "CO_2 addition and pressure effects on laminar and turbulent lean premixed CH_4 air flames," in *Proceedings of the Combustion Institute*, vol. 32, pp. 1803–1810, 2009.

[109] H. Kobayashi, H. Hagiwara, H. Kaneko, and Y. Ogami, "Effects of CO_2 dilution on turbulent premixed flames at high pressure and high temperature," in *Proceedings of the* 31^{st} *Syposium (International) on Combustion*, vol. 31, pp. 1451–1458, 2007.

[110] O. Blichner, "A fluid dynamic study of a spherical and a cylindrical stirred reactor," in 8^{th} *Symposium (International) on Combustion*, pp. 995–1002, 1960.

[111] H. C. Hottel, G. C. Williams, and M. L. Baker, "Combustion studies in a stirred reactor," in 6^{th} *Symposium (International) on Combustion*, pp. 398–411, 1957.

[112] A. E. Clarke, J. Odgers, F. W. Stringer, and A. J. Harrison, "Combustion processes in a spherical reactor," in 10^{th} *Symposium (International) on Combustion*, pp. 1151–1166, 1965.

[113] H. C. Hottel, G. C. Williams, and G. A. Miles, "Mixedness in the well-stirred reactor," in 11^{th} *Symposium (International) on Combustion*, pp. 271–278, 1967.

[114] W. S. Blazowski, "Soot production in back-mixed combustion," *Combustion Science and Technology*, vol. 21, pp. 87–96, 1980.

[115] W. S. Blazowski, "Dependence of soot production on fuel blend characteristics and combustion conditions," *Journal of Engineering for Power*, vol. 102, pp. 403–408, 1980.

[116] W. S. Blazowski, A. F. Sarofim, and J. C. Keck, "The interrelationship between soot and fuel NO_x control in gas turbine combustors," *Journal of Engineering for Power*, vol. 103, pp. 43–48, 1981.

[117] F. J. Wright, "Carbon formation under well-stirred conditions, part II," *Combustion and Flame*, vol. 15, pp. 217–222, 1970.

[118] V. S. Engleman, W. Bartok, J. P. Longwell, and R. B. Edelman, "Experimental and theoretical studies of NO_x formation in a jet-stirred reactor," in 14^{th} *Symposium (International) on Combustion*, pp. 755–765, 1973.

[119] A. Y. Abdalla, D. Bradley, S. B. Chin, and C. Lam, "Temperature fluctuations in a jet-stirred reactor and modelling implications," in 19^{th} *Symposium (International) on Combustion*, pp. 495–502, 1982.

[120] D. R. Jenkins, V. S. Yumlu, and D. B. Spaulding, "Combustion of hydrogen and oxygen in a steady-flow adiabatic stirred reactor," in 11^{th} *Symposium (International) on Combustion*, pp. 779–790, 1967.

[121] D. T. Pratt and E. S. Starkman, "High-temperature kinetics of ammonia-air combustion," in 12^{th} *Symposium (International) on Combustion*, pp. 891–899, 1969.

[122] J. J. Evangelista, R. Shinnar, and S. Katz, "The effect of imperfect mixing on stirred reactors," in 12^{th} *Symposium (International) and Combustion*, pp. 901–912, 1969.

[123] R. A. Corr, P. C. Malte, and N. M. Marinov, "Evaluation of NO_x mechanisms for lean, premixed combustion," *Journal of Engineering for Gas Turbines and Power*, vol. 114, pp. 425–434, 1992.

[124] G. C. Williams, H. C. Hottel, and A. c. Morgan, "The combustion of methane in a jet-mixed reactor," in 12^{th} *Symposium (International) on Combustion*, pp. 913–925, 1969.

[125] J. E. Nenniger, *Polycyclic Aromatic Hydrocarbon Production in a Jet Stirred Combustor*. PhD thesis, Massachusetts Institute of Technology, 1983.

[126] J. E. Nenniger, A. Kridiotis, J. Chomiak, J. P. Longwell, and A. F. Sarofim, "Characterization of a toroidal well stirred reactor," in 20^{th} *Symposium (International) on Combustion*, pp. 473–479, 1984.

[127] J. Zelina and D. R. Ballal, "Combustion and emissions studies using a well stirred reactor," in *30th AIAA/ASME/SAE/ASEE Joint Propulstion Conference*, no. AIAA 94-2903, 1994.

[128] S. L. Manzello, D. B. Lenhert, C. B. Stroud, and W. Tsang, "The effects of aromatic species on soot particle size distribution and species concentration in a well stirred reactor/plug flow reactor," in 5^{th} *US Combustion Meeting*, 2007.

[129] S. D. Stouffer, R. C. Striebich, C. W. Frayne, and J. Zelina, "Combustion particulates mitigation investigation using a well-stirred reactor," in *AIAA*, 2002.

[130] S. D. Stouffer, J. Heyne, G. Justinger, D. Ballal, R. Pawlik, and J. Zelina, "Combustion performance and emissions characteristics for a well-stirred reactor for low volatility hydrocarbon fuels," in *AIAA*, no. 2007-5663, 2007.

[131] S. D. Stouffer, D. R. Ballal, J. Zelina, D. T. Shouse, R. D. Hancock, and H. C. Mongia, "Development and combustion performance of a high pressure WSR and TAPS combustor," in *AIAA*, no. 2005-1416, 2005.

[132] J. W. Blust, *EFFECTS OF FUEL STRUCTURE ON EMISSIONS AND STABILITY IN THE WELL STIRRED REACTOR*. PhD thesis, University of Dayton, 1998.

[133] J. W. Blust, D. P. Ballal, and G. J. Sturgess, "Fuel effects on lean blowout and emissions from a well-stirred reactor," *Journal of Propulsion and Power*, vol. 15, pp. 216–223, 1999.

[134] J. M. Beér and K. B. Lee, "The effect of the residence time distribution on the performance and efficiency of combustors," in 10^{th} *Symposium (International) on Combustion*, pp. 1187–1202, 1965.

[135] R. J. Kee, J. A. Miller, and T. H. Jefferson, "CHEMKIN a general-purpose, problem-independent, transportable, FORTRAN chemical kinetics code package," Tech. Rep. SAND 80-8003, Sandia National Laboratories, 1980.

[136] R. J. Kee, F. M. Rupley, and J. A. Miller, "CHEMKIN-II: A fortran chemical kinetics package for the analysis of gas-phase kinetics," Tech. Rep. SAND 89-8009, Sandia National Laboratories, 1990.

[137] R. J. Kee, F. M. Rupley, E. Meeks, and J. A. Miller, "CHEMKIN-III: A FORTRAN chemical kinetics package for the analysis of gas-phase chemical and plasma kinetics," Tech. Rep. SAND 96-8216, Sandia National Laboratories, 1996.

[138] I. V. Novosselov, P. C. Malte, S. Yuan, R. Srinivasan, and J. C. Y. Lee, "Chemical reactor network application to emissions prediction for industrial DLE gas turbine," in *Proceedings of the 2006 ASME Gas Turbine Expo*, 2006.

[139] R. L. Curl, "Dispersed phase mixing: 1. theory and effects in simple reactors," *AIChE Journal*, vol. 2, pp. 175–181, 1963.

[140] P. Glarborg, R. J. Kee, J. F. Grcar, and J. A. Miller, "PSR: A Fortran program for modelling well-stirred reactors," Tech. Rep. SAND 86-8209, Sandia National Laboratories, 1986.

[141] F. Hermann, T. Ruck, J. Klingmann, and F. Mauss, "Flammability limits of low Btu gases: Computations in a perfectly stirred reactor and experiments," in *Proceedings of the ASME Turbo Expo*, no. 2001-GT-0004, (New Orleans), ASME, 2001.

[142] R. G. Gilbert, K. Luther, and J. Troe, "Theroy of thermal unimolecular reactions in the fall-off range. II. Weak collision rate constants," *Berichte der Bunsengesellschaft für physikalische Chemie*, vol. 87, pp. 169–177, 1983.

[143] P. H. Stewart, C. W. Larson, and D. M. Golden, "Pressure and temperature dependence of reactions proceeding via a bound complex. 2. application to $2CH_3 \leftarrow C_2H_5 + H$," *Combustion and Flame*, vol. 75, pp. 25–31, 1989.

[144] S. Li and L. Petzold, "Software and algorithms for sensitivity analysis of large-scale differential algebraic systems," *Journal of Computational and Applied Mathematics*, vol. 125, pp. 131–145, 2000.

[145] D. Bradley, S. B. Chin, M. S. Draper, and G. Hankinson, "Aerodynamic and flame structure within a jet-stirred reactor," in 16^{th} *Syposium (International) on Combustion*, (Pittsburgh), pp. 1571–1581, The Combustion Institute, 1976.

[146] C. K. Westbrook and F. L. Dryer, "Simplified reaction mechanisms for the oxidation of hydrocarbon fuels in flames," *Combustion Science and Technology*, vol. 27, pp. 31–43, 1981.

[147] C. K. Westbrook and F. L. Dryer, "Chemical kinetic modeling of hydrocarbon combustion," *Progress in Energy and Combustion Science*, vol. 10, pp. 1–57, 1984.

[148] W. P. Jones and R. P. Lindstedt, "Global reaction schemes for hydrocarbon combustion," *Combustion and Flame*, vol. 73, pp. 233–249, 1988.

[149] G. P. Smith, D. M. Golden, M. Frenklach, N. W. Moriarty, B. Eiteneer, M. Goldenberg, C. T. Bowman, R. K. Hanson, S. Song, W. C. Gardner, V. V. Lissianski, and Z. Qin, "GRI-Mech 3.0 mechanism." Online, http:/www.me.berkely.edu/gri_mech, April 2012.

[150] San Diego Mechanism Web Page, Mechanical and Aerospace Engineering (Combustion Research), University of California San Diego, "Chemical-kinetic mechanism for combustion applications." Online, http://www.combustion.ucsd.edu, April 2012.

[151] P. Glarborg and L. L. B. Bentzen, "Chemical effects of a high CO_2 concentration in oxy-fuel combustion of methane," *Energy & Fuels*, vol. 22, pp. 291–296, 2008.

[152] M. Frenklach, *Numerical Approaches to Combustion*, vol. 135 of *Progress in Astronautics and Aeronautics*, ch. 5 Reduction of Chemical Models, pp. 129–154. American Institute of Aeronautics and Astronautics, Inc, 1991.

[153] H. Wang and M. Frenklach, "Detailed reduction of reaction mechanims for flame modeling," *Combustion and Flame*, vol. 87, pp. 365–370, 1991.

[154] A. Kazakov and M. Frenklach, "Reduced GRI-Mech 1.2 mechanism." Online, http://www.me.berkely.edu/drm, April 2012.

[155] G. Sturgess, "Combustor lbo design model evaluation," Tech. Rep. WL-TR-95-2089, Wright Laboratory, USAF, 1995.

[156] B. Lilleberg, I. S. Ertesvåg, and K. E. Rian, "Modeling instabilities in lean premixed turbulent combustors using detailed chemical kinetics," *Combustion Science and Technology*, vol. 118, pp. 1107–1122, 2009.

[157] S. Jahangirian and A. Engeda, "Biogas combustion and chemical kinetics for gas turbine applications," in *Proceedings of the IMECE2008*, no. IMECE2008-66667, (Boston, Massachusetts, USA), ASME, 2008.

[158] R. J. Kee, J. F. Grcar, M. D. Smooke, and J. A. Miller, "A fortran program for modeling steady laminar one-dimensional premixed flames," Tech. Rep. SAND85-8240, Sandia National Laboratories, 1985.

[159] J. Bibrzycki, T. Poinsot, and A. Zajdel, "Investigation of laminar flame speed of $CH_4/N_2/O_2$ and $CH_4/CO_2/O_2$ mixtures using reduced chemical kinetic mechanisms," *Archivum Combustionis*, vol. 30, no. 4, pp. 287–296, 2010.

[160] F. Liu, H. Guo, G. J. Smallwood, and Ö. L. Gulder, "The chemical effects of carbon dioxide as an additive in an ethylene diffusion flame: Implications for soot and NOx formation," *Combustion and Flame*, vol. 125, pp. 778–787, 2001.

[161] S. Hoffmann, P. Habisreuther, and B. Lenze, "Development and assessment of correlations for predicting stability limits of swirling flames," *Chemical Engineering Processing: Process Intensification*, vol. 33, pp. 393–400, 1994.

[162] J. W. Blust, M. G. Getz, and S. Zabarnick, "Probe design optimization for the well-stirred reactor," in 35^{th} *AIAA Aerospace Sciences Meeting and Exhibit*, no. 0907, 1997.

[163] M. J. Moran and H. N. Shapiro, *Fundamentals of Engineering Thermodynamics*. John Wiley & Sons, Inc., 5^{th} ed., 2004.

[164] A. Rashad and A. El Maihy, "Energy and exergy analysis of a steam power plant in Egypt," in *Proccedings of the* 13^{th} *International Conference on Aerospace Science and Aviation Technology*, 2009.

[165] I. H. Aljundi, "Energy and exergy analysis of a steam power plant in Jordan," *Applied Thermal Engineering*, vol. 29, pp. 324–328, 2009.

[166] K. N. Hassan, Q. A. Rishack, and A. K. Mohammed, "Study of the condenser performance in Al-Nassiriyah thermal power plant," *Journal for Engineering Sciences*, vol. 2, 2011.

[167] V. Haldkar, A. K. Sharma, R. K. Ranjan, and V. K. Bajpai, "Parametric analysis of surface condenser for thermal power plant," *International Journal of Heat and Mass Transfer*, vol. 3, pp. 155–159, 2013.

[168] S. L. Mirjana, S. V. L. M. M. Stojiljkovic, V. P. Stefanovic, and D. D. Mitrovic, "Impact of the cold end operating conditions on energy efficiency of the stream power plants," *Thermal Science*, vol. 14, pp. S53–S66, 2010.

[169] H. Forster and J. Lilliestam, "Modeling thermoelectric power generation in view of climate change," *Regional Environmental Change*, vol. 10, pp. 327–338, 2010.

[170] B. M. Johnson, R. T. allemann, D. W. Faletti, B. C. Fryer, and F. R. Zaloudek, "Dry cooling of power generating station: A summary of the economic evaluation of several advanced concepts via a design and cost estimate," Technical Report BNWL-21120, Battelle Pacific Northwest Labs, 1976.

[171] R. T. Allemann, B. M. Johnson, and E. V. Werry, "Wet-dry cooling demonstration: a transfer of technology," Tech. Rep. CS-5016, Electric Power Research Institute, 1987.

[172] D. Y. Goswami, "Solar thermal power technology: Present status and ideas for the future," *Energy Sources*, vol. 20, pp. 137–145, 1998.

[173] A. S. Hegazy, "Use of cooling thermal storage as a heat sink for steam power plant," *JSME Journal of Thermal Science and Technology*, vol. 3, pp. 330–341, 2008.

[174] A. S. Hegazy, "Improving performance of refrigerant cooled steam power plant using cooling thermal storage," *ASME Journal of Engineering for Gas Turbines and Power*, vol. 131, p. 053002, 2009.

[175] K. A. Yousif, A. Assef, A. S. Hegazy, and A. Engeda, "Comparative study of using water and R-134a as a cooling medium in the condenser of a steam power plant," in *Proceedings of the ASME Turbo Expo*, no. GT2014-25034, 2014.

[176] K. A. Yousif, A. Assefa, A. S. Hegazy, and A. Engeda, "Comparative study of using R-410a, R-407c, R-22, and R-134a as a cooling medium in the condenser of a steam power plant," in *Proceedings of the ASME Turbo Expo*, no. GT2014-25033, 2014.

[177] W. Nusselt, "Die oberflachen-kondensation des wasserdampfes," *VDI Zeitung*, vol. 60, pp. 541–757, 1916.

[178] I. G. Shekriladze and V. I. Gomelauri, "Theoretical study of laminar film condensation of a flowing vapor," *International Journal of Heat and Mass Transfer*, vol. 9, pp. 581–591, 1966.

[179] D. Butterworth, "Developments in the design of shell-and-tube condensers," in *ASME WA/HT-24*, no. No. 77, (Atlanta), ASME, 1977.

[180] T. Fujii, *Power condenser heat transfer technology*, ch. Vapor shear and condensate inundation: an overview. Hemisphere Publishing, 1981.

[181] B. V. Lakshmi, T. Subrahmanyam, V. D. Rao, and K. V. Sharma, "Turbulent film condensation of pure vapor flowing normal to a horizontal condenser tube - constant heat flux at the tube wall," *International Journal of Automotive and Mechanical Engineering*, vol. 4, pp. 455–470, 2011.

[182] Y. Haseli, I. Dincer, and G. F. Naterer, "Optimum temperatures in a shell and tube condenser with respect to exergy," *International Journal of Heat and Mass Transfer*, vol. 51, pp. 2462–2470, 2008.

[183] A. Vidal, R. Best, R. Rivero, and J. Cervantes, "Analysis of a combined power and refrigeration cycle by the exergy method," *Energy*, vol. 31, pp. 3401–3414, 2006.

[184] T. Wu and K. Vierow, "Local heat transfer measurements of steam/air mixtures in horizontal condenser tubes," *International Journal of Heat and Mass Transfer*, vol. 49, pp. 2491–2501, 2006.